Line-connected permanent magnet synchronous generator with adjustable excitation for variable-frequency AC aircraft power system

By

Haoyu Liu

A thesis submitted in fulfilment of the requirements for the degree of

Doctor of Philosophy

Department of Electronic and Electrical Engineering

Faulty of Engineering

The University of Sheffield

October 2024

Abstract

Electrical generators are a key enabling technique for aircraft electrification which is a growing trend in the aerospace industry. Whereas the wound-field synchronous generators allow the direct line connection to the aircraft power network, their power density and efficiency are lower than permanent magnet synchronous generators. However, the latter needs a power converter to regulate the output voltage magnitude and frequency, compromising the power density and fault tolerant capability of the overall power generation system. Therefore, this thesis proposes a direct line-connected variable-flux permanent magnet synchronous generator which does not require a power converter for the aircraft power network connection. To regulate the output voltage, two movable flux-diverting endplates are employed to regulate the flux crossing the main working airgap. Extensive three-dimensional finite element analysis is performed to demonstrate the voltage regulation principle with various space-off distances between the flux-diverting endplates and the active rotor stack. To achieve the voltage regulation and power quality requirements, a series of designs are performed by changing the aspect ratio, tooth tip geometry, airgap length, winding pitch, and the rotor profile. Global optimisation of the rotor profile leads to an asymmetric geometry which reduces the voltage distortion factor while increasing the power output. The final optimised design successfully achieves the voltage regulation requirement of 113Vrms ± 5V at 360-800Hz frequency range and the power quality requirement of within 5% distortion factor, as per MIL-STD-704F standard for aircraft electrical systems. A mechanical structure for manual setting of the flux-diverting endplate position is designed to demonstrate the mechanism to control the position of the endplates. The proposed generator with flux-diverting endplates and their manual actuation system are manufactured and mostly assembled to test the performances of this prototype.

Acknowledgements

Contents

List of Figures

XI

List of Tables

List of symbols and abbreviations

Symbol	Definition	Unit
A_{123}	Coil conductor	
D	Stator outer diameter	mm
L	Axial length	mm
R_{ABC}	Equivalent terminal resistance	Ω
$\overrightarrow{V_{an}}$	Potential differences between phase terminal resistor and neutral point	V

Abbreviation	Description
AC	Alternative current
APU	Auxiliary Power Units
ATU	Autotransformer rectifier unit
CO_2	Carbon dioxide
CSD	Constant speed drive
DC	Direct current
DEM	Doubly excited machines
ECS	Environmental control system
EDM	Electro-discharge machine
EMF	Electromotive force
FE	Finite element
FEA	Finite element analysis
FFT	Fast Fourier transform

FSPM	Flux-switching permanent magnet machine
GCU	Generator control unit
HEM	Hybrid excitation machine
IDG	Integrated drive generator
IPM	Interior permanent magnet machine
MEA	More-electric aircraft
PM	Permanent magnet
PMA	Permanent magnet alternator
PVR	Point voltage reference
RAT	Ram air turbine
RMS	Root mean square
SPM	Surface mounted permanent magnet
THD	Total harmonic distortion
TRU	Transformer rectifier unit
VF	Variable frequency
VFAC	Variable frequency alternative current

Chapter 1 - Introduction

1.1 Structure of the thesis

This thesis is organized into 7 chapters:

The first chapter introduces the rationale behind this research project. As clarifies the evolution of the aircraft electrical system, noting that with the trend represented by the MEA, the power demand on board has significantly increased. Compared to listed conventional aerospace generators, the permanent magnet generator offers higher power density and efficiency with corresponding converter system. However, its fixed excitation poses challenges for direct line connection which simplified the electrical system to a greater extent. Therefore, this project aims to investigate a variable excitation permanent magnet generator for direct grid connection.

The second chapter will review the majority of flux manipulation methods for permanent magnet machines.

The third chapter will outline the design criteria and begins by examining the existing converter-fed permanent magnet generator, thereby establishing a baseline model for evaluation.

The fourth chapter will focus on optimizing the baseline model to meet the designing criteria.

The fifth chapter will demonstrate the development process of mechanical aspect of machine structure.

The sixth chapter will present the complete procedure and result of prototype construction and testing.

The final chapter will summarize the findings of this project and layout the plan for the future work.

1.2 Trends in the electrification of aircraft

Since the Wright brothers successfully flew their prototype aircraft in 1903, technological development of aircraft has received growing attention. These developments have resulted in higher speeds, greater payload, improved safety and reduced fuel consumption. As well as technical improvements in aerodynamics, aerostructures and engines, key technologies in the advancement of aircraft have been avionics and the on-board power systems. Electrification of aircraft is a growing trend in the aerospace industry with a number of different electrical systems being considered for future aircraft.

1.2.1 Electric aircraft propulsion

A topic that has received growing attention for future aircraft is all-electric, hybrid-electric or turbo-electric propulsion. Electrification of the propulsion systems offers one route to zero-emissions flight and increase efficiency. Although the efficiency of gas turbines engines has increased by some 60% since the very first civil gas-turbines of the 1950a [1], when compared with pure electric propulsion systems, there is still a very big gap in CO_2 emissions. There are 3 basic types of electric propulsion which shown in Fig 1-1 are being investigated for electric propulsion [2].

(a) Turbo-electric

(c) Parallel hybrid-electric

(b) Series hybrid-electric
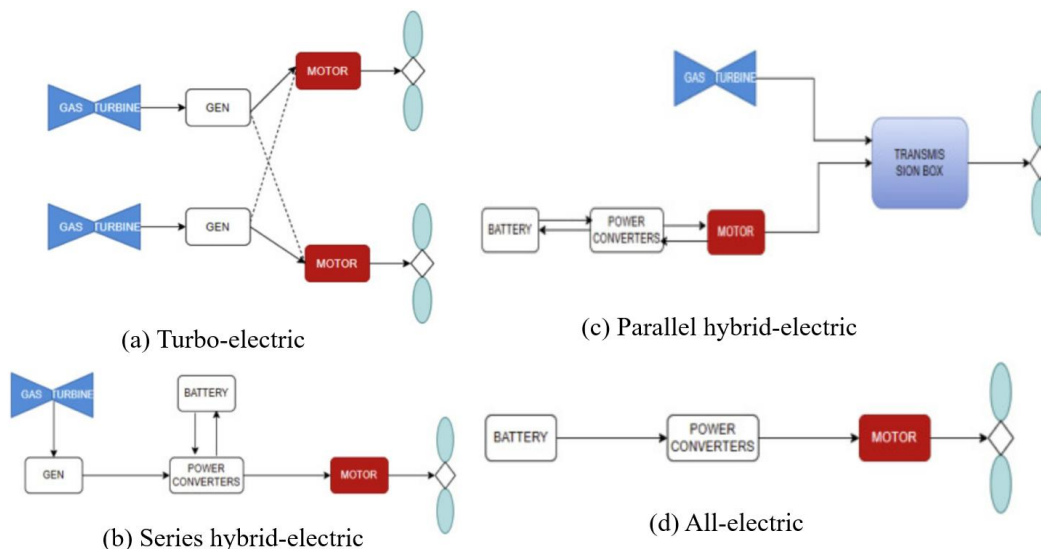
(d) All-electric

Fig 1-1 Alternative electric propulsion architectures [2]

The energy density of battery technology is too low for all-electric propulsion electrical aircraft, as a review of electrification in 2022 [2] noted that in 2022 state-of-the-art Lithium-ion batteries had power density of 250Wh/kg. This compares with projections

2

that all-electric aircraft for general aviation and regional aircraft will require battery energy densities of 400Wh/kg and 750Wh/kg, respectively. The same review noted that in 2022 state-of-the-art Lithium-ion batteries had power density of 250Wh/kg compared to 12,000Wh/kg for aviation fuel. Even allowing for the higher efficiency of all-electric propulsion, this difference shows the difficulties of moving to electrical propulsion for large and long-range aircraft. Although the target for aircraft remains all-electric propulsion, it is inevitable that gas-turbines which burn sustainable aviation fuel will remain the dominant technology for medium and large aircraft. However, even if the main propulsion power remains dominated by gas-turbines, the requirements for electrical power on aircraft will continue to grow as more sub-systems migrate to electrical power.

1.2.2 More-electric aircraft

In aircraft, the power systems are often divided into primary systems which provide the main propulsion power and secondary power systems which supply the numerous systems on the aircraft for control and actuation, cabin environment and other ancillaries. On most commercial aircraft, secondary power systems provide power in the form of direct mechanical, hydraulic, pneumatic or electrical power depending on the requirements of the sub-system they are supplying.

There has been a longstanding interest in moving from hydraulic, pneumatic and mechanical systems to electrical systems. This interest has resulted in the notion of a more-electric aircraft (MEA) based on sub-systems such as that shown in Fig 1-2 [3]. It is important to note that the term 'more-electric' aircraft does not cover aircraft with some form of electric propulsion but refers to aircraft which use electrical power for most of the secondary systems. In the example shown in Fig 1-2, electrical power is used for the cabin air environmental control system (ECS), actuation of control surfaces though either electromechanical [4] or electro-hydraulic [5] actuators, de-icing and other electrical loads on the aircraft. The ultimate version of the more-electric aircraft would have gas-turbine engines which produce propulsion and electrical power only.
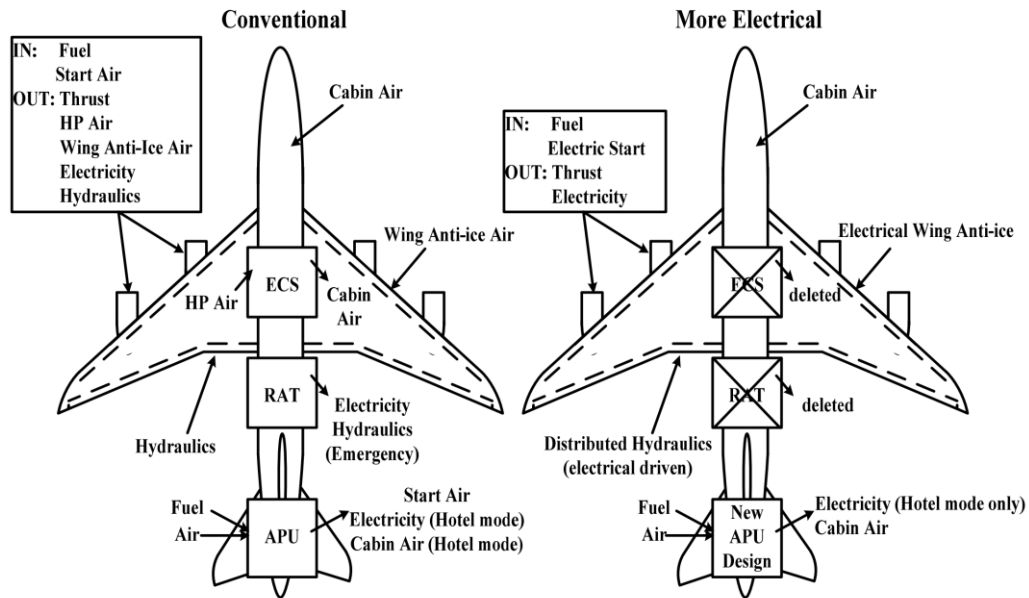
Fig 1-2 Comparison between conventional and more-electric aircraft [3]

Among the claimed benefits of adopting a more-electric aircraft approach to the secondary power systems are:

- Reduced weight which can be up to 10% on current estimates with potential to exceed this in next generation systems [6].

- Improved controllability in terms of reduced response time for single component and fewer mechanical linkages between each component.

- Improved fault tolerance capability and redundancy with the ability of electrical systems to be divided into several separate and isolated sub-systems [9].

- Reduced maintenance requirements with benefits in cost and downtime [7][8][9].

System-wide health monitoring of electrical systems is more achievable compared with equivalent mechanical and hydraulic systems [10].

Electrical power requirements on aircraft have grown significantly in recent years as shown by Fig 1-3. The Boeing 787, also known as the Dreamliner, remains the large commercial civil aircraft with the highest degree of electrification with a number of 250kVA rated generators [11].
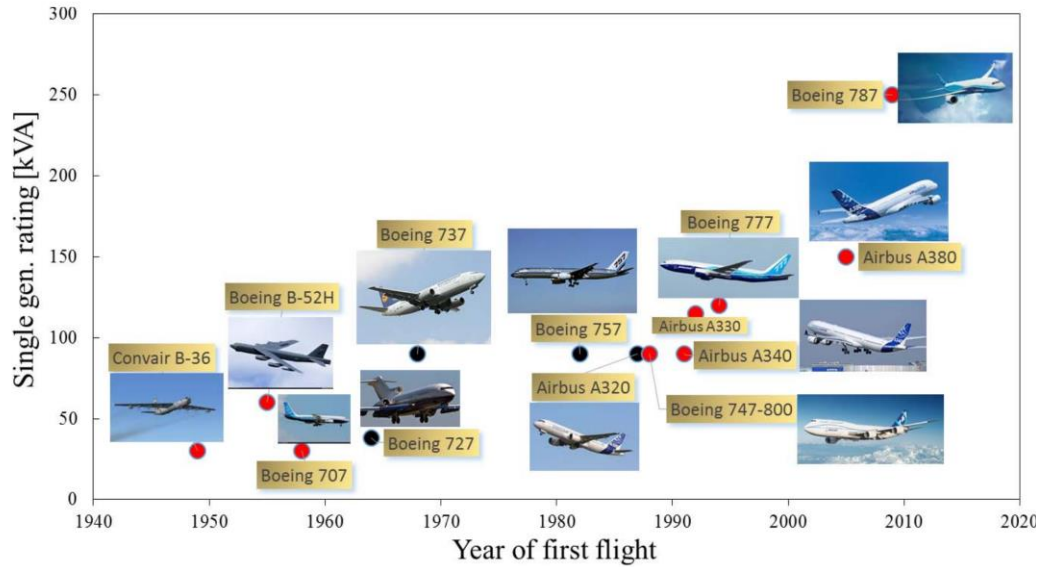
Fig 1-3 Increase in generator ratings over the past 70 years [12]

1.3 Aircraft electrical systems on commercial aircraft

1.3.1 Electrical network architectures

A typical modern aircraft electrical power system architecture is shown in Fig 1-4, in this case for a Boeing 787. As shown in Fig 1-4, for this twin-engine aircraft there are two separate 250kVA generators on each engine, giving a total installed capacity of 1MVA from 4 generators. As shown by Fig 1-4, the overall system is very complex with many features to allow reconfiguration of the network to ensure continued provision of electrical power even with the loss of engine or a generator. It is interesting to note that despite this parallel power supply layout, the 2 variable frequency starter generators will not always have the same frequency. These 4 generators supply all the secondary system via 4 separate 230V AC bus bar, with 2 Auxiliary power unit starter generator and 1 ram air turbine generator as backup power sources. When one of the generators experience malfunctions, the bus power control unit is responsible for redistributing the remaining bus bar to maintain the system working.
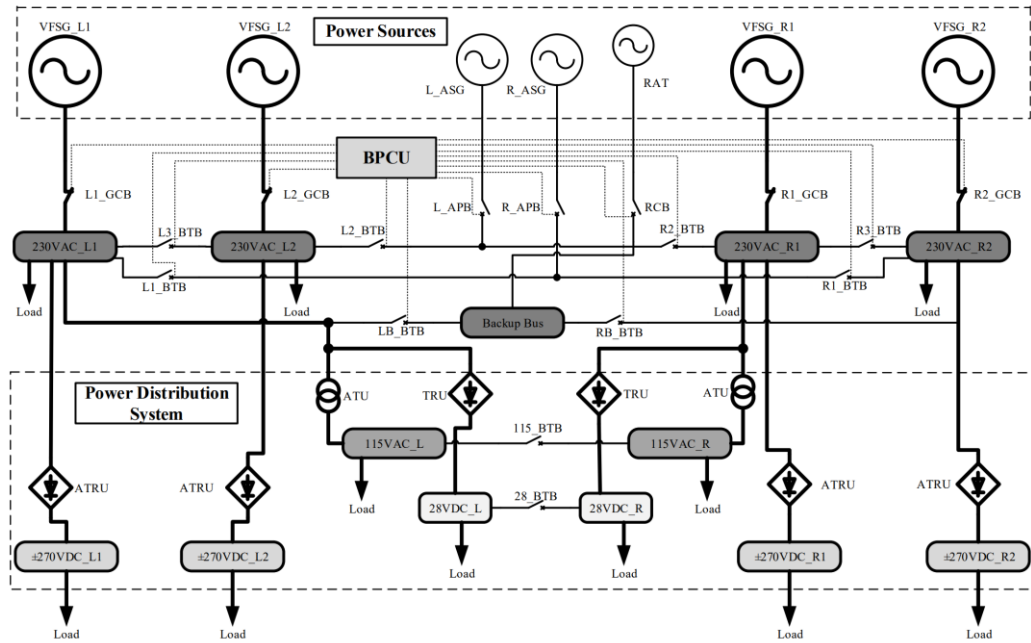
Fig 1-4 Power system architectures of a Boeing 787 [11]

1.3.2 Variable-frequency and fixed-frequency electrical networks

In older aircraft with AC power networks, i.e. pre 1990s, electric power was supplied at a fixed 400Hz. The need to maintain a fixed 400Hz electrical supply with synchronous generators meant that the mechanical speed of the generator was precisely controlled at a fixed speed, e.g. 24,000 for a 2-pole machine, reducing to 6,000 rpm for an 8-pole machine. However, although the ratio of the accessory gearbox output speed and the engine shaft speed can be set by the gear-ratio, the gearbox output shaft tracks the speed of the engine shafts. Hence, for a 400Hz fixed frequency aircraft there is a need to produce a fixed mechanical speed into the electrical generator from a variable-speed accessory gearbox output.

The approach which remains in use on many older commercial aircraft in service is to use a constant speed drive (CSD) in combination with a generator to form an integrated drive generator (IDG). In an IDG, a mechanical device converts a variable speed input into a fixed speed output which in turn drives the generator, thus ensuring that the electrical frequency remain independent of the engine speed [13]. A typical IDG is shown in Fig 1-5. Although using a CSD as part of an IDG provides a straightforward

solution from a system architectures point of view, these CSD devices are bulky, inefficient and require regular maintenance.
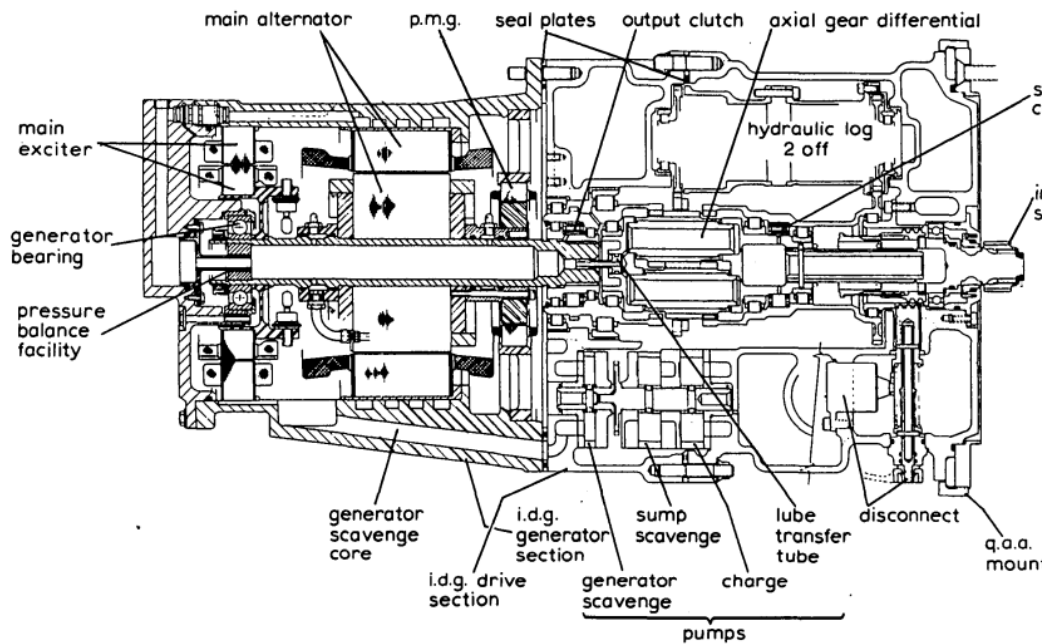
Fig 1-5 Constant speed integrated drive generator [14]

As the electrical power requirements of aircraft continued to increase, the inefficiencies and poor power densities of IDGs became unacceptable and so a new approach of a variable frequency (VF) power networks was developed in the 1980s and came into service in the 1990s [12]. In a VF power system, the magnitude of the supply voltage remains fixed (usually at a nominal phase voltage of 115Vrms or 230Vrms) but the frequency is allowed to vary over a defined range of 360-800Hz. This allows a direct connection between the accessory gearbox and the generator eliminating the need for a constant speed drive.

1.3.3 Electrical power quality standards for aircraft

Modern aircraft integrate many hundreds of systems, sub-systems and components, often manufactured by a number of different suppliers. In order to ensure that these operate successfully and to enhance the safety of the aircraft, the various components must meet various industry standards. There are several standards for aircraft electrical systems, with significant overlaps between the standards. The most well-known

standard for aircraft electrical system is MIL-STD-704 release initially by the US Defence Department in 1959 and updated several times since., with the latest version being MIL-STD-704F [15]. Standards such as MIL-STD-704F set out specifications for different aspects of electrical power systems and all equipment designed and manufactured for aircraft must meet the relevant standard.

For the research reported in this thesis on direct line connect generators, the terminal power quality is critical to evaluate the performance of any novel designs and concepts. Table 1-1 below summarizes the key specifications for the power quality which were extracted from MIL-STD-704F [15], DO-160G [16], EN 2282 – 1992 [17] and ISO 1540-2006 [19]. It is worth noting that all the values used within the standard are rms values.

Table 1-1 Key power quality specifications for a direct line connected generator

Standard	Voltage range	Frequency range	Total harmonic distortion of terminal voltage waveform (THD)
DO-160G	111Vrms ± 9.5V	360-800Hz	10% for total contents 6% for individual harmonic contents
EN 2282-1992	113Vrms ± 5V	400Hz fixed	8% for total contents 5% for individual harmonic contents
MIL-STD-704F	113Vrms ± 5V	360-800Hz	5% for total contents
ISO 1540-2006	111Vrms ± 9.5V	360-800Hz	10% for total contents 7.5% for individual harmonic contents

The harmonic content of the waveform is limited in the standards by the specification of a single distortion factor, which is defined according to the following: Equation 1-1:

$$THD_x = \frac{\sqrt[2]{\sum_{n=2}^{\infty} X_x^2}}{x_1} \qquad \text{Equation 1-1}$$

Whereas MIL704-F sets a voltage total distortion limit of 5%, this does vary between standards. DO-160 sets a limit of 10%, ISO1540 – 2006 set a limit of 10% and EN 2282 – 1992 sets a limit of 8%. As can be seen, MIL-STD-704F has the strictest limitation on the distortion factor and hence this limit was adopted as the value for the research in this thesis.

Another important factor in the performance of generators with star connections is whether the star-point is connected to the system ground or left floating. In aircraft, the local 'ground' for the power system within the aircraft is known as the point of voltage reference or PVR which is the reference 0V shared by all aircraft electrical equipment[18]. The star-point of the AC power sources are electrically connected to the PVR to provide a common electrical reference potential. During refuelling or maintenance, the PVR is connected to an earth ground. The impact of grounding or floating the star-point of the generator is investigated in detail in chapter 4.

1.4 Conventional aircraft generator technology

The mechanical drive for the main electrical generators in current commercial aircraft is provided by the rotating shafts of the gas-turbine engines. The power is usually taken off via a radial driveshaft and an accessory gearbox as shown in Fig 1-6 for the particular case of a Rolls-Royce Trent 1000 engine which is used on the Boeing 787. To optimize the propulsion performance of the gas-turbine, the speed of the various shafts varies significantly over the operating envelope of the engine and hence the mechanical input to the generator follows this variation, but often with a fixed gear ratio. The proportion of the shaft power taken off by the generator as electrical power is small and the large moment of inertia of engine shafts means that the mechanical input to the generator is very stiff in terms of speed and power capability and so can be regarded as an idealized mechanical input.
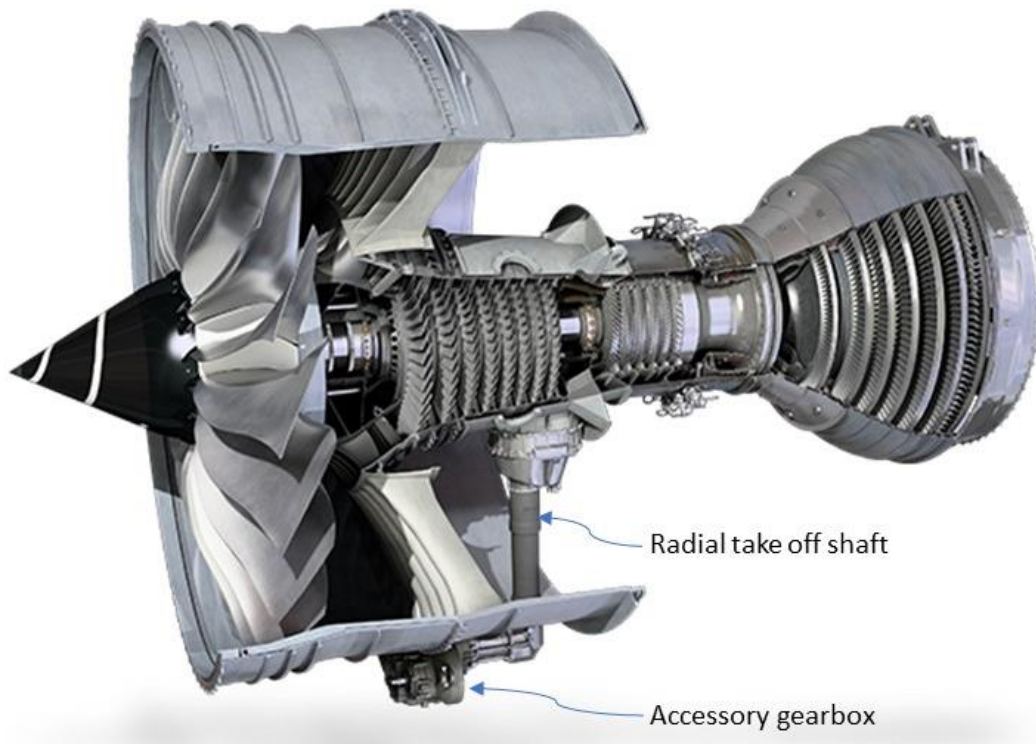
Fig 1-6 Cut-away section of a Trent 1000 engine showing the radial take-off shaft and the accessory gearbox which drives the electrical generators

1.4.1 Wound-field synchronous generators

Major new civil aircraft programs over the past 20+ years have adopted a variable-frequency system with a wound-field synchronous machine. A wound field synchronous machine allows the direct connection of the generator terminals to the power network without the need for an intermediate power converter. Aerospace wound-field generators have a brushless exciter configuration of the general form shown in Fig 1-7 [12]. The small permanent magnet section of the rotor generates an AC voltage in the associated small stator winding which is rectified and used to power for the main exciter unit which adjust the magnitude of the DC current in the main exciter to ultimately regulate the generator output voltage. The AC armature of the main exciter generates a voltage which is rectified by rectifier diodes mounted on the rotor to produce the field which then generates the AC voltage in the main generator AC winding. The frequency of this output voltage is proportional to the mechanical speed of the generator shaft and the magnitude can be regulated by controlling the DC current in the main exciter.
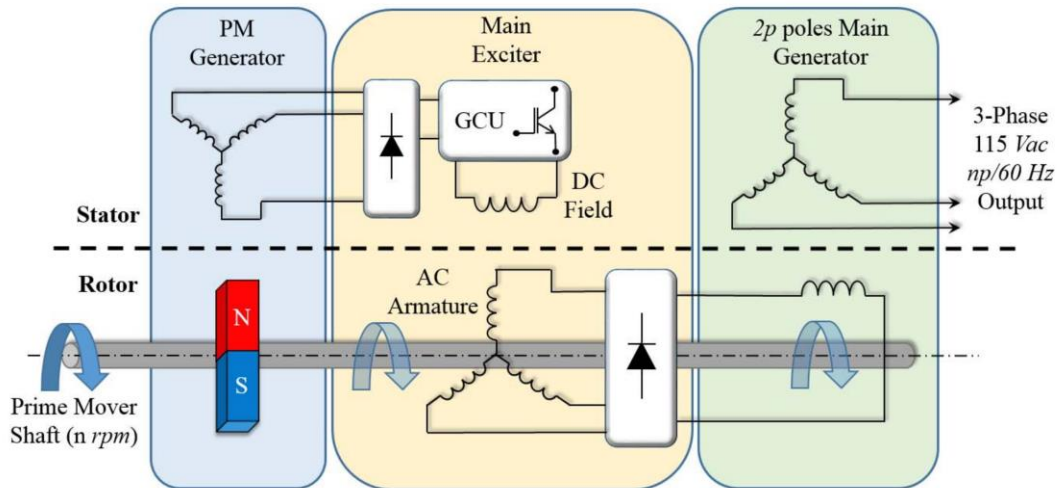
Fig 1-7 Typical architecture of a wound-field synchronous generator with a brushless exciter [12]

Wound-field synchronous generators offer the flexibility to control the excitation and hence the generator output voltage magnitude as both the speed and the current drawn by the load vary over the operating range of the generator. The generator control unit (GCU) which controlled the main exciter DC field is only rated at a small fraction of the shaft power and is hence a small unit.

1.4.2 Converter connected generators

An alternative to direct line connection of a synchronous generator is the use of a full-rated power converter or converters between the generator terminals and the network. These power converters de-couple the magnitude and frequency of the power supplied to the network from the output voltage and frequency of the generator. Hence, this approach takes variable amplitude and variable frequency from the generator and produces a fixed frequency (usually 400Hz) and regulates and controls the waveform shape of the 3-phase output voltage. Since the output frequency can be controlled this type of system can interface to a VF network including synchronizing to the network.

There are several possible alternatives based on various architectures as shown in Fig 1-8. In Fig 1-8a, the generator output is diode rectified to produce an unregulated DC link of variable magnitude which is then converter via grid-facing inverter to a regulated magnitude and fixed frequency 3-phase AC output. The arrangement in Fig 1-8b is

similar but uses a three-phase converter operating as an active rectifier to produce a regulated DC link as input the grid-facing converter. This back-to-back 3 phase converter option is inevitably a more complex and higher cost option than its diode rectifier equivalent but will tend to have higher performance and controls the current waveforms from in the generator which can have benefits in terms of core loss. The final option in Fig 1-8c employs a direct AC to AC conversion in a single stage power converter which is often realized with a matrix converter [20]. Configurations Fig 1-8b and Fig 1-8c allow bi-directional power flow and can hence be used as a means of providing electric starting of the engine or shaft power transfer [21].
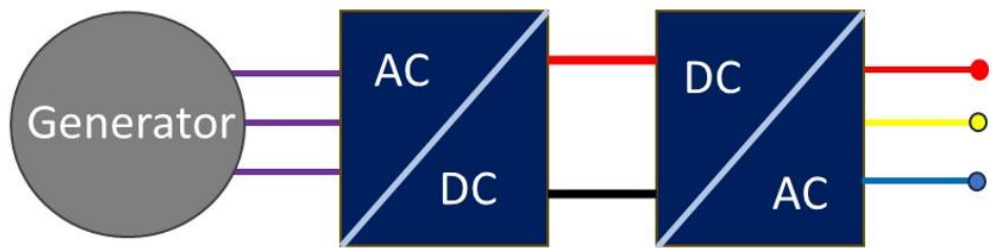
(a) Back-to-back arrangement of an active rectifier and a grid-facing inverter
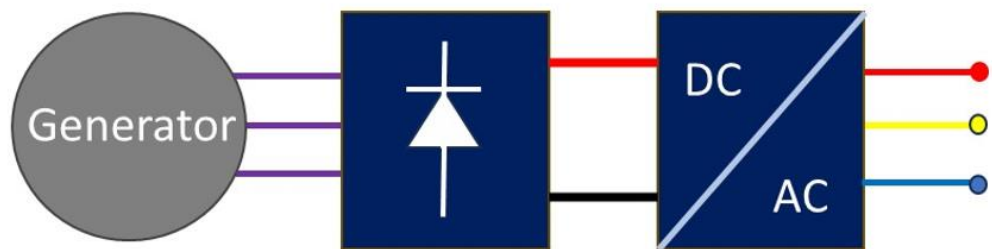
(b) Uncontrolled diode rectifier and a grid-facing inverter
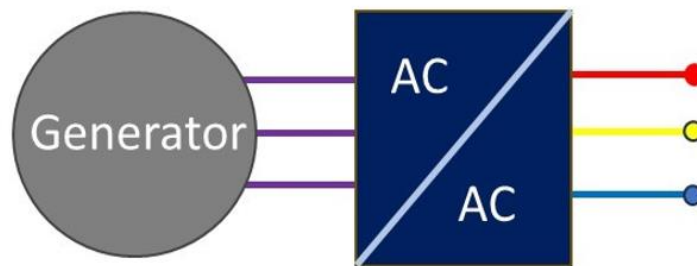
(c) Direct AC to AC converter

Fig 1-8 Converter connected generators system architecture

Since all of these arrangements decouple the magnitude of the voltage supplied to the network generator from the terminal voltage of the generator, it is possible to use permanent magnet (PM) machines in these types of systems. This offers the potential

to increase the power density of the machine compared to wound-field machines and eliminate the rotating diodes which impose onerous temperature constraints on the rotor if reliable operation is to be ensured.

There have been several published studies on permanent magnet machines with back-to-back power converters for aircraft power generation, often extended to give electric starting capability. As an example, a 100kW continuous (135kW peak) permanent magnet starter generator was reported in [22]. The proposed system architecture for this generator is shown in Fig 1-9. This allows a high-speed permanent generator with fixed excitation to be used which is generally the machine type which can achieve the highest power density to be used.

However, this back-to-back arrangement requires two fully rated, i.e. 135kW peak, power converters. Whereas such a system is very flexible and highly controllable, the need for two fully power rated converters with the associated mass, volume, cost and losses makes it challenging for such an arrangement to compete at system-level with a direct line connected wound-field machine despite the significant enhancements in machine performance that might be possible in moving from a wound-field machine to a permanent magnet machine. It is also worth noting that these converters would introduce a large number of additional failure modes and reliability issues to consider. Against this background, it is apparent why direct line connected wound-field remain the incumbent technology, although the case for converter fed permanent magnet machines does improve if electrical starting is required.
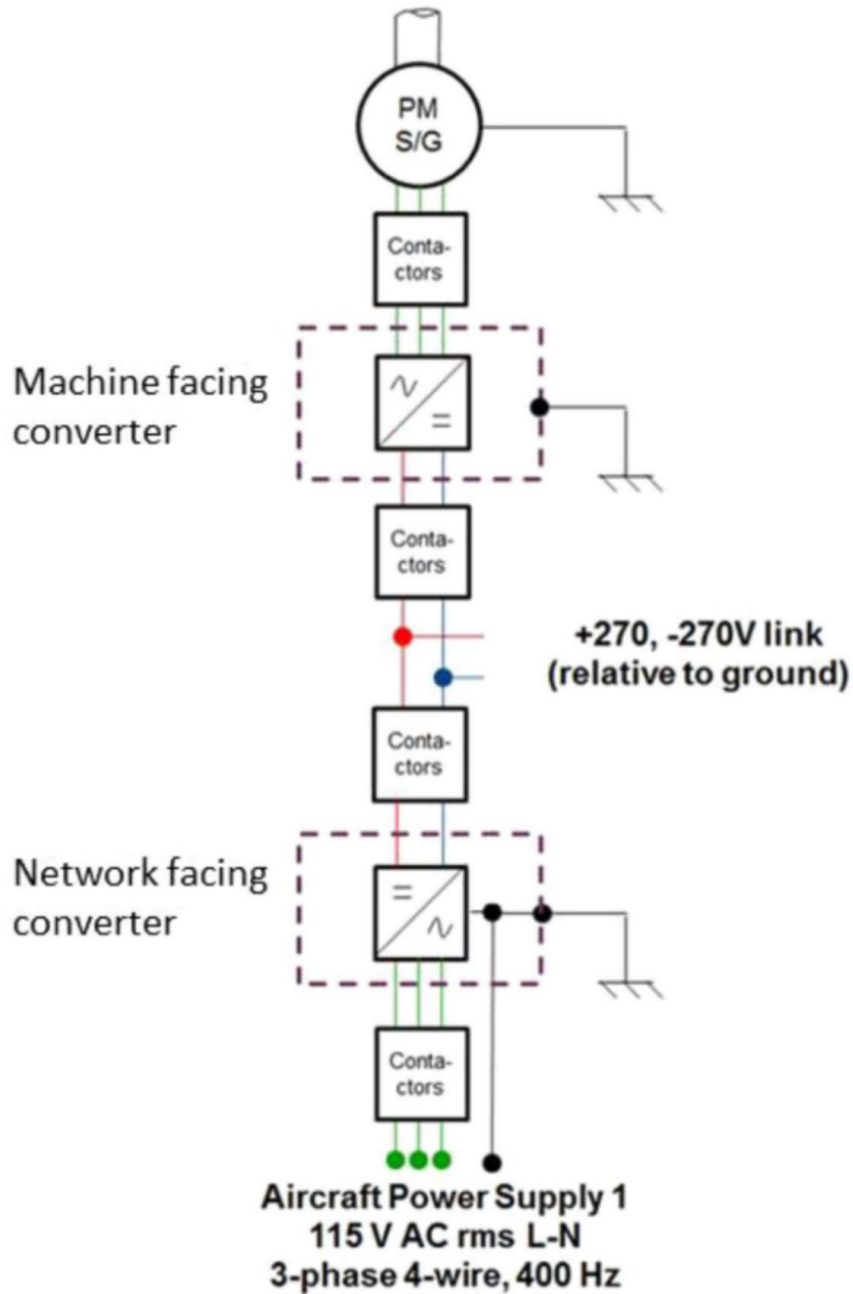
Fig 1-9 PM generator with back-to-back converter system architecture [22]

1.4.3 Auxiliary generators

As well as the main generators, there are also a pair of Auxiliary Power Units (APUs) rated at 270V each in the example network shown previously in Fig 1-4. These provide electric power for the various aircraft systems before the main engines are started. An APU consists of a small gas-turbine which directly drives an electrical generator. Fig 1-10 shows the APU from a Boeing 787 which has a total electrical output of 450kVA at sea level.
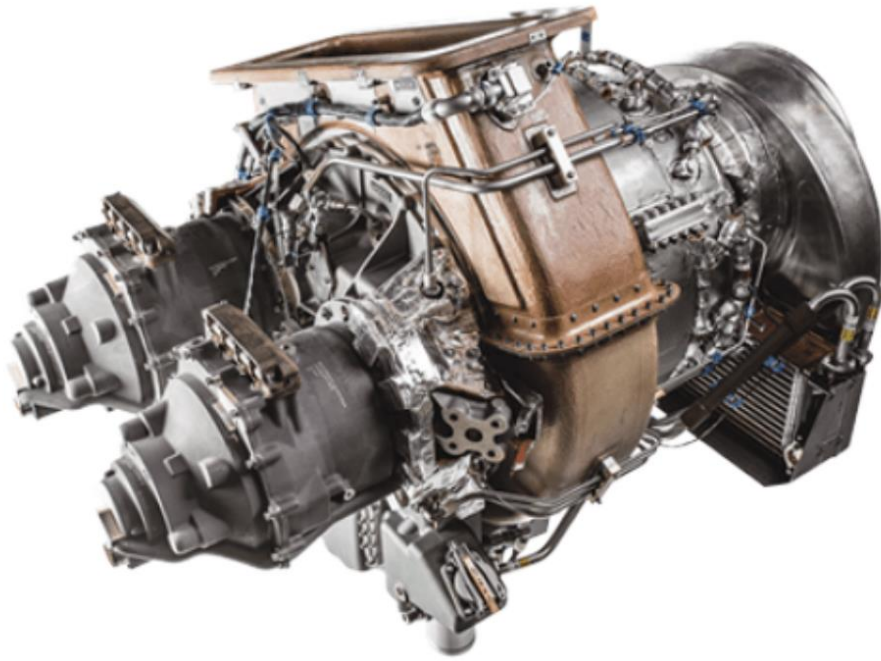
Fig 1-10 Pratt and Whitney all-electric APS5000 APU for Boeing 787 [23]

As with all aircraft, the network shown previously in 1-4 also includes a ram air turbine (RAT) which is a propeller driven generator which is deployed from a panel in the airframe in an emergency to provide power for essential systems. A typical commercial RAT is shown in Fig 1-11.

Fig 1-11 Typical Ram-Air turbine (RAT) for emergency [24]

For modern civil aircraft the dominant technology for power generation is variable-frequency ultimately, the maximum speed for a given pole number is set by the maximum electrical output frequency of 800Hz for the frequency range, which mainly depends on the operation speed of the generator and if the history of the frequency standard was traced, the other choices had been from 60 Hz to 800 Hz back to 1940s, the US Army Air Corps in 1943 chose 400 Hz as the standard for the fixed frequency and 360-800 Hz for the variable frequency [25].

On the other hand, for the voltage level, due to the breakdown voltage between two electrodes given the distance between them fixed, will decrease the along with the altitude consider the pressure is decreasing when the altitude rising based on Paschen's Law, therefore, which indirectly limit the voltage level that can be used for the aircraft electrical system. In addition to these two critical parameters, other key parameters also under strict review which consequently, the general standards were introduced and one of the most acceptable standards is the MIL-STD-704 standard [15] and due to the nature of generator application, this is one of the most important criteria during the designing stage and will be further explained in later sections.

A direct line connecting generator that can produce required output terminal voltage to the grid according to the standard will be a viable approach to increase the efficiency of the aircraft electrical system considering the system power density. Due to the nature of being directly connected, the generator should be able to output the voltage level that meets quality requirements for the grid and also consider self-regulation capability for different driven shaft speed and different load requirements. It's noticeable that the direct connect generator still needs working with the grid that has its own autotransformer rectifier unit (ATU) or the transformer rectifier unit (TRU) which means the distribution function of the electrical system is excluded for this project. For the output voltage quality, according to the MIL-STD-704 Standard, the most important parameter that can be used to evaluate the quality is the distortion factor which also will be further elaborated in the later sections.

1.5 Variable flux permanent magnet generators for direct line connection

As noted previously, permanent magnet machines tend to offer the highest performance of different machine types, particularly in power density and efficiency. However, the fixed excitation would not allow them to operate successfully as a direct line connected generator for several reasons:

- Since the back emf is proportional to speed for a fixed excitation, the open-circuit voltage would vary by a factor of 2.22 over the VF speed range.
- Due to the impedance of the generator, the output voltage will vary as the load current varies even at a fixed speed.
- A fault in the generator could result in a continuous fault current which could be several times greater than the rated current. Since there is no method to reduce the excitation, which is driving the short-circuit current, it will continue to flow some catastrophic failure of the winding occurs.

These three limitations could be overcome if a method could be found to vary the excitation contribution to the stator flux-linkage from the rotor permanent magnets by a factor of at least 2.22 although as will be shown in this thesis to have full control over the output voltage requires a flux variation with is greater than a factor of 2.2.

There are 4 operating points which define the operating envelope of the generator as shown in Fig 1-12. As shown, the maximum flux operating point corresponds to delivering rated current at the minimum speed (corresponding to 360Hz) and the minimum flux condition would be open-circuit at maximum speed (corresponding to 800Hz). In this thesis, the flux variation is often specified in terms of the flux turn-down ratio from the maximum flux condition. It is not straightforward to determine the turn-down ratio as this depends on the reactive volts drop when the machine is loaded. However, it should be clear from Fig 1-12 that it needs to be at least 2.22:1 just to accommodate open-circuit conditions.
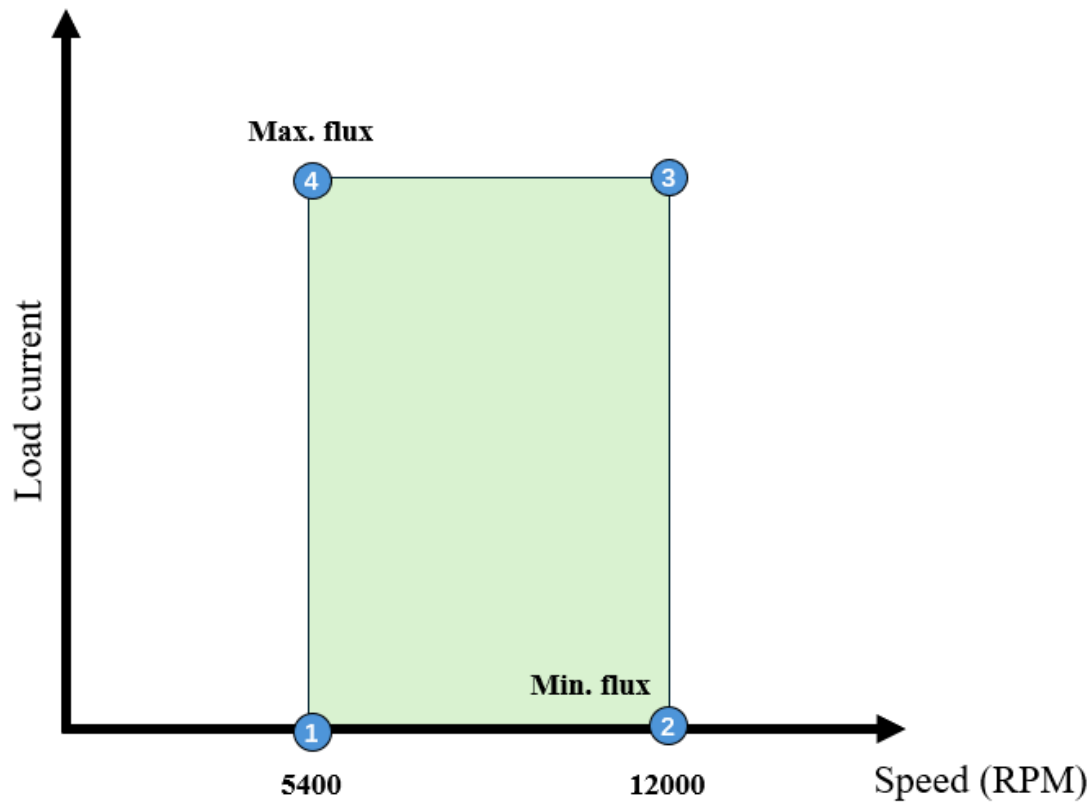
Fig 1-12 Schematic of operating envelope of a variable flux generator

The different methods for achieving variation in the permanent magnet flux are reviewed in detail in chapter 2.

1.6 Key novelty in the research

The research has resulted in the following key novel contributions to knowledge in electrical machines research

- The combination of an IPM type rotor with movable magnetic diverting endplates to achieve voltage regulation.
- An in-depth design study into features which allow sufficient variation in permanent magnet excitation to meet the requirements of a VFAC supply.
- Global optimisation of rotor pole-piece geometry to refine power quality of the generator output voltage, including allowing asymmetric geometries.

1.7 Publication produced during this research

H. Liu, G. W. Jewell and X. Chen, "Line-connected permanent magnet generator with adjustable excitation for variable-frequency AC aircraft power systems," *2023 IEEE International Electric Machines & Drives Conference (IEMDC)*, San Francisco, CA, USA, 2023, pp. 1-7, doi: 10.1109/IEMDC55163.2023.10239086.

Chapter 2 - A review of variable-flux permanent magnet machines

In this chapter, different flux variation methods were reviewed and compared given the direct-line connection features of aerospace starter generator, in particular, different proposals are summarised based on the specification outlined in section 1.3.3.

2.1 Introduction

The discussion of aircraft electrical systems and associated generator technologies in chapter 1 demonstrated the challenges for permanent magnet machines to displace wound-field generator in aircraft electrical power systems. Permanent magnet machines offer many potential advantages over wound-field machines in terms of power density, efficiency and the absence of diodes mounted on the rotor. However, at a system level the need for full rated power converters is a significant drawback of permanent magnet machines, particularly when the additional failure modes and reliability concerns are taken into account.

However, variable-flux permanent magnet machines in which some other form of control can be exercised over the magnet flux provides a potential route to obtain the performance of the benefits of permanent magnet machines, i.e. high-power density and a robust rotor, but with direct line connection of the generator to the wider power network. This chapter reviews various topologies and concepts for achieving variable flux excitation in permanent magnet machines and culminates in the selection of a preferred machine topology.

2.2 Types of variable flux permanent magnet machines

The concept of variable flux permanent machines has been investigated for numerous potential applications. These have included applications with continuous variation of magnet flux to exercise control over electrical performance without the need for a converter [26] but also applications with rapid and large reductions in magnet flux to

manage fault conditions [27] In all cases, the basic principle of operation is to use a mechanical or electrical means to vary the net permanent magnet excitation in the armature winding. There are many different approaches to varying the excitation flux in permanent magnet machines with features having been proposed for both the rotor and stator. An extensive review of variable flux permanent magnet machines in [28] classified the various approaches as shown in Fig 2-1. This demonstrates that both mechanical adjustment of different structures and features and various means of incorporating additional coil excitation into a permanent magnet machine have been proposed in previous studies. This chapter reviews these previous studies in the context of using variable-flux permanent magnet machines for a direct line connected aircraft generator.
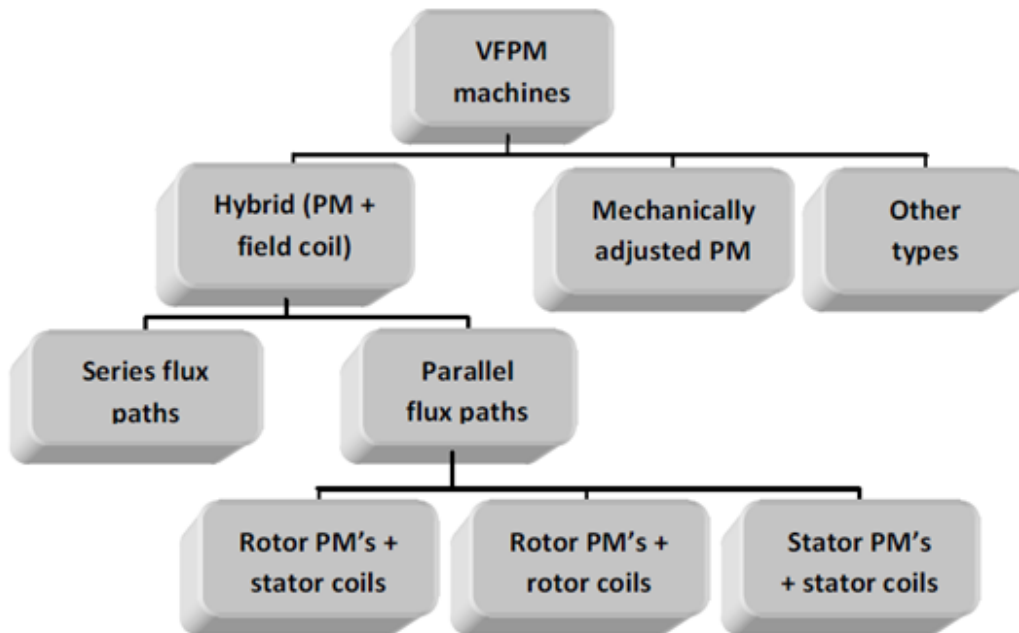
Fig 2-1 Categorization of VFPM [28]

2.2.1 Variable flux machine via demagnetization

The idea of memory motor was introduced in [29] This type of machine uses demagnetization of the permanent magnet to reduce the flux linkage. This type of machine combines Alnico permanent magnets and soft iron in a sandwich type structure in the rotor. Alnico permanent magnets are a class of permanent magnets which were the first commercially produced permanent magnets and although they have a high

remanence, they have low coercivities and hence can be easily magnetized and demagnetized [30]. By applying a current pulse, part of the rotor magnet can be demagnetized therefore reducing the net flux linkage shown in Fig 2-2. In this figure,
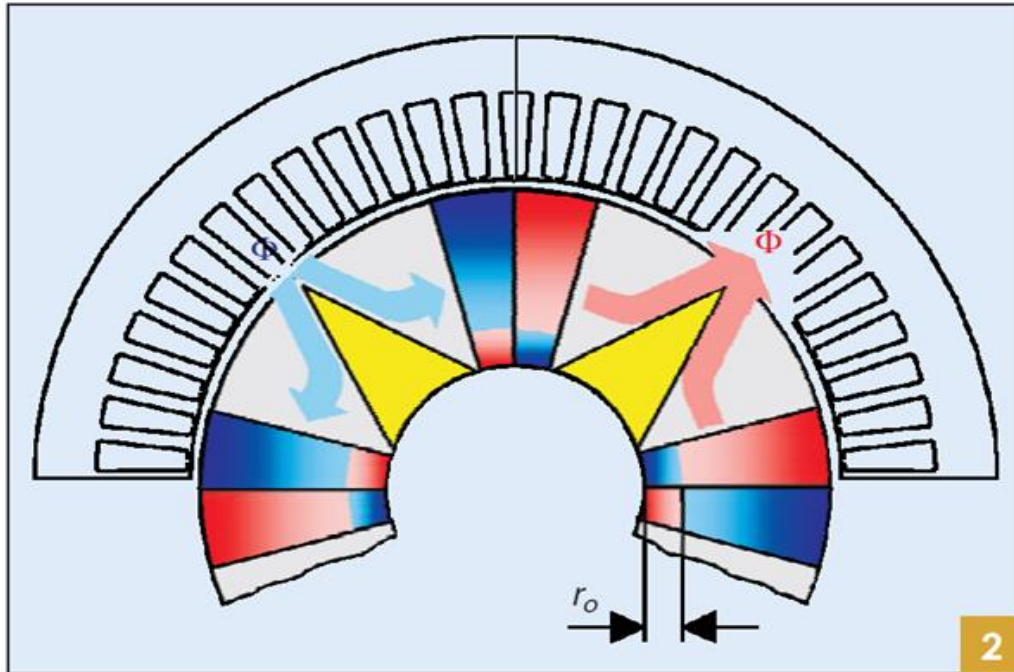
Fig 2-2 Typical Variable-flux memory motor structure [29]

whereas memory motors can be a useful solution for wide speed range motoring applications, they have several limitations in terms of power density and flux-enhancement. Moreover, partial demagnetization of the permanent magnets can introduce significant harmonics into the back-emf and hence generator terminal voltage which is problematic for a direct line-connected generator. It is also necessary to introduce some form of power converter to achieve the demagnetization which precludes this type of machine for a direct line connected generator unless a secondary demagnetization winding is added into the machine. A further variant proposed shown in Fig 2-3 using the combination of NdFeB and CeFeB material to replace the Alnico and ferrite magnet to improve performance [31].
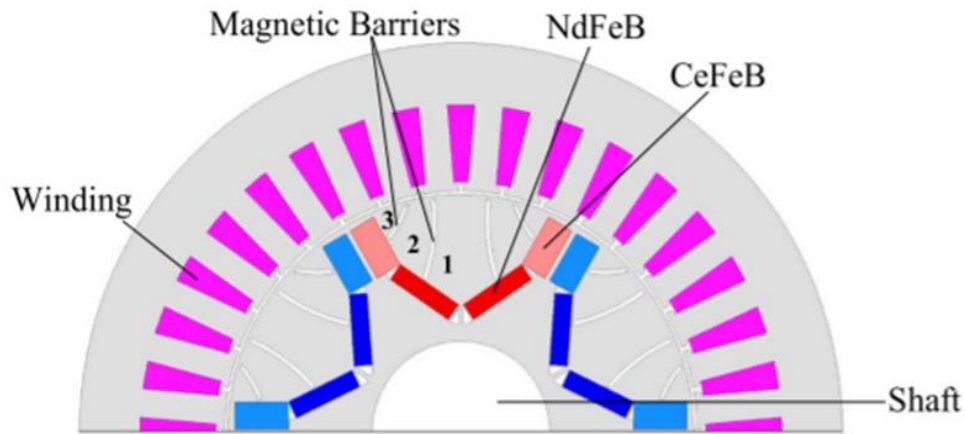
Fig 2-3 VFPM using CeFeB material [31]

2.2.2 Variable flux operation via controllable alternative axial flux paths

As an alternative to reducing the flux produced by the rotor permanent magnet themselves, several concepts for variable flux permanent magnet machines involve providing alternative and controllable low magnetic reluctance paths to divert flux away from the working airgap [32]-[35].This is usually achieved by incorporating magnetic design features in the rotor or in the stator. As an example, in [34] a concept is proposed which uses a pair of adjustable iron plates mounted at each end of the rotor of interior permanent magnet machine (IPM) as shown in Fig 2-4. These iron plates promote axial flux leakage into the end plate and then circumferentially within the plate to return to the opposite pole of the magnet thus reducing the magnet flux which cross the main airgap. The flux reduction in the airgap can be controlled by adjusting the axial separation between the iron plates and the end face of the IPM rotor. Retracting the plates away from the end-face of the rotor will increase the proportion of the magnet flux which passes through the main working airgap and further retraction will tend towards the airgap flux that would be seen in the same IPM with no iron plates. As the iron plates are brought closer to the end of the rotor, the main airgap flux will tend to reduce.
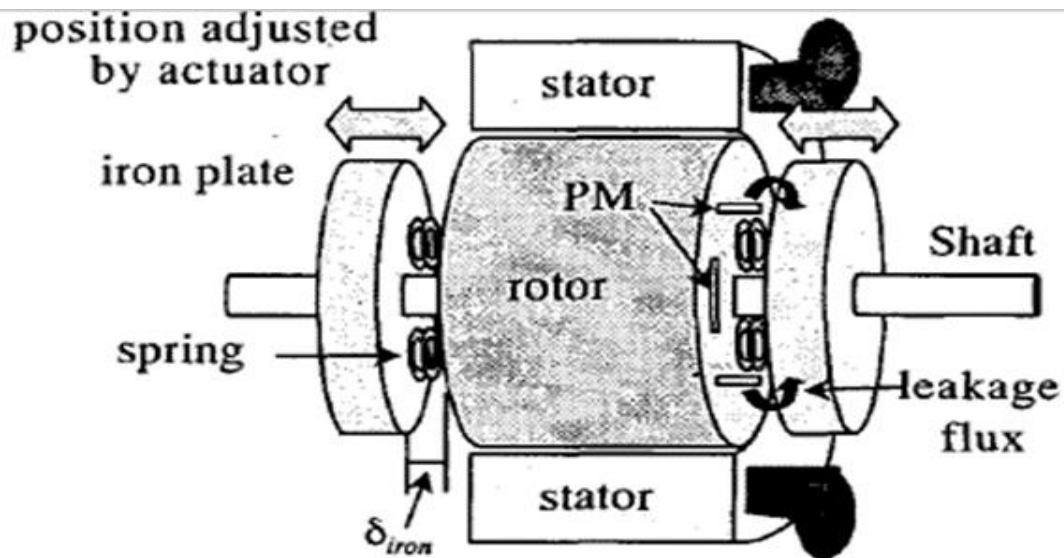
Fig 2-4 IPM with adjustable magnetic end plates [34]

2.2.3 Variable flux operation in flux-switching machines with stator flux guides

An important class of permanent magnet machines which has received significant attention in recent years are so-called flux-switching permanent magnet machine (FSPM) including design studies focused on aerospace [36]. A standard version of an FSPM without any variable flux features is shown in Fig 2-5 [37]. As can be seen, in this type of machine the stator incorporates both permanent magnets and the coils which make it attractive in terms of the simple, robust rotor.
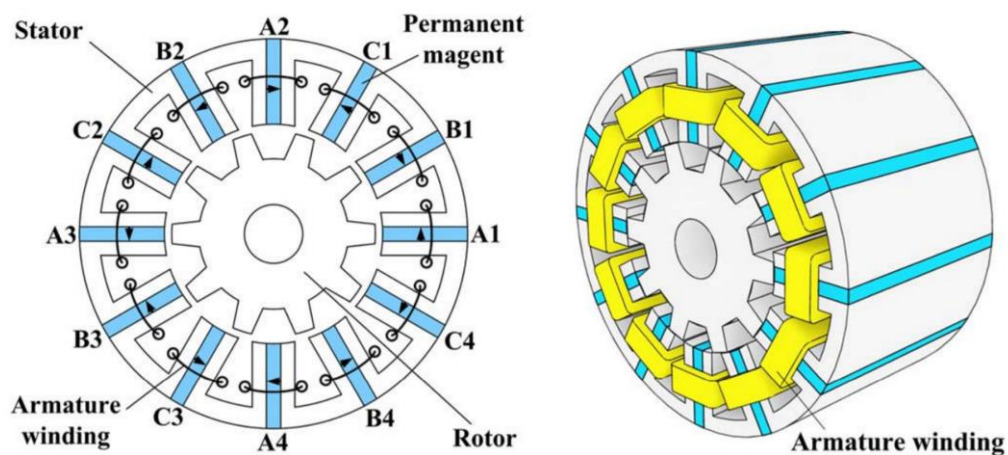
Fig 2-5 3-phase, 12 pole flux-switching permanent magnet [37]

A variation on the FSPM machine was proposed in [33] in which rotatable flux guides were added at the back of the stator. As shown the simple rectilinear representation of the stator in Fig 2-6. When the flux guides are aligned with the top of the stator C-cores, the magnet flux is largely unaffected by their presence and the machine operates with permanent magnet excitation which is close the value in a standard machine. However, when the series of flux guides outside the main stator core are rotated so that they span a magnet they short-circuit a large proportion of the permanent magnet flux hence reducing the net excitation in the working airgap. It was shown in [33] that this can realise useful levels of excitation turn-down but involves a very complex mechanical arrangement with an actuator that must overcome a very large cogging torque to rotate that flux-guides since individual alignment forces on each tooth are all in phase. It is also possible that rather than rotating the flux guides to move them radially outwards to increase the effective airgap and so reduce the amount of permanent magnet flux which is diverted through the flux guides.
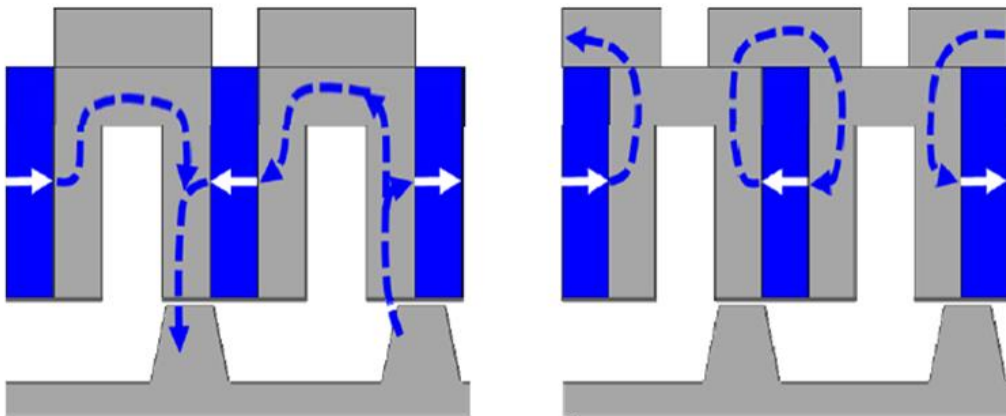
Fig 2-6 SFPM with movable external flux guides [33]

2.2.4 Variable flux operation via mechanical displacement of rotor components

The split-rotor concept shown in Fig 2-7 was proposed in [38] and [39]. In this concept, the rotor is split into two separate regions whose relative angular alignment can be adjusted by a mechanism to vary the net flux-linkage of the winding. The maximum flux linkage occurs when the two rotor sections are fully aligned while the minimum

flux occurs when the N pole of one section is aligned with S of the other section. The degree of maximum flux variation is set by the relative axial lengths of the two rotor sections. The performance of concept was simulated in detail in [38] within the context of an aerospace permanent magnet alternator (PMA) and was shown significantly reduce fault levels. This machine was connected to a voltage regulator and not line connected with the rotor adjustment acting to regulate the voltage. Moreover, no details were provided in either [38] or [39] on the mechanical mechanism used to control the alignment of the rotor sections. Although some kind of centrifugally activated mechanism could automatically rotate one rotor as a function of mechanical speed end hence could keep the back-emf constant over a defined speed range, it would not be controllable to deal with load regulation.
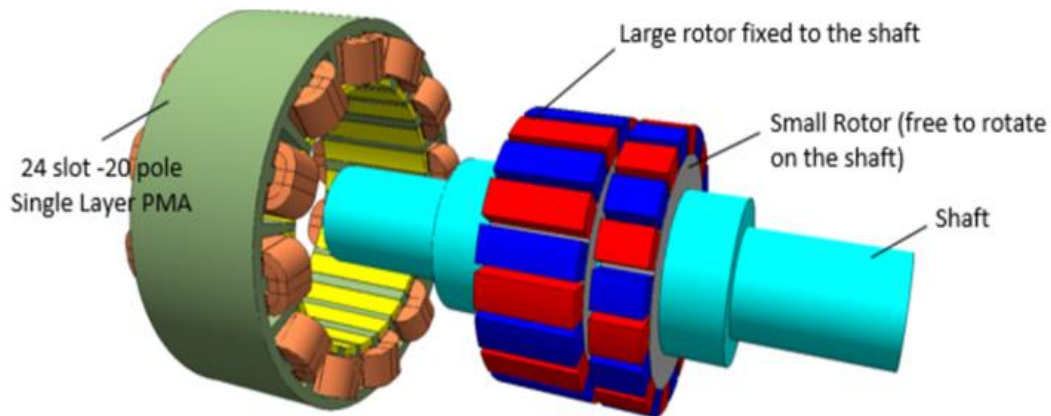
Fig 2-7 Split rotor machine [38]

Another concept that mechanically changes the machine structure as a function of speed involves using centrifugal force to change the location of a flux barrier [40] as shown in the schematic of Fig 2-8. The device works by the displacement of a magnetic insert with increasing speed to reduce the magnetic reluctance of the internal rotor leakage paths hence reducing the proportion of the flux which reaches the main This concept was developed for field-weakening rather than full regulation of the output voltage and operates open-loop with the flux variation with speed fixed at the design stage.

26
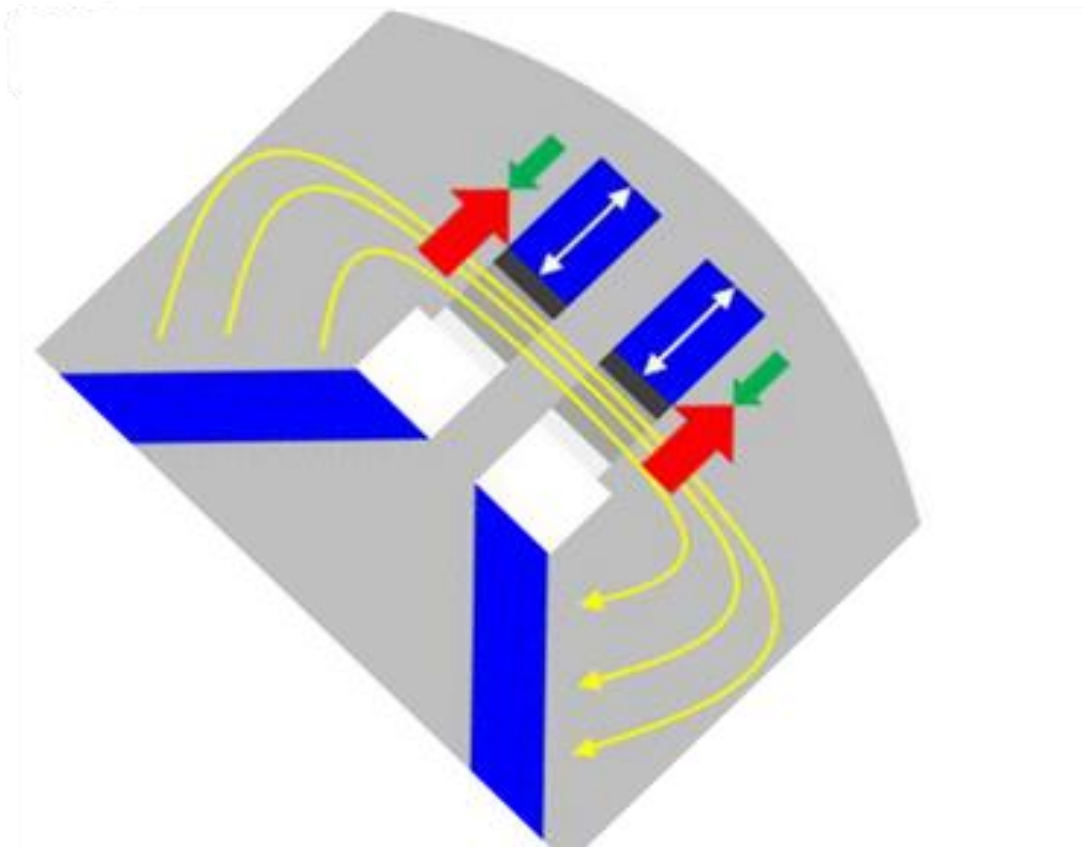
Fig 2-8 PMSM with centrifugal activated flux barrier [40]

A variation on this idea was proposed in [41] in which a flux barrier formed by a slot within the rotor structure is gradually filled with an iron insert which moves axially into the flux barrier slot as shown in Fig 2-9. In this case, the centrifugal force acting on the weight near the end of the shaft causes an axial movement of the iron insert which gradually increase the proportion of the rotor axial length in which the flux barrier is magnetically short-circuited by the iron insert. Even allowing for the fact that the drawing in Fig 2-9 is a schematic and not a detailed design, the range of movement that could be achieved with this mechanism is likely to be small.

These rotor features can provide some level of speed dependent variation in the either the net winding flux linkage (in the case of the split-rotor) or in the airgap flux density in the case of the two actuated iron inserts. However, all of these changes are open-loop and cannot be used to achieve closed-loop regulation of the output voltage since there is no means for an external controller to influence the changes in the rotor. Hence, precise closed loop regulation of the output voltage will need a concept in which control is exercised in the stationary frame. It is also worth noting that in all these cases, an

experimental prototype was not manufactured and tested, and the ideas remain theoretical.

(a) Cross-section of the rotor

(b) Longitudinal section
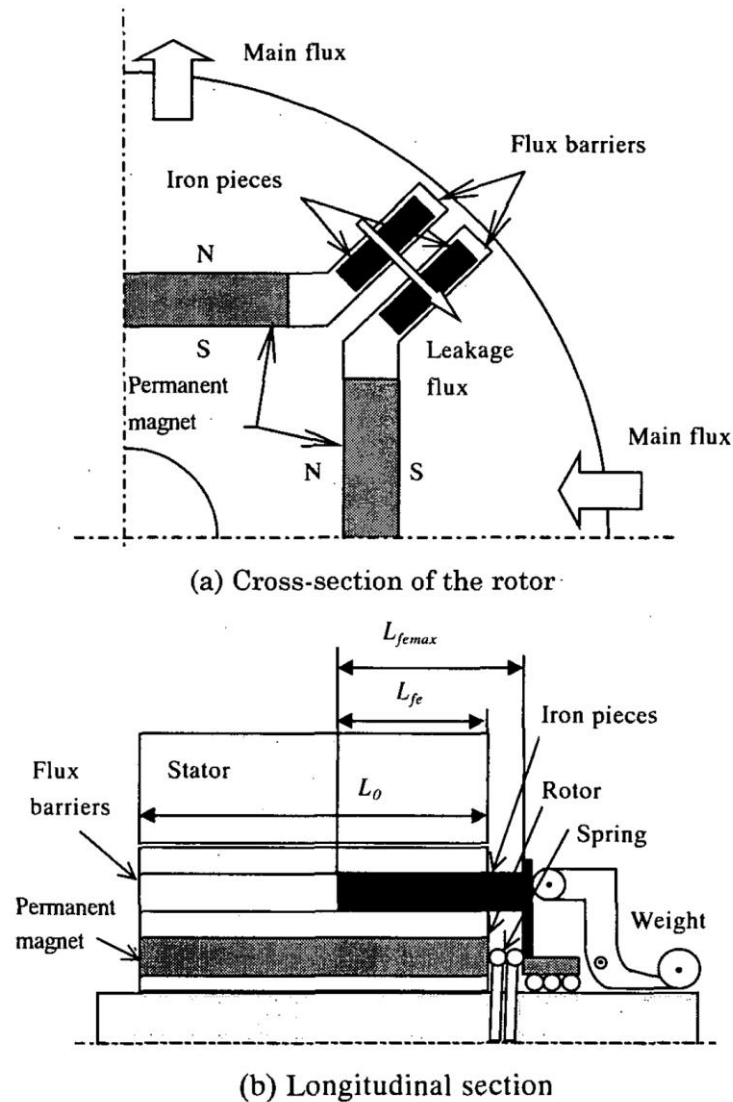
Fig 2-9 Concept for mechanical automatic actuation of an iron piece [41]

2.2.5 Variable flux operation via additional controllable excitation sources

Another set of concepts which have been proposed for variable excitation flux in permanent magnet machines involves adding an additional and controllable excitation source into the machine to produce a hybrid excitation machine (HEM) or doubly excited machines (DEM). These extra excitation sources can be either in stator [42] or in the rotor [43] as shown in Fig 2-10. Topologies with stator excitation coils will tend to offer the best option in terms of straightforward practical realisation.
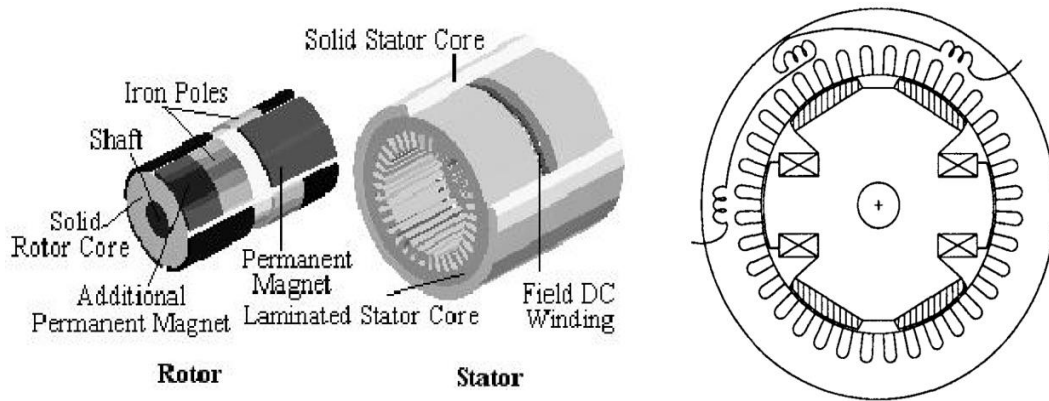
(a) Stator mounted DC excitation coil [42]   (b) Rotor mounted DC excitation coil [43]
Fig 2-10 Alternative topologies of hybrid-excited permanent magnet machines with supplementary DC excitation coils

The drawbacks of coil excitation are the extra space required in the stator or rotor to locate the excitation coils, the extra losses in these coils and the need to include different low reluctance paths for the coil flux which tend to promote permanent magnet leakage flux in the stator. Hence, incorporating coil excitation often involves a significant reduction in power density compared to a fixed excitation machine.

2.2.6 Variable flux machine via air gap adjustment

Adjustment of length of the working magnetic air gap provides a means of varying the level of excitation. In a radial-field machine, the length of the airgap can be adjusted by using a conical rotor and stator [44]. Axially moving the conical rotor in and out of the conical stator bore results in the change in the effective magnetic airgap as shown in the schematic of Fig 2-11. This type of arrangement results in a large axial reluctance attraction force which must be counteracted by a spring. A study in [45] reported on a permanent magnet synchronous machine for field-weakening in electric vehicles. A combination of analytical calculations and three-dimensional finite element analysis was used to optimise a small-scale 140W demonstrator which achieved a flux weakening ratio of 19.3% with a conical angle of 5.7° and an axial displacement of 3.15mm.
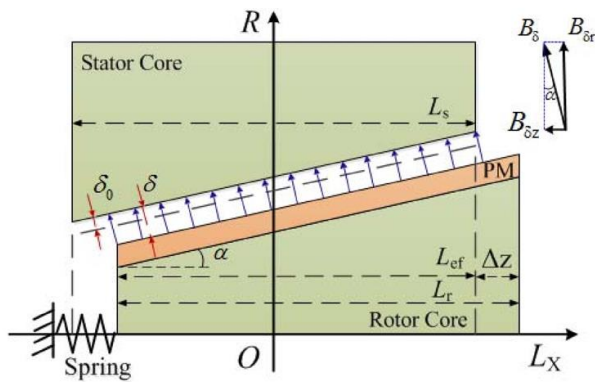
(a) Schematic showing principle of operation   (b) Demonstrator 140W machine

Fig 2-11 Schematic of a conical rotor and stator machine for airgap adjustment [45]

Axial-field machines are better suited to variable airgap operation since no changes to the rotor and stator geometry are required other than to include some mechanical adjustment mechanism to control the separation between the rotor(s) and stator(s). A schematic of an adjustable airgap axial-field machine with a single rotor and stator is shown in Fig 2-12 along with a simplified representation of the effect of the airgap on the torque speed curve [46].
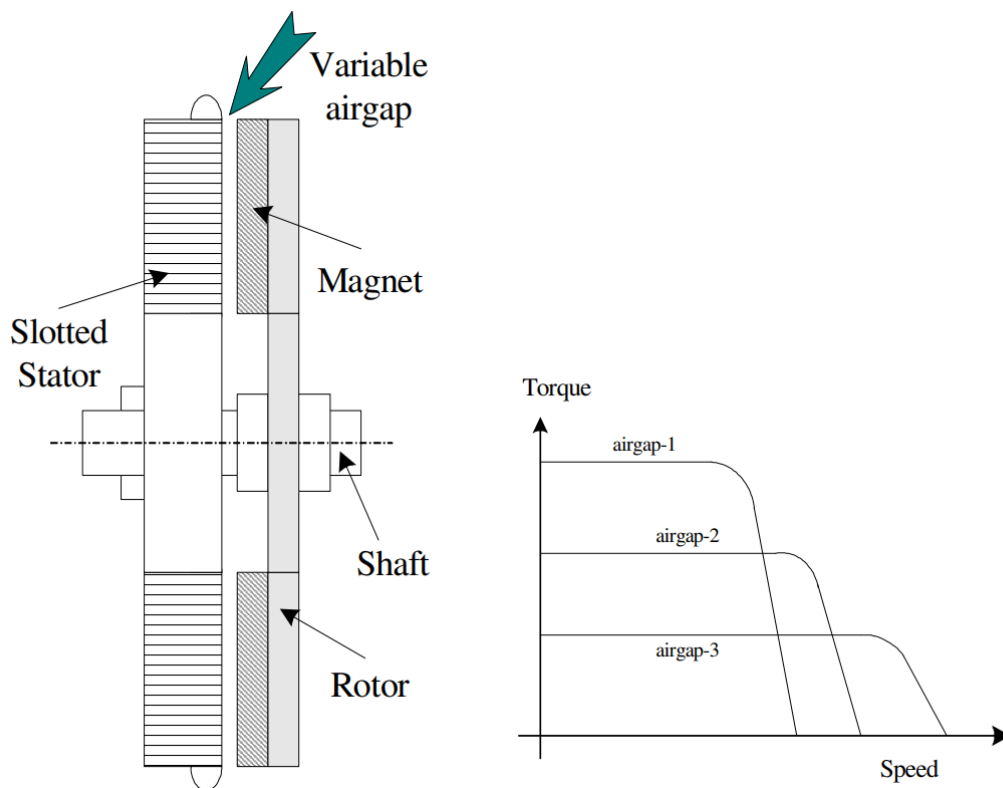
Fig 2-12 Schematic of the mechanical air gap adjustment axial field permanent magnet machine[47]

2.2.7 Variable flux by rotor withdrawal from the stator

Another method for reducing the flux in a radial-field machine is to axially withdraw the rotor from the stator core as shown in the design shown in Fig 2-13 which is taken from a patent application [48] .This approach allows the machine to be designed from an electromagnetic point of view with no modifications from a normal machine, but it does require a much longer machine casing depending on the degree of adjustment required. This mechanism could be retro-fitted to a standard machine design and hence does not require any innovation from an electromagnetic point of view. The example shown involves displacing the rotor which requires a complex linear bearing arrangement. In principle, the stator could be the moving component which could simplify the rotor bearing arrangement but would require a complex sliding mechanism for the entire stator core.
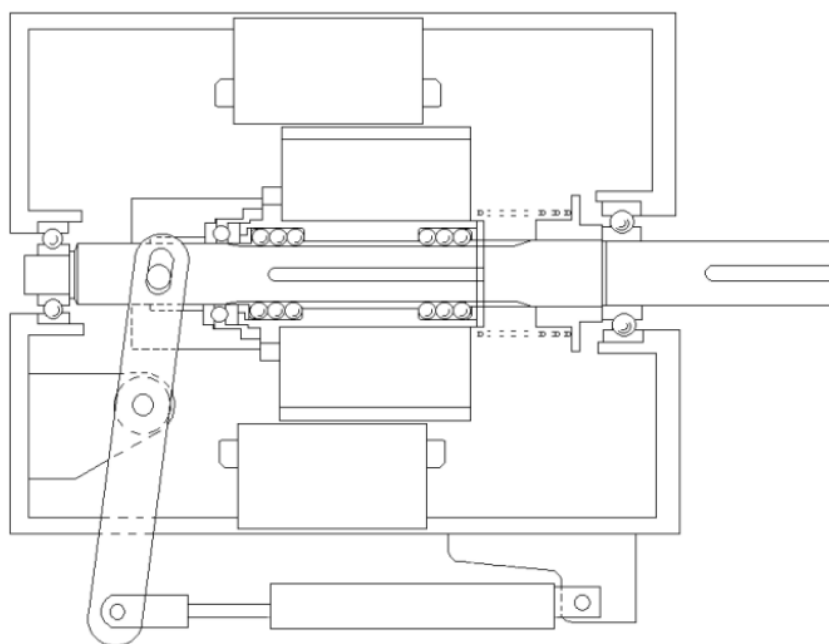
Fig 2-13 Patent drawing for a machine with a retracting rotor [48]

2.2.8 Changes in flux-linkage via number of series turns in circuit

Almost all practical permanent magnet machines have windings with fixed configurations and connections. Some large machines can be reconfigured, e.g. star to

delta, pole-changing, but generally the complexity of such arrangements mean that they are limited to niche applications. A concept proposed in [49] is based on using a centrifugal switch to change the winding between 2 turn and 4 turn rectangular bar windings. This provide a means of realising field-weakening with a single discrete change in the back-emf constant but cannot be used for the continuous regulation of output voltage.

2.3 Literature review summary

On Table 2-1, the different flux control methods are summarised and their feasibility is analysed in corresponding with the requirements outlined in the previous sections of the thesis.

Table 2-1 Comparison of flux control methods: Advantages, disadvantages and suitability for aerospace generator

Machine topology	Advantages	Disadvantages	Suitability for aerospace generator
PM Demagnetization	1. Rapid response 2. Fine flux tuning	Risk of irreversible demagnetization	Viable with real-time monitoring
Controllable alternative axial flux path	1. Minimal interference with the main flux path 2. Simple system design	1. Mechanical challenge 2. Thermal risk due to leakage flux	Attractive option if overall reliability is satisfied
FSPM with stator flux guides	1. Relatively compact structure 2. Wide operating range	Mechanical challenge	Need precision control of flux guides
Mechanical displacement of rotor component	Wide operating range	1.Mechanical challenge 2. Unsuitable for direct-line connection	Less favourable
Additional controllable excitation sources	1. Direct flux control 2. Simple mechanical structure	1. Increase system complexity 2. Thermal risk due to the DC winding	Favourable with simple additional excitation system
Air gap adjustment	1. High precision in flux variation 2. Wide adjustment range	Significant mechanical challenges	Suitable for axial field machine, Unsuitable for aerospace generator
Alignment control between rotor and stator	1. Minimal modifications to existing machine structures 2. Applicable to various machine types	Multiple mechanical challenge	Unfavourable due to low reliability
Variable winding turns number	1. Wide operation range 2. Direct flux control	1. Transient instability 2. Mechanical challenges from switching mechanisms	electromagnetic and mechanical reliability risk

This chapter has reviewed the numerous mechanical and electrical methods that have been proposed to vary the excitation flux in permanent magnet machines. Some general conclusions can be drawn from these previous studies:

- Although it is possible to vary the flux with rotor speed by incorporating design features, these approaches do not facilitate the closed loop control required to regulate output voltage with both speed and load current.
- The various mechanical adjustment techniques can involve counteracting very large magnetic attraction forces using a combination of springs and actuators.
- Some of the mechanisms, e.g. conical rotors, split rotors or moving flux barriers, can involve significant electromagnetic compromises in the design which will tend to reduce the power density of the machine in its full-power mode.
- Rotor retraction in section 2.2.7 and the magnetic end-plates of section 2.2.3 allow the machine to be designed almost as normal and hence can maintain most of the power density of a fixed excitation permanent magnet machine.

The magnetic end-plate approach in section 2.2.3 involves significant electromagnetic innovation and optimization whereas the rotor retraction approach is largely an issue of mechanical design of a mechanism for a standard machine design. Hence, the magnetic end-plate approach was adopted as the preferred method for research in this thesis because of the electromagnetic challenge that it offers.

Chapter 3 - Preliminary design of a variable-flux permanent magnet generator

This chapter will focus on defining the initial model along with the relevant evaluation including the mesh tuning and the geometry of end-plates. Starting from an existed machine prototype geometry as reference to gradually build the preliminary model.

3.1 Introduction

As noted at the end of chapter 2, consider the direct-line connection features and mechanical feasibility, movable iron end-plates was selected as the preferred option for flux variation, which as essential components of research for direct-line connected generator for aerospace application. This chapter describes the preliminary stages in the design of a machine which can be connected directly to a standard aerospace variable-frequency AC supply and meet the specification set out in Table 1-1 in chapter 1.

The main aim of this design study is to understand the performance compromise of adopting a direct line connected generator compared to an approach based on a high-performance permanent magnet generator which is connected to the AC network using an arrangement of converters shown previously in Fig 1-9 in chapter 1.

Hence, instead of starting with a power specification for the generator, a set of main dimensions were obtained from a published study on a high performance, converter connected starter generator [50] These dimensions were used as the baseline of the design study with the output power produced by the variable flux, direct line-connected generator is therefore an outcome from the design study and not an input.

3.2 Reference PM generator design

3.2.1 Performance specification and leading dimensions

The design study reported in this chapter starts from an existing machine specification which represents a power density at the upper end of published aerospace generator designs that have been built and tested. The machine selected is an oil-cooled, high-speed permanent magnet starter-generator with a continuous power rating of 100kW and a transient peak power rating of 135kW[50]. This would connect to the aircraft VF or fixed frequency AC supply grid via a back-to-back arrangement of converters although only the machine facing converter was built and tested in the study reported in [50].

The leading dimensions and main performance measures of this machine are shown in Table 3-1. This is a 3-phase concentrated winding machine with a standard 1.5 slots per pole configuration and surface mounted loaf-shaped magnets. The associated power converter is divided into two separate power channels and so the machine has two sets of windings, each of which is a star-connected three phase winding with two coils per phase. The machine has a reported power density of 4.4kW/kg including the structural components.

Table 3-1 Reference machine leading dimensions and performance [50]

Quantity	Value
Stator outer diameter	173.6 mm
Stator Bore diameter	119 mm
Rotor inner diameter	88 mm
Airgap Length	1 mm
Axial length	98 mm
Machine mass (incl. shaft and casing)	22.75kg
Pole-slot combination	8/12
Continuous generator output power rating	100kW
Peak generator output power rating	135kW
Output power from machine facing converter	95kW
Rated Speed	14,677 rpm
Maximum speed	26,584 rpm

As shown previously in Table 1-1 in chapter 1, a direct line-connected generator must

meet a comprehensive set of power quality standards, in this case from MIL-704-F. A generator and its associated pair of back-to-back converters only needs to meet at the power quality standard at the point of connection to the wider electrical supply. Since the power quality fed into the wider electrical supply is determined by the operation and filtering used in the grid-facing converter, the generator in [50] was designed without any compromises in power density in order to manage the generator compliance with power quality standards.

The back-emf predicted by both two-dimensional and three-dimensional finite element analysis for the reference machine in [50] are shown in Fig 3-1. As would be expected from a machine with simple concentrated coils in an 8 pole / 12 slot combination, the back-emf exhibits some elements of a trapezoid rather than a pure sinusoid. The authors of [50] did not provide a measure of the total harmonic distortion of this back emf since this machine feeds into a machine facing converter but it is unlikely to meet the MIL-704-F requirements for total harmonic distortion.
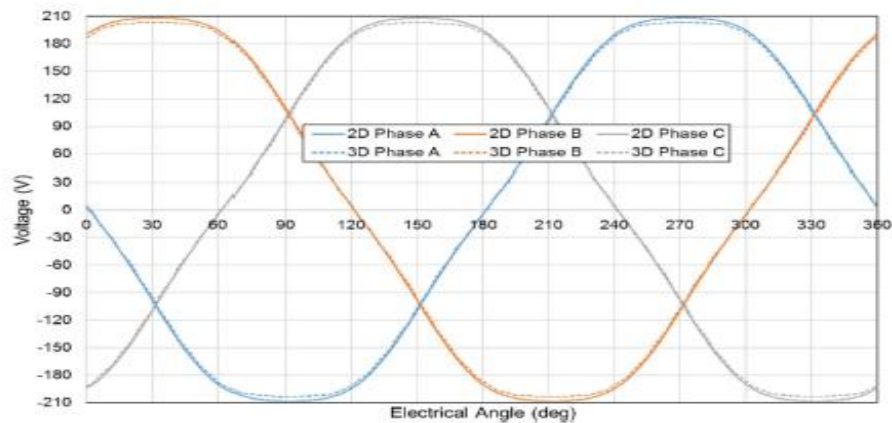
Fig 3-1 Phase Back-EMF waveform from 2D and 3D FE analysis [50]

A series of different variations on the reference machine detailed in [50] were modelled using two-dimensional finite element analysis. The first machine considered had a surface mounted permanent magnet (SPM) rotor based on the reference model in [50] even though this rotor topology is not suitable for the concept proposed in chapter 2 for diversion of the magnet flux through iron plates at either end of the rotor. Although the main dimensions of the reference machine were provided in[50], it was necessary to scale and estimate some of the remaining main dimensions, e.g. a 4mm thick magnet (in the direction of magnetisation) was selected. The second machine considered was

an IPM with spoked magnet arrangement using the same 12-slot stator dimensions. A further variant of the spoke-type IPM with a 7.5mm thick magnet was also modelled. This machine has the same rotor magnet volume as the SPM design. Cross-sections through these three machine designs are shown in Fig 3-2. Each coil in the machine has 1 series turns.

| (a) SPM rotor variant | (b) Spoke type IPM rotor variant with 4mm thick magnet | (c) Spoke type IPM rotor variant with 7.5mm thick magnet |
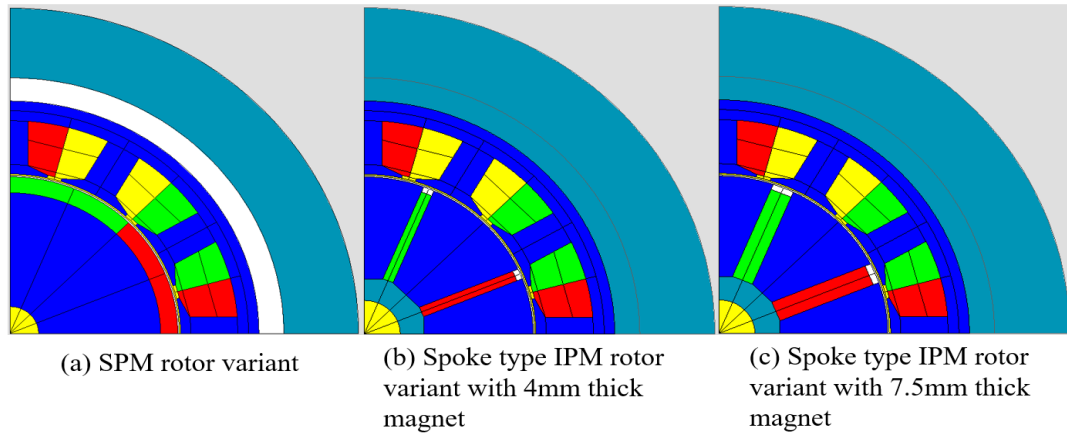
Fig 3-2 Cross-sections through SPM and IPM designs

The two-dimensional finite element predicted open-circuit back-emf waveforms (line to star-point) at the base speed of 5,400 rpm is shown in Fig 3-3 while the harmonic spectrum calculated using an FFT is shown in Fig 3-4. The peak magnitudes of the fundamental for the SPM, the 4mm thick magnet version of the IPM and the 7.5mm thick magnet version of the IPM are 25.3V, 24.4V and 27.8V respectively.
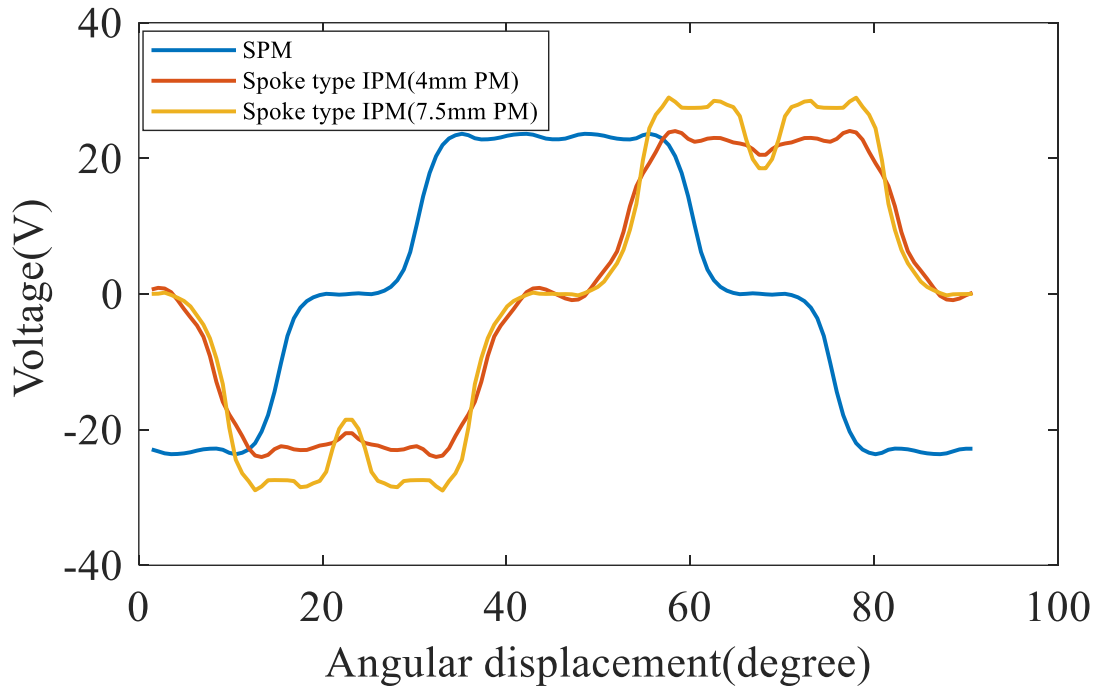
Fig 3-3 Finite element predicted open-circuit output voltage waveforms under open-circuit conditions at 5,400 rpm for SPM rotor and the two IPM spoke rotors in a12 slot stator.
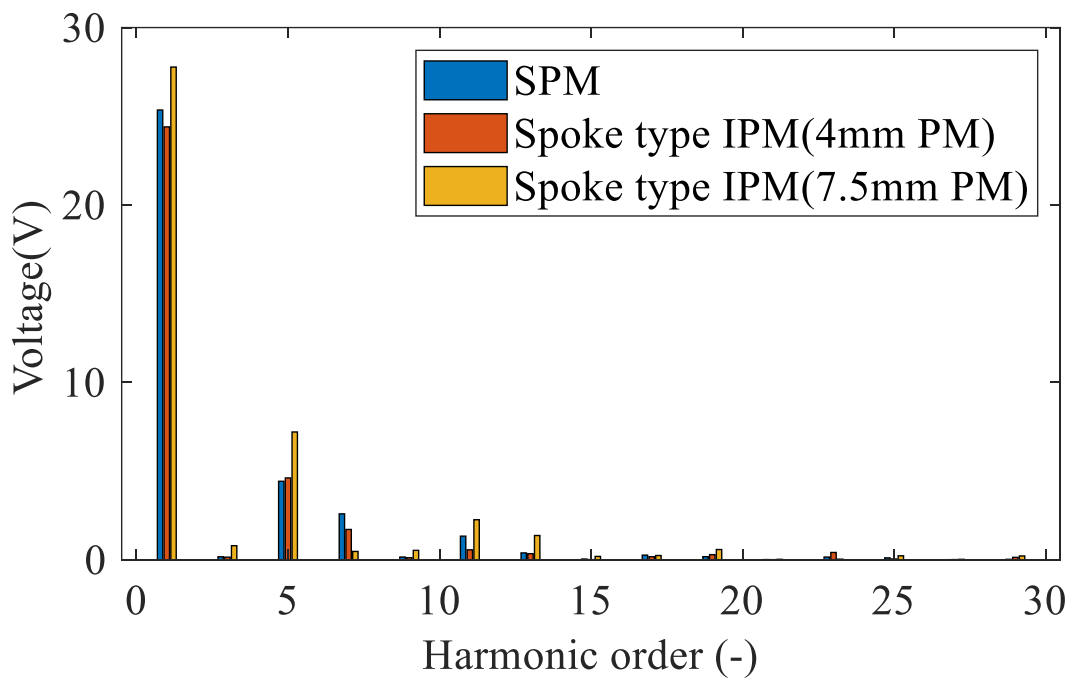
Fig 3-4 Output voltage waveform FFT spectrum under open-circuit conditions at 5,400 rpm for SPM rotor and the two IPM spoke rotors in a12 slot stator.

The finite element simulation results in Fig 3-3 and Fig 3-4 illustrate several key points:

1.Spoke type IPM permanent magnet rotors will tend produce a more distorted output

waveform quality compared to an equivalent the SPM rotor as shown quantitatively in the FFT spectrums of Fig 3-4.

2.The IPM rotor with the same magnet volume as the SPM variant produces an open-circuit back emf with a 10% higher fundamental component than the equivalent SPM although this is achieved at the expense of a 15% higher harmonic content. However, it is important to note than when a permanent magnet machine is operating as a generator into a passive load or a stiff supply, the power envelope is determined by a combination of the back-emf constant and the machine impedance (which is usually dominated by the reactance in high power machines).

3.2.2 Investigation into the influence of the rotor geometry

Ultimately the harmonic content of the terminal voltage of the generator depends on a combination of the airgap flux density harmonics produced by the rotor, the influence of stator slots and the winding distribution and winding factors of the stator winding. However, it is useful to isolate the contribution of the rotor geometry to the terminal voltage THD in order to understand the extra challenges posed by the use of an IPM machine to achieved variable flux operation. The simplified finite element models shown in Fig 3-2 were used. The spoke-type IPM machine in the version with the thinner 4mm magnet poles and 7.5mm thicker magnet poles along with original SPM with 6mm thick magnet. In these models, the stator region was removed, and an idealised normal flux boundary condition (Neumann boundary) was applied in the middle of airgap from models in Fig 3-2. This simplified model shown in Fig 3-5 eliminates the effect of slotting and allows the spatial harmonics generated by different rotor types to be compared. Fig 3-6 shows the corresponding resulting flux distribution throughout the finite models while Fig 3-7 shows the flux density profiles in the middle of the airgap. The harmonic content of these waveforms calculated with an FFT are shown in Fig 3-8. As shown in Fig 3-8, and as would expected from Fig 3-7, the SPM rotor generates higher magnitudes of spatial harmonics compared with both spoke type IPM rotors.
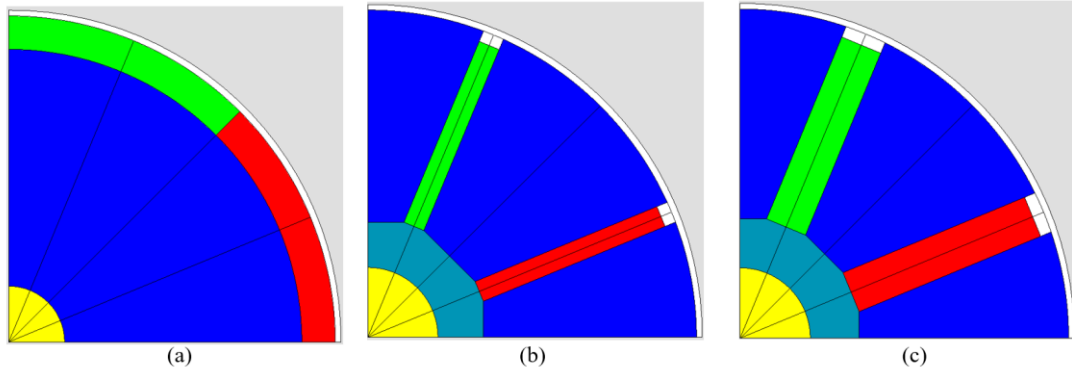
Fig 3-5 Different rotor topologies with simplified representation of airgap with Neumann boundary condition(a) SPM (b) Spoke with 4mm thick PM (c) Spoke with 7.5mm thick PM
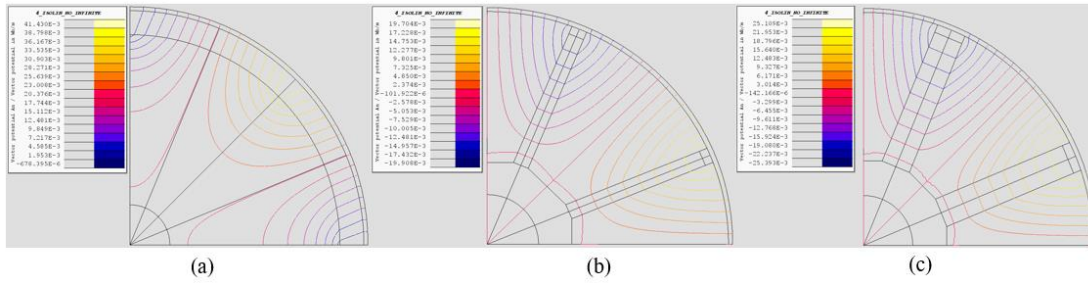
Fig 3-6 Two-dimensional finite element predicted field distributions for different rotor topologies
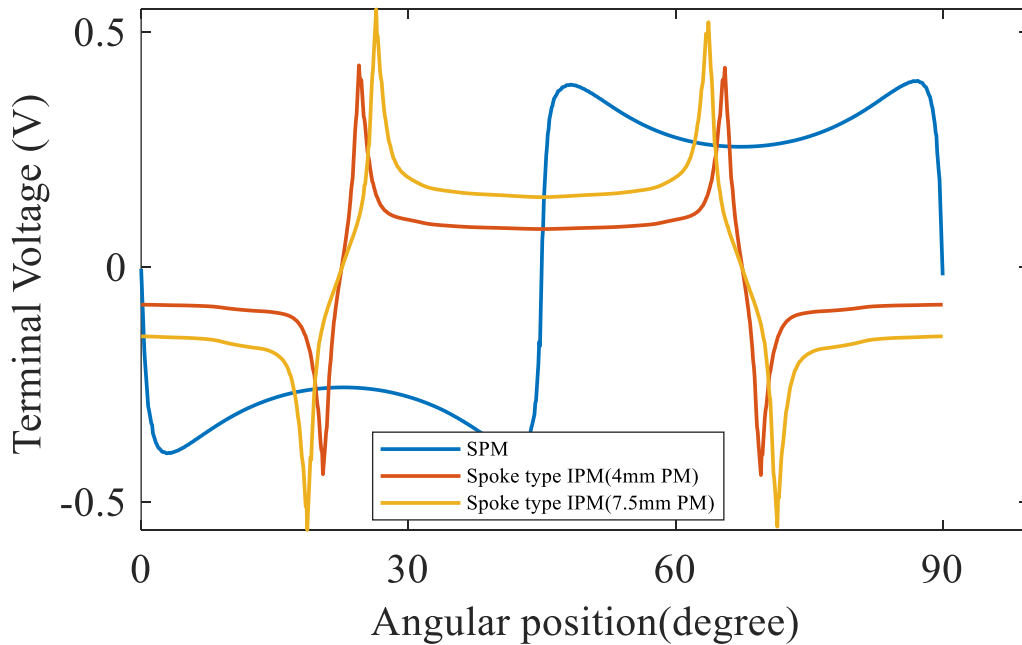
Fig 3-7 Flux linkage profiles across 90 a degree (mech) arc at the middle of the airgap displacement
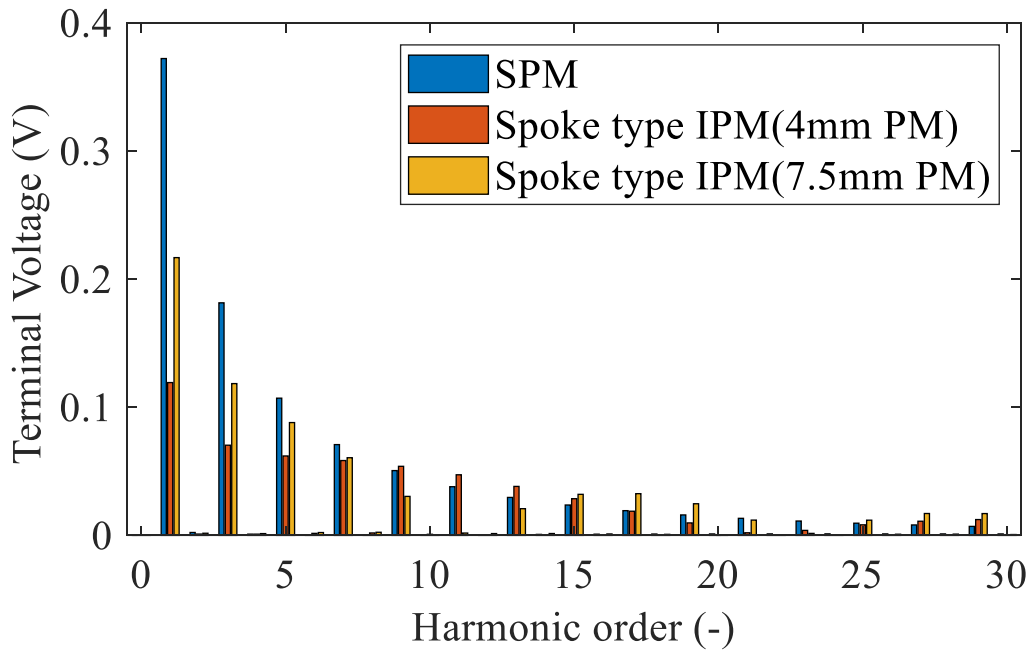
Fig 3-8 FFT spectrum of flux density profiles over a 90-degree (mech) arc

3.2.3 Design features of initial design

To produce a machine design capable of meeting the performance specification for a direct line connected machine it is necessary to make some changes to some features of the converter connected permanent magnet machine in [50]. However, in order to provide a meaningful comparison, the main dimensions were kept fixed, but some important changes were made:

1. Slot / pole number combination – The 12slot/8pole combination in the reference machine of [50] is useful to minimise the end-winding length and did not need to take power quality into account. However, the fundamental winding factor of this type of winding is only 0.866. As shown in previous finite element simulations of the back-emf waveforms, the resulting output voltage quality of the reference machine in [50] cannot meet the required power quality specification which is an essential feature for the direct line-connect machines. Hence, persisting with a 12 slot / 8 pole combination is not a good strategy for a line connected machine. An integer slot winding with 48 slots and 8 pole was selected for the direct line-connected machine. Not only does this have a higher winding factor of 0.966, but according to[51], the integer slot winding will exhibit lower voltage distortion due to the PM leakage flux. It also provides further

scope for refining the winding arrangement with features such as double-layered windings and short-pitching of coils. Considering the overall structure of direct-line connection, although the fraction-slot structure such as 12slot/10pole can offers better fault tolerance capabilities and lower cogging torque, without an inverter the low-order harmonic contents generated by such configurations may cause greater interference to the overall systems.

2. IPM rotor dimensions – The adoption of a spoke-type IPM machine for the variable-flux features means that several IPM design decisions must be made. The thickness of the magnet poles in the direction of magnetisation was set to 4mm and the width of the magnets in the radial direction was set to 35mm. This results in a total rotor magnet volume of 13,720mm^3 compared to 25,676mm^3 for the reference SPM machine design in[50]. The bridge thickness of the rotor core in the vicinity of the airgap was set at 2mm.

3. Stator core dimensions - The stator yoke thickness was set to 1/3 of thickness of the stator annulus and the stator tooth body width was set as 3mm, which is same as slot opening for this 48 slots machine. The tooth tip angle was set to 30° for large slot area. The preliminary 48 slot/8-pole design is summarised in Table 3-2.

Table 3-2 Preliminary design geometry

Parameter	Value
Stator outer diameter	173.6 mm
Stator Bore diameter	119 mm
Rotor inner diameter	88 mm
Axial length	98 mm
Slot/pole combination	48/8
Hub distance	14.3 mm
PM thickness (in direction of magnetisation)	4 mm
PM width (in radial direction)	35 mm
Slot opening	3 mm
Stator slot width	5 mm

3.2.4 Two-dimensional finite element modelling of the initial design

The finite element model of the initial design is shown in Fig 3-9. The symmetry of the winding and the 8-pole rotor was exploited to reduce the problem domain to a 45° segment. The two-dimensional model of Fig 3-9 was coupled to an electric circuit to simulate the baseline performance in terms of the output voltage of generator waveform when directly connect to a stiff power grid.
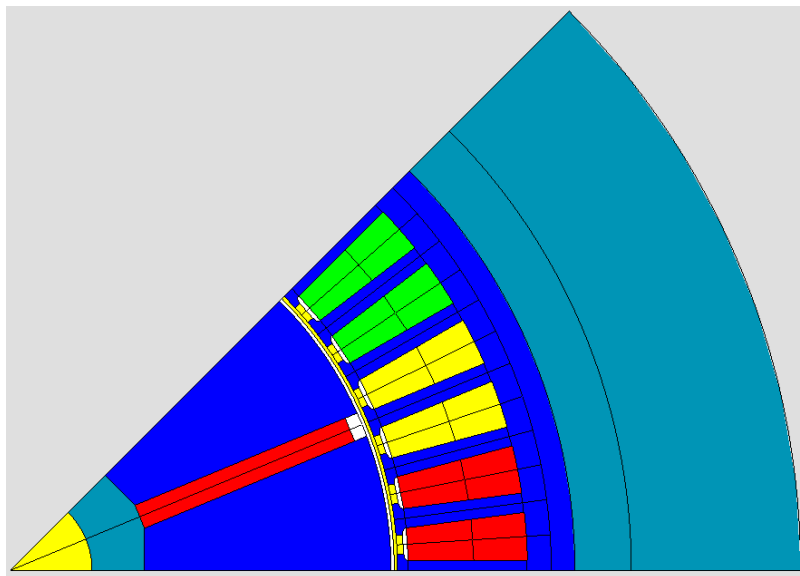
Fig 3-9 Preliminary FE model of 48/8 machine with an IPM rotor

However, the two-dimensional model cannot represent the variable-flux features of the proposed concept or other end-effects in the machine. These factors required three-dimensional finite element analysis. The two-dimensional simulation platform is Altair Flux2D, a FE simulation package from Altair. The following settings were adopted in the simulations:

1. **Winding -** The winding configuration in the model is a single layer winding with a nominal single turn per coil. This allows various aspects of performance to be scaled by the appropriate turns-ratio.

2. **Rotational speed** – The simulations were performed at the lower end of the 360Hz-800Hz VF frequency range. For an 8-pole rotor, the minimum speed 5,400 RPM. It is worth noting that is much lower than the base-speed of 14,647 rpm for the machine

in[50]. This demonstrates that direct line connection imposes a speed range on machine which is not necessarily the case for machine such as the reference machine in [50] which connect to the grid via a power electronic converter.

3. Stator core material - The stator core material was set to Carpenter Hiperco-50 which is a similar grade of high saturation Cobalt iron to that used in the reference machine from[50].

4. Permanent magnet material – The rotor permanent magnets were Sm_2Co_{17}, specifically Recoma-35E grade which is high performance magnet materials with a room temperature remanence of 1.2 T.

Open-circuit magneto-static simulations were performed by setting the three-phase load resistors connected to the generator within the electrical circuit which is coupled to the finite element model within FLUX2D to values of 10kΩ. These simulations were performed over a single electrical cycle with 130 increments including an additional static initial simulation step. The full load simulations were performed by varying the value of the 3-phase load resistors which are connected across the generator. The flow of significant current in the machine winding and the start-up transient which in inherent in time-stepped simulations means that an additional two electrical cycle of simulation were required to reach near steady-state conditions.

Fig 3-10 shows the two-dimensional finite element predicted open-circuit terminal voltage in the three phases at 5,400rpm while Fig 3-11 shows the terminal voltage when the machine is loaded with a star connected resistive load of 0.25Ω per phase. This load draws a current of 279.2A in this single-turn variant which corresponds to a load power of 19,488W. As will be apparent, even at this modest load, there is a significant drop in terminal voltage due to the impedance of the machine. This issue will be discussed in detail in chapter 4, but even initial set of simulations demonstrated that variable capability is required to accommodate load regulation requirements.
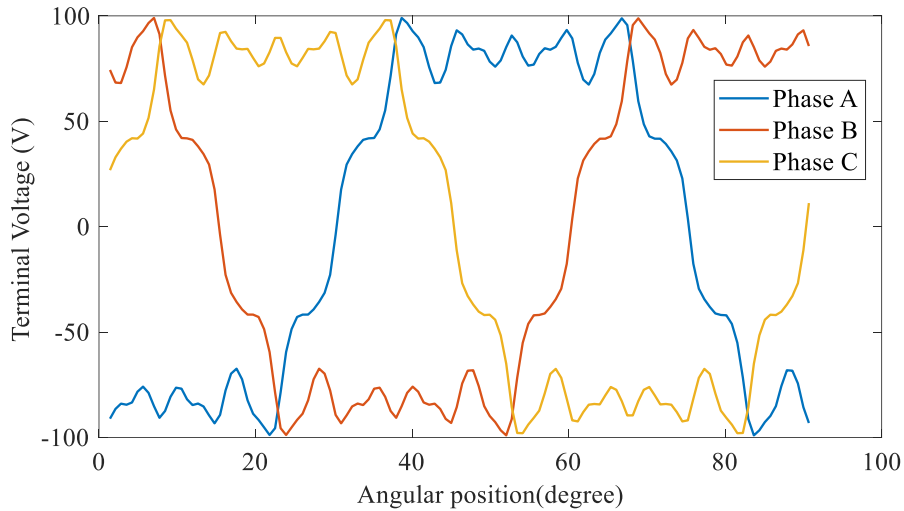
Fig 3-10 Two-dimensional finite element predicted output voltage waveform under open-circuit condition at 5400 RPM
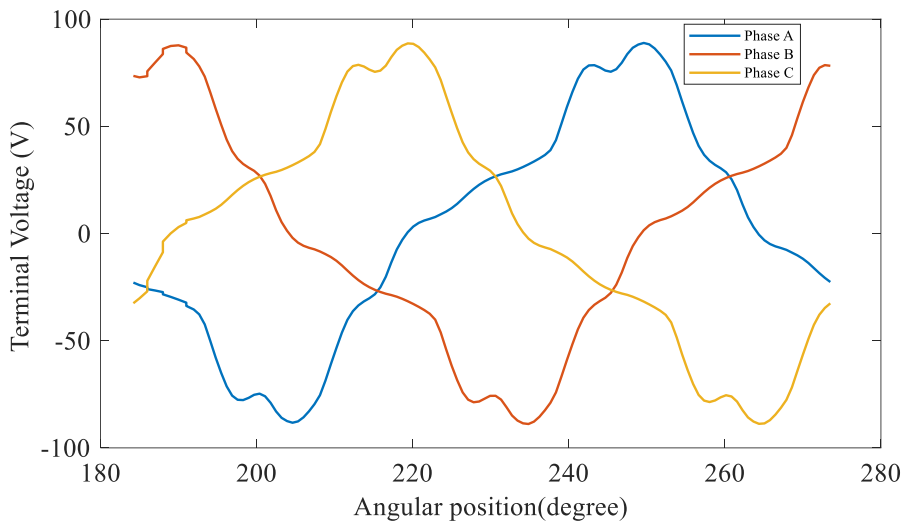
Fig 3-11 Two-dimensional finite element predicted output voltage waveform at 5400 RPM with the generator loaded with a star-connected, three phase load of 0.25Ω per phase with 2 electrical cycles skipped to avoid transient phenomena.

The corresponding harmonic spectra for these two operating conditions are shown in Fig 3-12 and Fig 3-13. It is important to note that these simulations are based on a single turn winding irrespective of the number of slots and conductor cross-sections and hence the magnitudes of the voltages cannot be directly compared to the 12-slot version. Both spectrums demonstrate the significant harmonic content.

A summary of the performance of this first preliminary design is shown in Table 3-3 which demonstrates that as expected the distortion factor is far too high to meet the 5% specification set out in MIL-704-F.

Table 3-3 Key features of two-dimensional finite element predicted output voltage waveforms for a 48 slot / 8 pole machine shown previously in Fig 3-12 and Fig 3-13

	Open-circuit	Full Load
Distortion factor	27%	26.6%
Fundamental Component	101V	69.3V
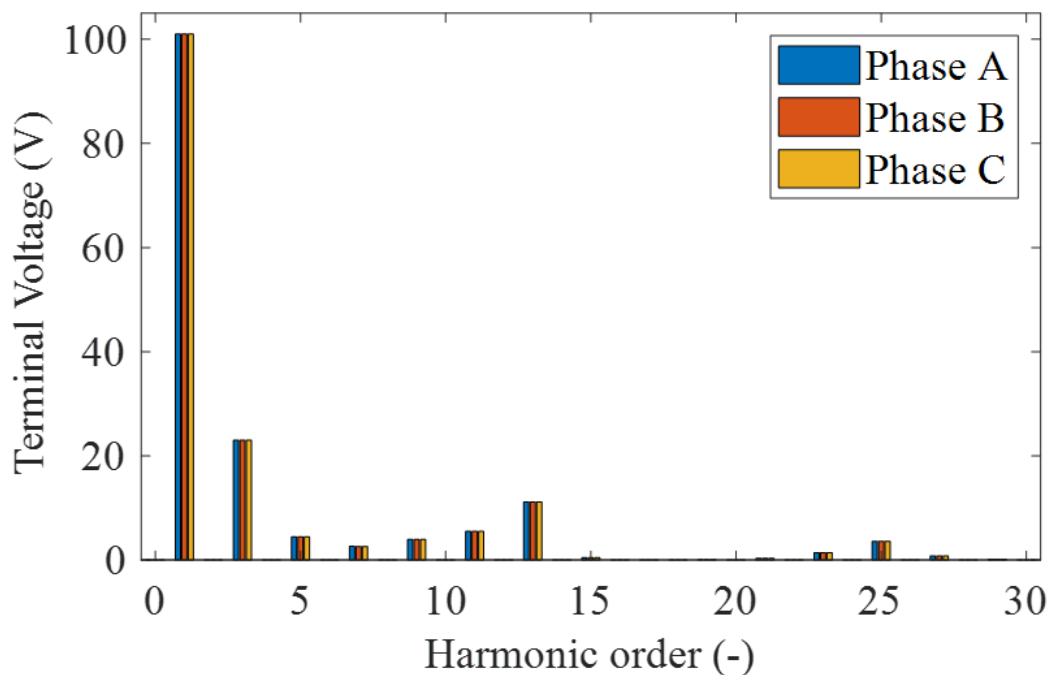
Fig 3-12 harmonic spectrum of figure 3-10 waveform
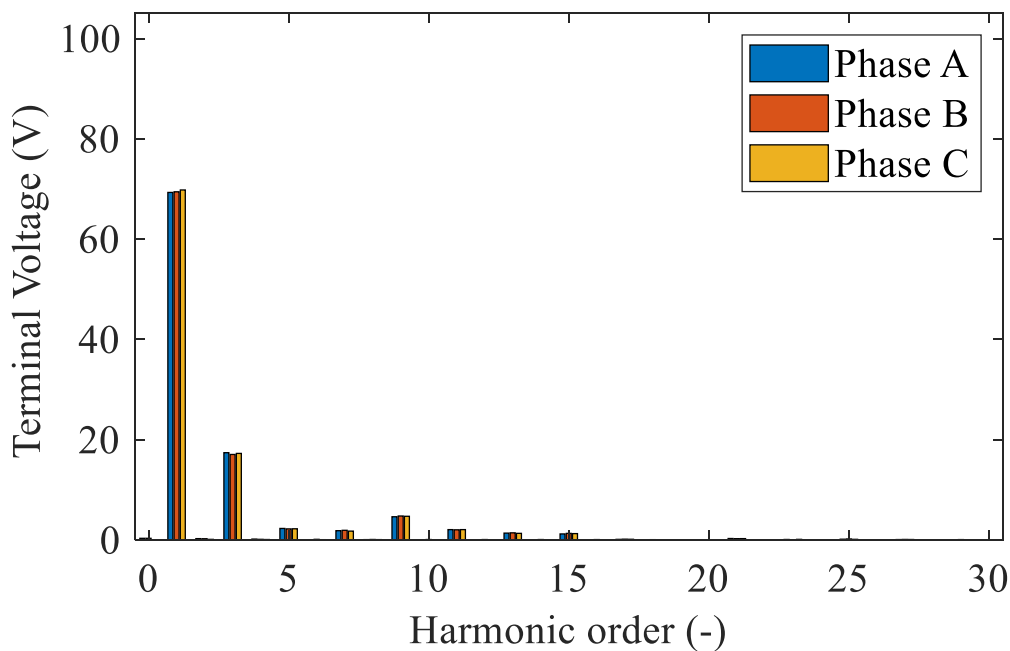
Fig 3-13 harmonic spectrum of figure 3-11 waveform

46

3.3 Three-dimensional finite element modelling of the initial design

3.3.1 Introduction

As noted previously, the two-dimensional finite element model provides a useful starting point for predicting the performance of the initial generator design, but it cannot model the end-plates and hence the variable-flux behaviour of the machine. The two-dimensional model also does not account for end-effects and therefore tends to overestimate the performance of any machine, particularly when the ratio of the diameter to the length is large. To assess the variable-flux behaviour of the initial design, a three-dimensional magnetostatic finite element model was constructed in FLUX3D.

3.3.2 Finite element model geometry and meshing

Although three-dimensional models are able to represent the machine more comprehensively with fewer geometric approximations, the model built for the initial design contains several simplifications to ease the construction of the model and reduce the computational time

1. **End-winding representation** - The winding was represented as a series of conductors which extend in a straight line for 10mm beyond of the core with the same cross-section as the regions within the core This simplified representation, which is shown in Fig 3-9, does not capture the regions which are remote from the machine in which the conductors pass circumferentially.

2. **Isotropic stator and rotor core** – The stator and rotor cores of almost all permanent magnet brushless machines are made from a stack of thin laminations. In most three-dimensional finite element models, the cores are modelled with isotropic magnetic properties which does not account for this laminated structure.

3. **Symmetry** – The axial and circumferential geometric and magnetic symmetry were

exploited to reduce the model to half the length and 1/8 of the circumference.

The three-dimensional model used in the simulation, with the surrounding air region made transparent to highlight the geometry, is shown in Fig 3-14. As can be seen in Fig 3-14(a), the end-plates were assumed to have the same outer diameter as the rotor.
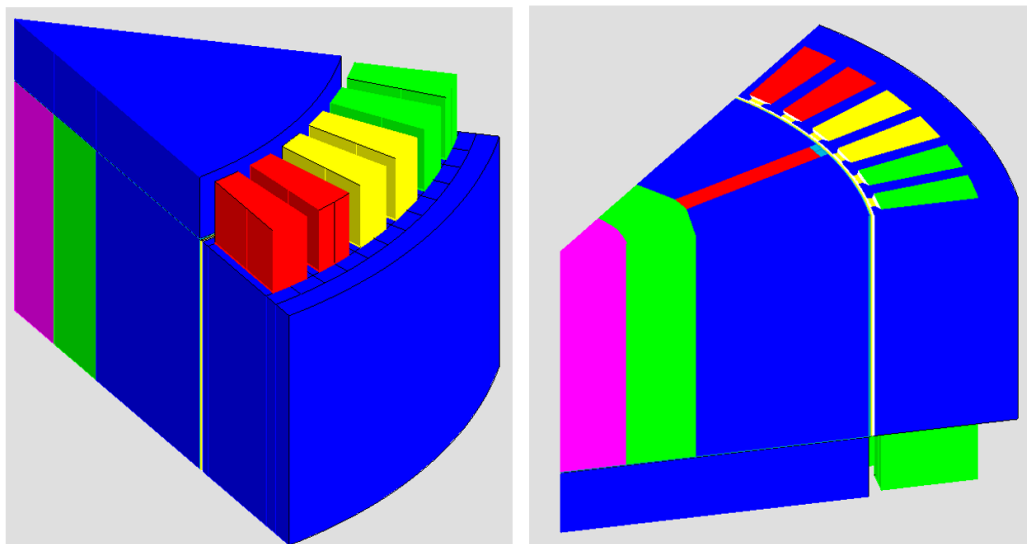
(a)Three-dimensional model NW view   (b)Three-dimensional model SE view

Fig 3-14 Preliminary 3D FE model of 48/8 IPM machine with endplate

The meshing of finite model is critical to the accuracy of the model. It is important to have sufficient good quality elements at key points in the model, e.g. around the working airgaps. However, the number of elements determines the solution and the memory requirements to allow the model to run at all. Hence, there needs to be a trade-off when selecting mesh densities in different regions of the model. This can be particularly challenging in three-dimensional models where visualisation of the mesh is difficult.

The mesh used for the initial three-dimensional model is shown in Fig 3-15 and Fig 3-16. Several areas of particular interest have been labelled as regions M1 to M4. The main working magnetic airgap in this machine, region M1 is represented with a three-layer mesh and elements that have reasonable aspect ratios. As would be expected, the mesh density in the stator lamination, where spatial field gradients are much lower have a coarser mesh. The region around the permanent magnets and the rotor hub, which is

labelled as M2 needs to have sufficient mesh density to reliably predict leakage. The region M3 is the axial airgap between the end-plates and the end of the rotor core and needs to be re-meshed with a different number of elements as the end-plate is moved further away. The axial mesh discretisation in the rotor and stator cores was set as shown as M4 with the main aim of ensuring a reasonable aspect ratio and allowing a straightforward extrusion of the rotor base geometry.
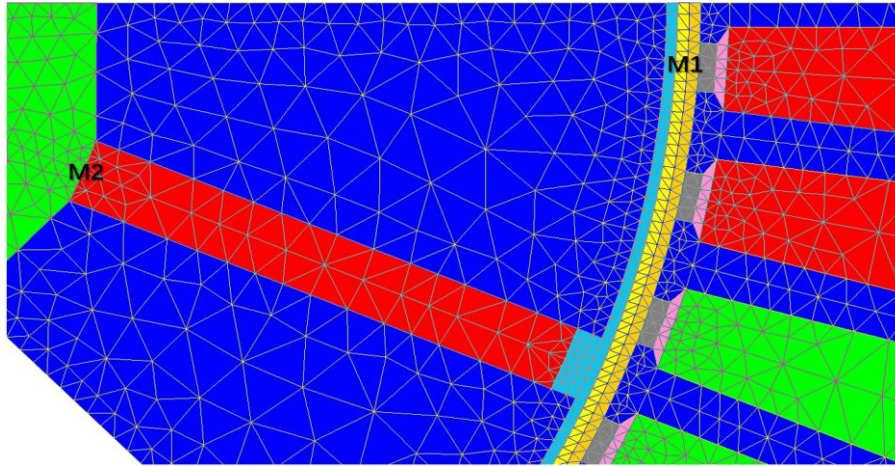
Fig 3-15 View of the mesh on the plane of axial symmetry – surrounding air and flux-mesh not visible
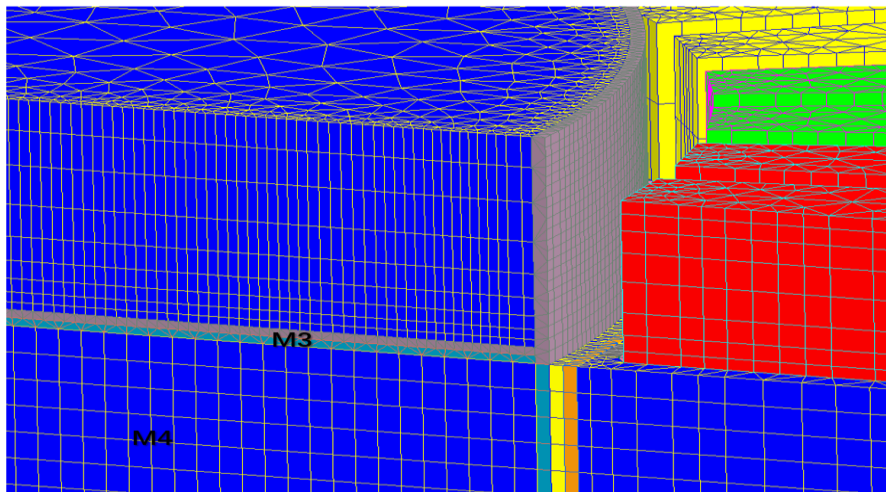
Fig 3-16 Side-on view of the mesh near the end of the rotor and around the flux-diverting plate (case shown has an axial gap of 4mm)

3.3.3 Simulation results

Before analysing the results of the finite element model, it is important to note that conversion from a 2D model to a 3D model often results in lower terminal voltage. This

is primarily because 3D models can capture edge effects, including axial flux leakage and asymmetric magnetic fields at the ends, which 2D models typically assume to be symmetric. As a result, 2D models are less capable of fully representing the real flux variations. Additionally, the presence of magnetic end plates further accentuates this inconsistency. Therefore, the best approach is to remove the magnetic end-plates in simulations to obtain a more accurate representation of the machine's electromagnetic performance.
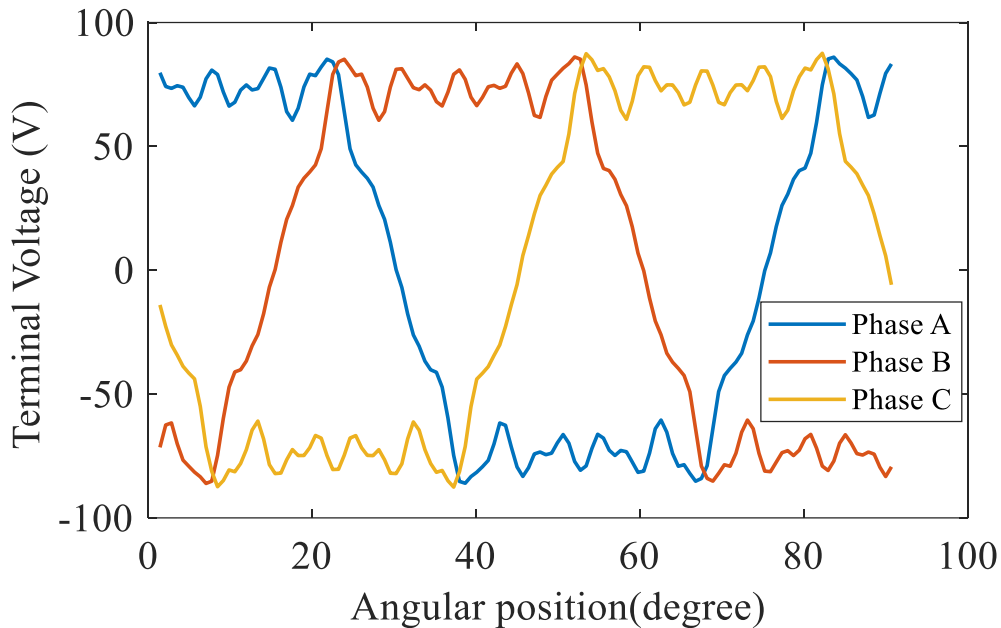
Fig 3-17 Three-dimensional finite element predicted output voltage waveform under open-circuit condition at 5400 RPM without magnetic end-plate

Table 3-4 Preliminary finite element model simulation result summary (5,400 rpm)

Simulation condition	Terminal voltage (peak to neutral) fundamental component - V	Total distortion factor (THD)	Terminal voltage RMS value - V
2D / OC	101	27.0%	73.9
3D / OC / No endplate	90.5	27.3%	66.4
3D / OC / 4mm gap	87.4	27.3%	64.1
2D / OL	69.3	26.7%	50.7
3D / OL / 4mm gap	60.3	28.0%	44.3

Fig 3-17 shows the finite element predicted open-circuit waveforms for the 48/8 IPM design without present of magnetic end-plate while Fig 3-18 shows the waveform with 13mm thick magnets and the magnetic end-plates located at a position which

corresponds to a gap of 4mm from the end of the rotor. Moreover, Fig 3-19 show the same machine loaded with resistive load at 0.25Ω per phase condition. The detail of numerical result is summarized in Table 3-4.
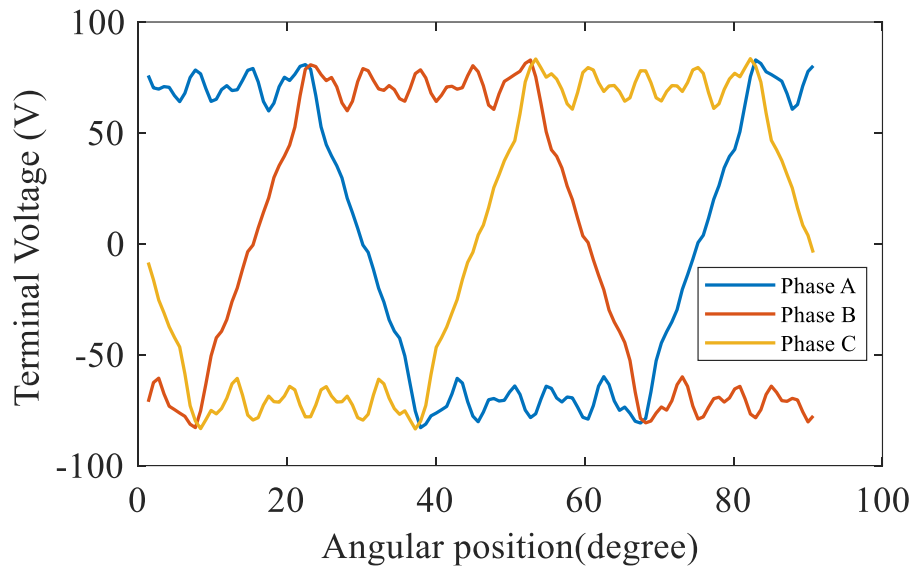
Fig 3-18 Three-dimensional finite element predicted output voltage waveform under open-circuit condition at 5400 RPM with 13mm thick magnetic end-plate at 4mm gap from rotor
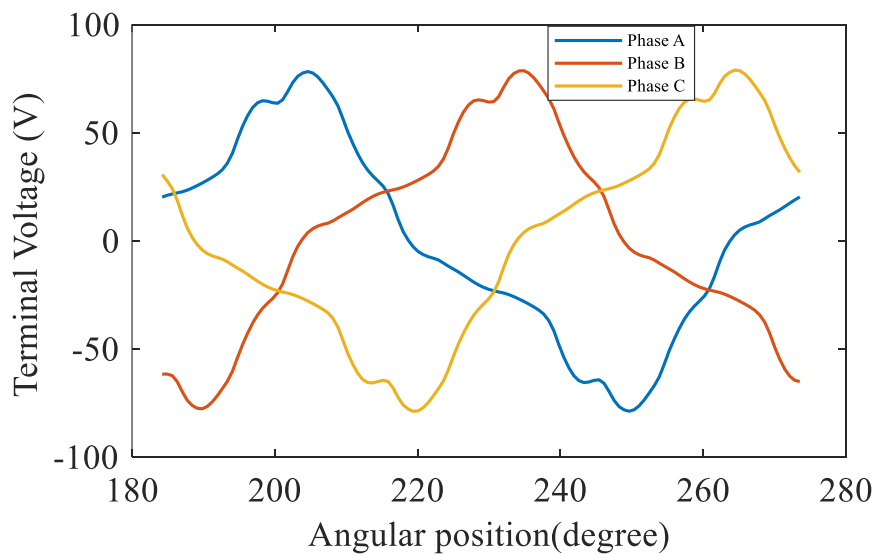
Fig 3-19 Three-dimensional finite element predicted output voltage waveform at 5400 RPM with 13mm thick magnetic end-plate at 4mm gap from rotor with the generator loaded with a star-connected, three phase load of 0.25Ω per phase skipped 2 electrical cycles

3.4 Evaluation of the end-plate geometry and space-off range

The primary reason for using three-dimensional finite element analysis in this particular phase of the design is to investigate the behavior of the stationary flux diverting end-plates located at both ends of the rotor. Two aspects have been considered, i.e. the thickness of the end-plates and then the relationship between the induced voltage and the space-off of the plates from the ends of the rotor.

3.4.1 End-plate thickness

It is anticipated that the minimum clearance or space-off of the plates from the ends of the rotor would be 0.25mm. This minimum airgap would correspond to the maximum flux passing through the end-plates which is the worst-case condition for magnetic saturation. Hence, a series of three-dimensional finite element simulations were performed at the lower end of the operating speed range, i.e. 5400rpm, for a fixed axis space-off of 0.25mm and flux-diverting plate thicknesses between 10 and 15mm in 1mm steps. The resulting variation in the fundamental component of the open-circuit terminal voltage as a function of plate thickness is shown in Fig 3-20. As shown in Fig 3-20, a 13mm endplate thickness achieves the lowest output voltage, corresponding to the maximum degree of magnetic flux diversion away from the main working airgap. Thinner plates that are 13mm exhibit some degree of localized magnetic saturation which limits their ability to divert flux away from the main working airgap of the generator.
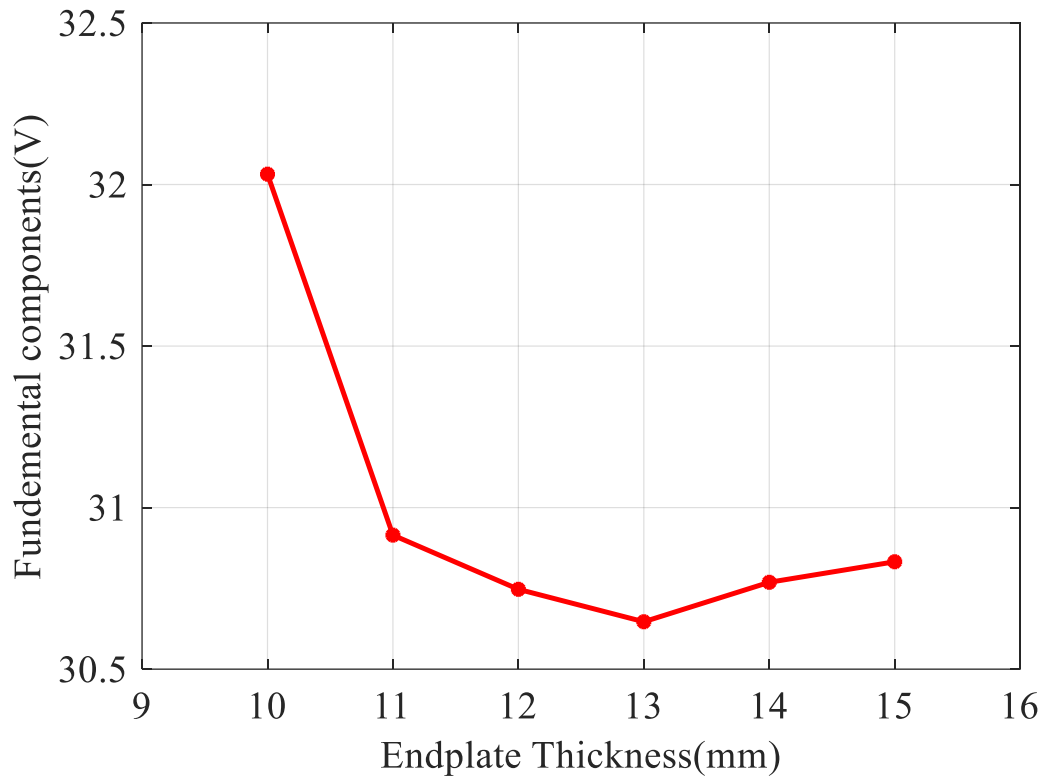
Fig 3-20 Preliminary 3D FE model Output voltage for different endplate thickness
at 0.25mm space-off and 5,400rpm

3.4.2 The endplate space off

Having determined the optimal endplate thickness for operation in the worst-case magnetic saturation conditions with a 0.25mm space-off from the end of the rotor, the variation in the magnitude of the fundamental voltage with increasing space-off of the flux diverting end-plates was calculated at 5,400 rpm, in all cases with the same endplate thickness of 13mm. Fig 3-21 shows the variation in the magnitude of the fundamental of the open-circuit voltage with space-off along with the corresponding value for a machine with no end-plates. As would be expected, when the endplate space-off is increased, the magnitude of the open-circuit voltage tends towards the value with no end-plates, reaching 87.9V at a space-off of 4mm. The remaining difference is due to some axial leakage flux from the rotor still passing through the end-plate. It is also worthing noting that the 'turn-down' ratio, i.e. the ratio of the maximum to minimum voltage is 1.8 for a full endplate excursion from 4mm to 0.25mm.
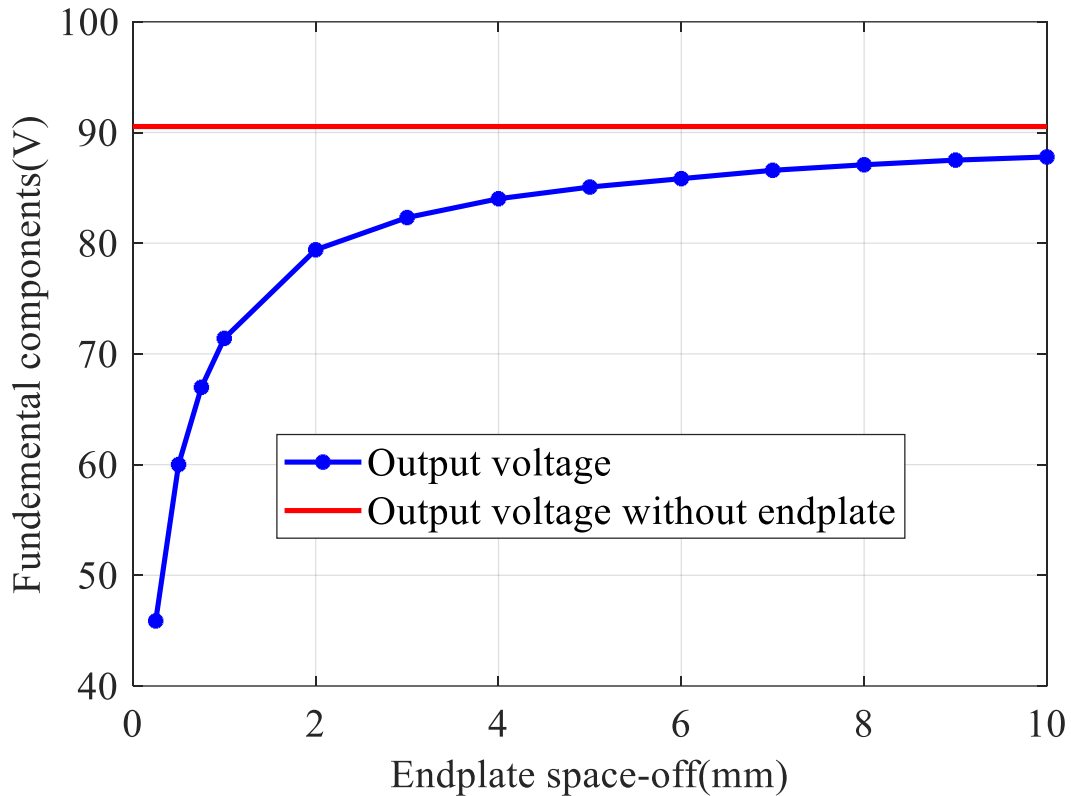
Fig 3-21 Preliminary 3D FE model open-circuit output voltage fundamental for different space-offs at 5,400rpm with a 13mm thick endplate

3.4.3 Endplate material

For the endplate material, the same material as the stator was selected (Carpenter Hiperco-50) to achieve optimal flux diverting capability. It is important to note that the endplate is in stationary frame during the operation. Therefore, to minimize losses, particularly eddy current losses, the endplate is not a single solid piece but is instead a toroidal laminated core.

3.5 Preliminary design summary

In this chapter, the sample models were introduced and due to the missing data, the rotor geometry was investigated in terms of comparative study of spatial harmonic contents of different magnet structures, which combining the stator from the sample models, the preliminary model was designed and simulated to determine the potential optimization options. Moreover, the flux diverting plate geometry was studies based on the specification.

Chapter 4 - The Generator electromagnetic optimization

4.1 Initial design evaluation

In the last chapter, the design of 8-pole, 48 slot machine spoke type PM machine preliminary model has been established by taking the main leading dimensions from the SILOET machine detailed in [50]. The initial stator outer diameter is 173.6mm with an axial length of 98mm. The flux-diverting plate is also included within the 3D model for flux modulation. However, the stator parameters for this design are inherited from the SILOET machine and the rotor geometry is based on empirical estimation. This was useful in terms of a proof-of-concept but unlikely to have been optimal in terms of variable-flux operation.

Therefore, it is important to have the preliminary design evaluated against the previous design criteria, to meet all the requirements for a direct line connect generator within the current variable frequency alternative current (VFAC) system. Moreover, from the previous discussion regarding the standard of the aerospace electrical system, the generator will operate over a mechanical speed range of 5,400rpm to 12,000rpm which is corresponding to 360-800Hz frequency range. Given the nature of direct line connection, the operating envelope of any generator under previous circumstance is bounded by 4 key operating points, viz. open-circuit at minimum and maximum speeds, and full load at minimum and maximum speeds. Hence, providing the terminal voltage that can be regulated within allowable limits at these four corner points, the machine will have sufficient PM flux variation capability to accommodate all intermediate operating points.

Furthermore, given the requirement of load regulation capability and speed regulation capability, the turn-down ratio of PM flux-linkage needs to be at least 2.2:1 (800/360 = 2.222). Hence, the first evaluation is to analyse the flux turn-down ratio. As Fig 3-21 shown with optima end-plate at 5,400 rpm, open-circuit condition, the turn-down ratio is 1.8:1.

Given that this chapter contains extensive content related to design iterations, for convenience and clarity, the preliminary model will be referred to as D1. Subsequent designs will follow the same progressive naming convention, i.e. D2, D3 etc.

4.1.1 Flux turn-down capability analysis

The initial approach to understanding the relationship between machine dimensions and turn-down capability was to investigate the flux density distributions on various cut-planes along the machine. Fig 4-1 illustrates the locations of each plane of interest long the machine. The particular condition considered is with endplate located at a 0.25 mm space-off the machine itself at open-circuit simulation condition.
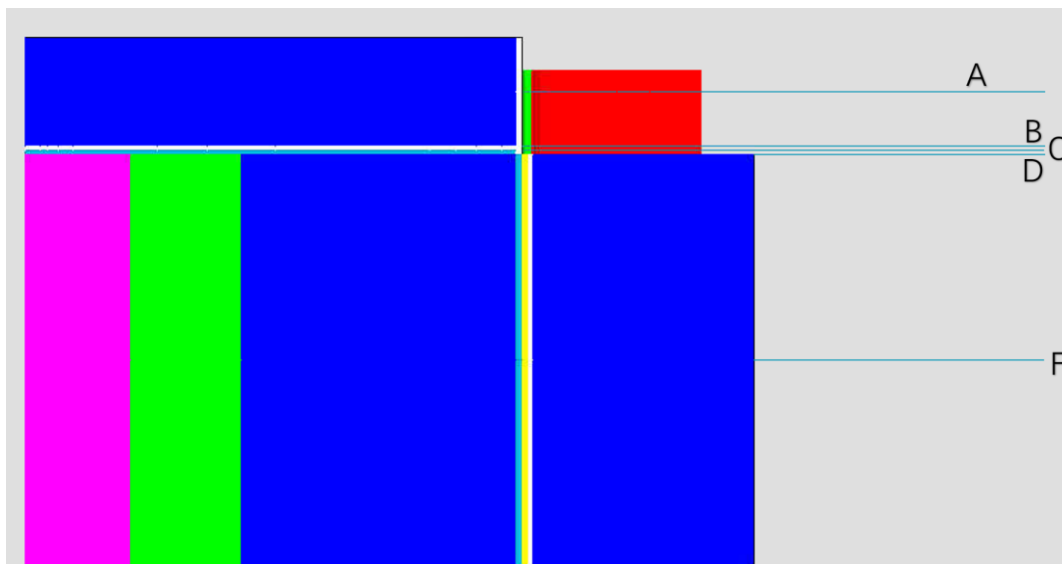
Fig 4-1 Cut-plane location demonstration
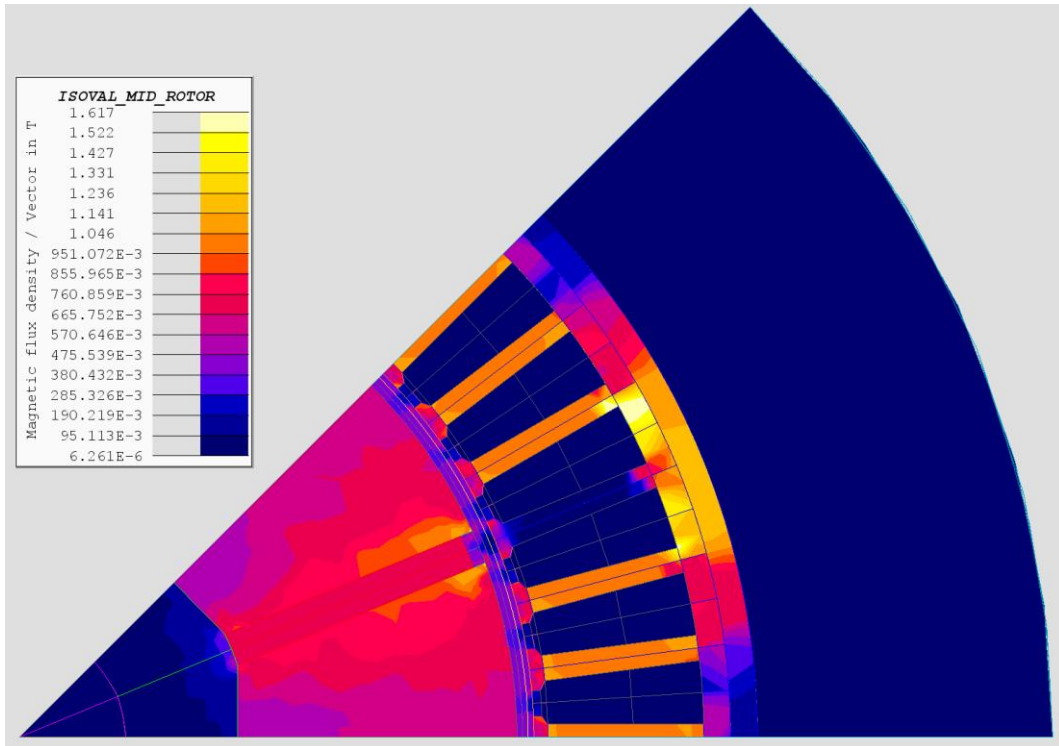
Fig 4-2 Flux density distribution on Plane F (rotor centre)
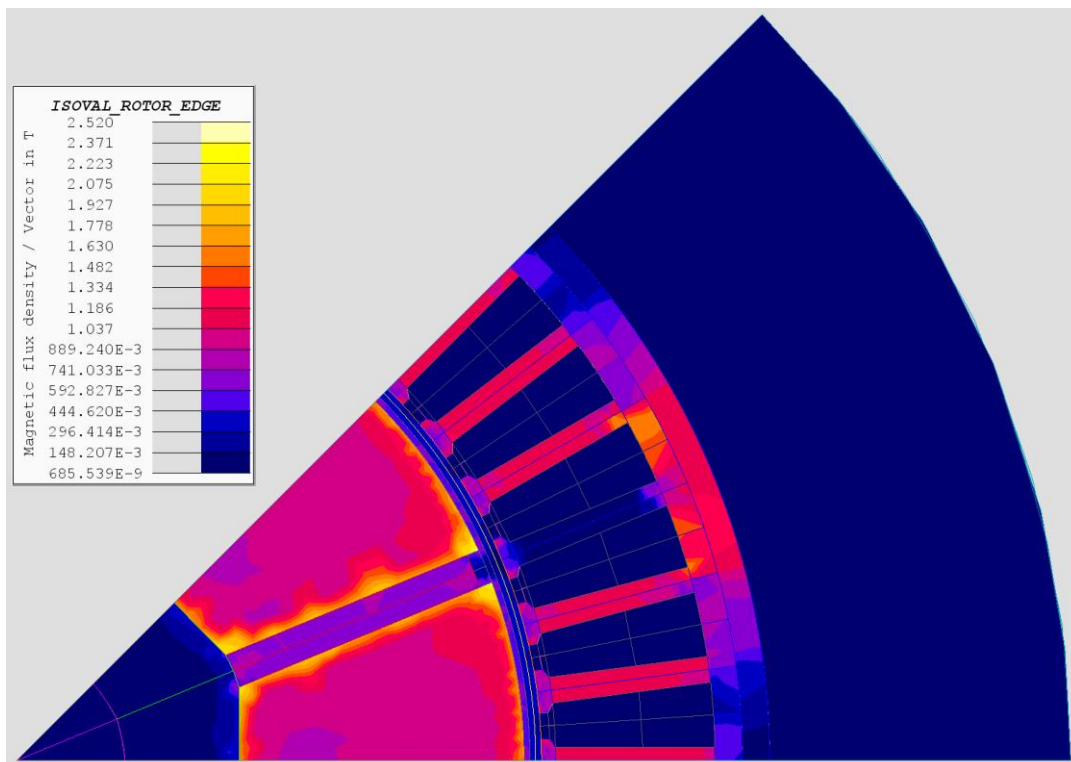
Fig 4-3 Flux density distribution on Plane D (rotor end face)

As showed in Fig 4-3, the flux density within the rotor lamination has localised values up to 2.5T, which means the rotor core (Cobalt iron) is heavily saturated. In the cut-plane of Fig 4-2, the flux density in the stator back-iron is ~1.6T. The presence of flux

shorting plate does divert most of flux from the main air-gap to side air-gap.

Moreover, from Fig 4-4 and Fig 4-5, the magnitude of flux density at space-off and endplate bottom is merely 1.2T. While in the endplate centre shown in Fig 4-6, the flux density is around 1T. Compared to the magnetic flux density on the rotor surface, particularly the differences in flux density at specific positions, it is evident that the current-sized endplate can still accommodate more magnetic flux.
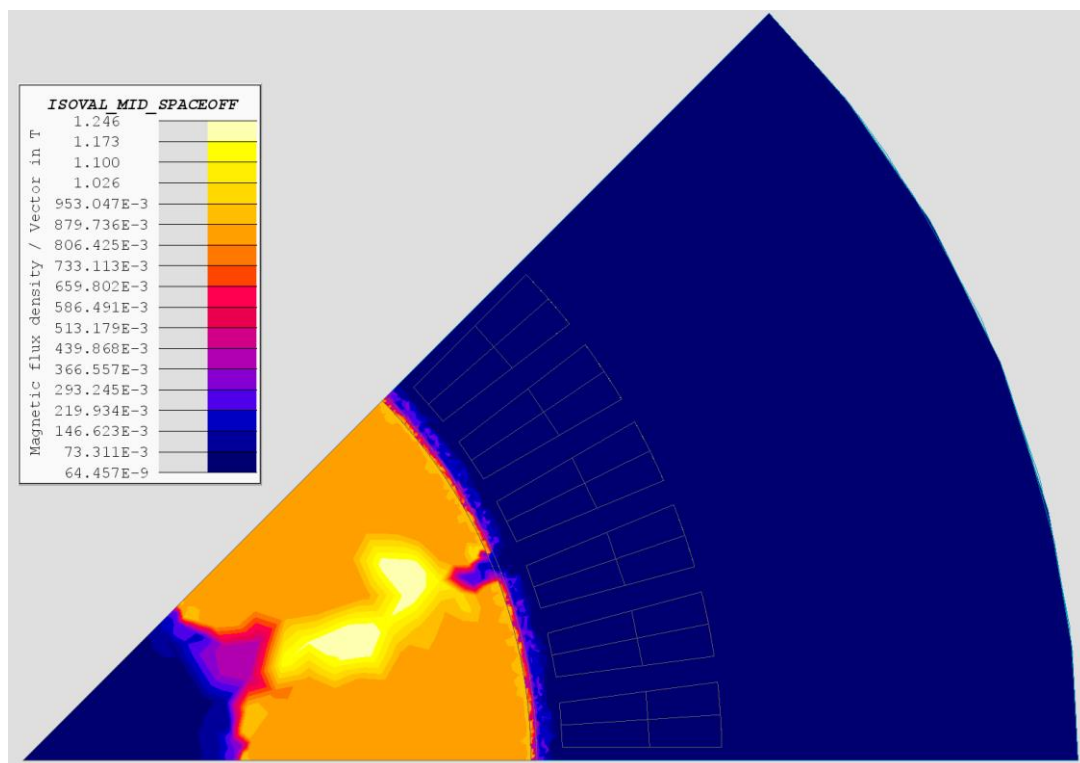
Fig 4-4 Flux distribution on Plane C (space-off centre)

It is worth noting that there is significant room for improvement in the efficiency of magnetic flux transmission along the path from the rotor to the endplate. Therefore, with the endplate thickness and space-off size determined, other improvements are feasible. For instance, adjusting the machines dimensions could enhance the magnetic flux conduction effectiveness of the endplate.
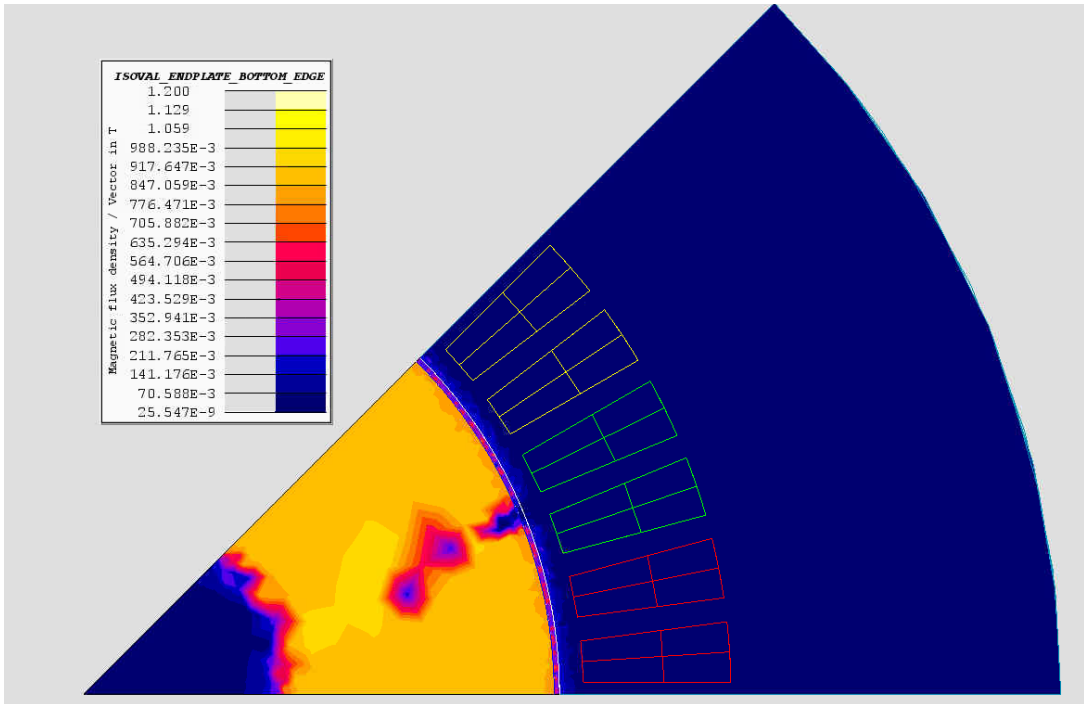
Fig 4-5 Flux distribution on Plane B (endplate bottom face)
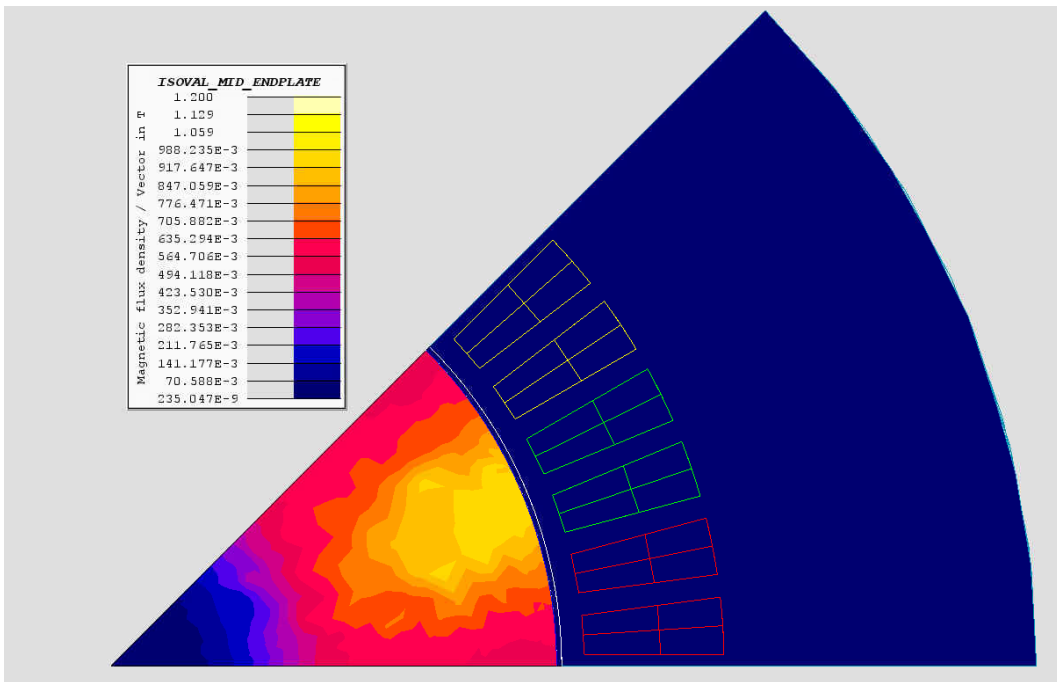
Fig 4-6 Flux distribution of Plane A (endplate centre)

Also, considering the flux path of a typical spoke type PM machine, it is essential to observe the flux density distribution from vertical perspectives, as shown in Fig 4-7. Whereas the predicted magnitude of flux density vertical components at bottom edge of endplate in Fig 4-5 is approximately 1.2 T, the flux density on the axial cut plane can reach ~1.8 T on the lower section of endplate, However, both directional components

of the magnetic flux density vectors from flux distribution map indicate that the endplate is far from reaching magnetic saturation.
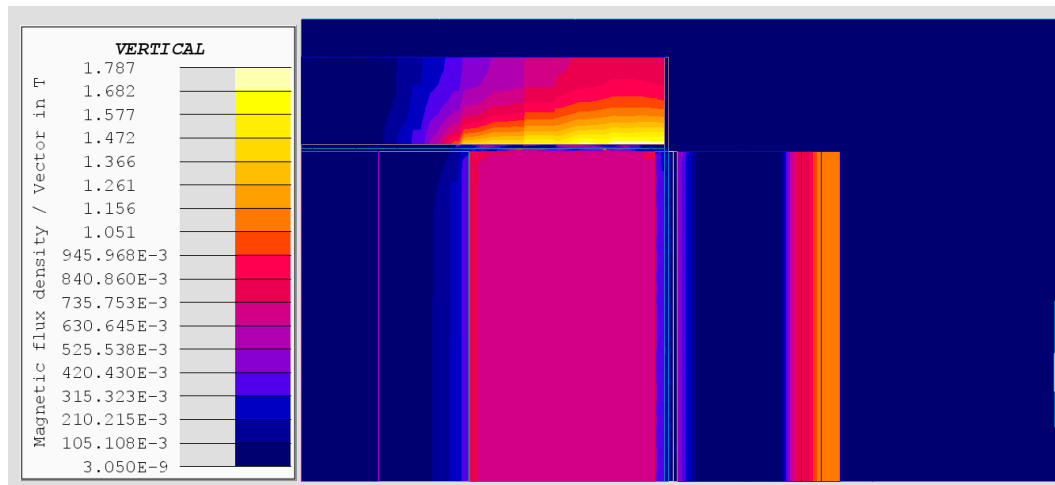
Fig 4-7 Flux density distribution on side view

In addition to that is the concern about asymmetric flux distribution shown in Fig 4-5, which is mainly due to the mesh issue given the mesh density settings on the endplate is inherited from the geometry construction which extrudes from the bottom plane of the rotor. This preliminary model aims to investigate the magnitude of flux linkage. The asymmetric flux is expected to have minimal impact on the results and will be optimized through detailed mesh settings during later performance evaluation stages.

4.2 Meeting turn-down ratio requirements

Given the preliminary design fail to meet the flux turn-down ratio requirements, which is the priority of the design, the first optimization approach will be geometry change of the machine to meet this requirement and given the flux diverting plate is the single measurement for flux control, which leads to the optimization which accommodate to this feature.

4.2.1 Change of machine aspect ratio

As shown previously, the initial design D1 does not meet the voltage regulation requirements and Fig 4-7 also demonstrates the potential for the endplate to perform the field weakening is not utilised as well given that the flux density at that region is far

from saturation. One approach is to increase the overall diameter of the machine which consequently increase the area that face the endplate while reducing the axial length. This changes the flux-focussing ratio between the magnets and the rotor end-face and also reduce the total magnetic reluctance in the axial direction.

In Fig 4-8, A1 represent the total area relevant to the flux passing through the end-face air-gap to the endplates and the A2 and A3 represent the area that corresponds to flux passing through the PM.

Neglecting the leakage flux through the inner region occupied by the nan-magnetic hub, the magnetic flux originating from the permanent magnets need to go through the areas A2 and A3, while the paths this flux takes when leaving the rotor body is subject to the ratio of reluctance for the air-gap regions associated with A5 and A1. According to the flux density distribution shown in Fig 4-3, where the flux density near the endplate-facing surface of the rotor body reaches 2.5T, it is evident that the existing A1 area is insufficient compared to A5 in providing an adequate flux path due to increase reluctance for diverting the magnetic flux originating from A2 and A21. This deficiency explains the extremely high, near saturated flux density levels and distribution observed on the A1 surface, which reduces the proportion of flux diverting to the endplate.

One solution is to change this ratio, which is to increase the size of the A1 area and correspondingly reduce the size of the A5 area. Increasing the A1 area would mean enlarging the rotor bore diameter, while reducing the A5 area would mean shortening the axial length of the machine, resulting in an aspect ratio change. The total active volume of the rotor can be kept the same while changing the aspect ratio, which would to first approximation maintain the same torque given the electric and magnetic loadings remain fixed.
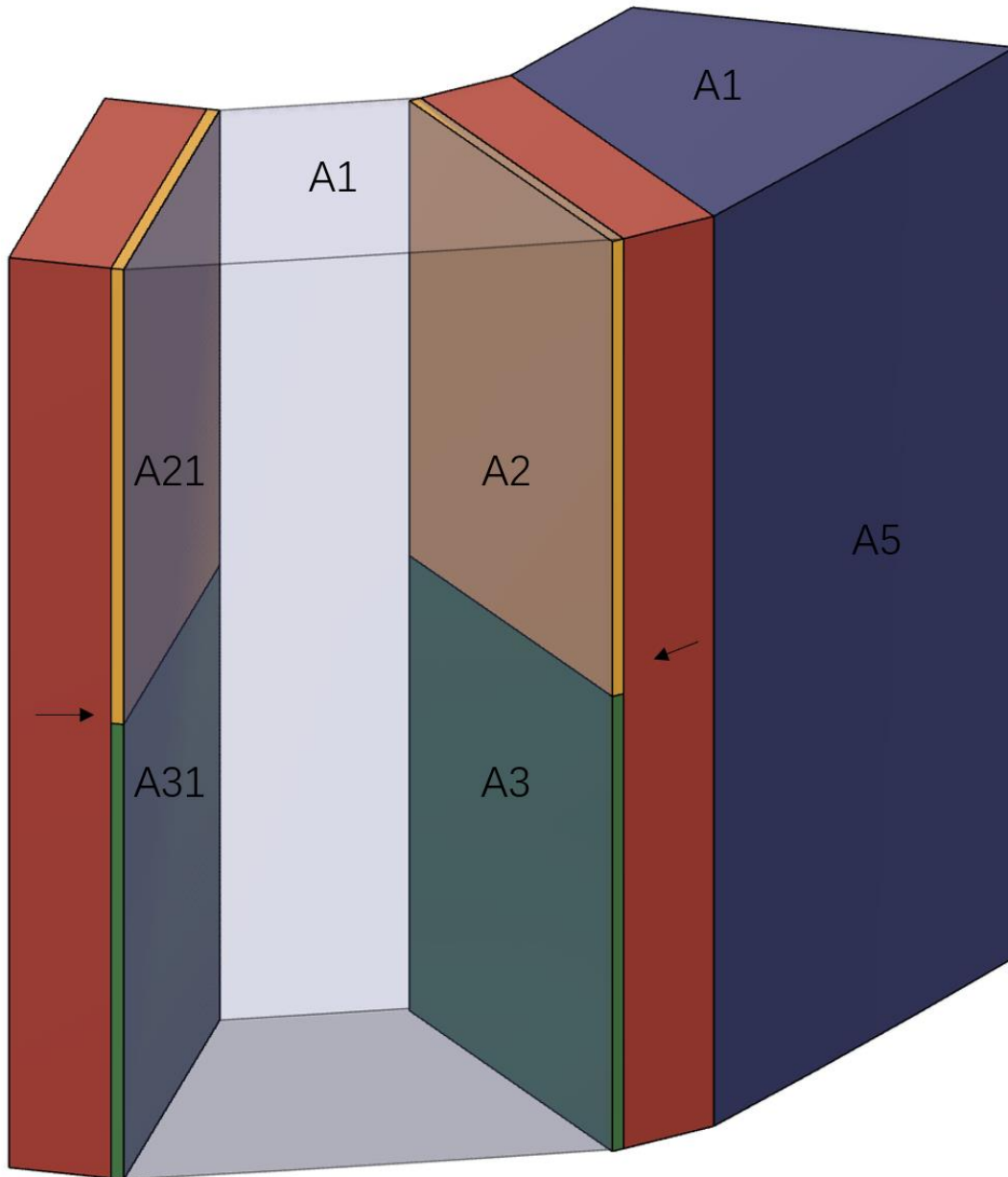
Fig 4-8 Rotor pole face illustration

The geometry of the initial model has an aspect ratio (L/D ratio) of approximately 0.56, with an estimated total active volume of 2.32×10^6 mm³. In an attempt to meet the flux turn-down ratio requirement, the stator outer diameter was increased to 191.5 mm while the axial length is reduced to 80 mm, resulting in a new aspect ratio of 0.42. The total active volume of the new machine was maintained at 2.3×106 mm. Fig 4-9 also visually shows s simplified representation of aspect ratio differences in these two rotors.
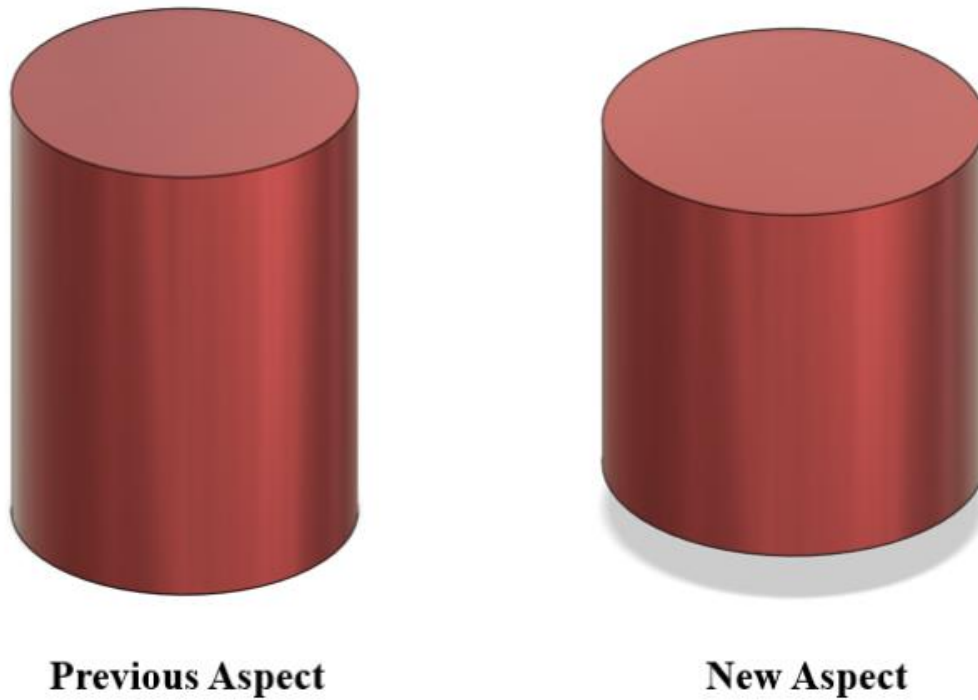
Fig 4-9 Aspect ratio change illustration

4.2.2 Change of size and air-gap

In addition to changing the aspect ratio, several other approaches can be adopted to increase the flux regulation capability. One such approach is to increase the length of radial air-gap of the machine from 1 mm to 2 mm. This change increases the reluctance from the PM to the stator through the main radial working airgap, consequently increasing the flux turn-down ratio.

However, this also reduce the magnetic loading of the machine to different extents. For the aspect ratio change, the total area of PM (perpendicular to the magnetisation direction) is reduced, given that the A2 and A3 areas are reduced despite maintaining the same total volume of the machine. Moreover, increasing the main air-gap length reduces magnetic loading to a greater extent, as the effective air-gap flux density is directly related to the air-gap length.

Therefore, it is important to note that these approaches are based on two selected features of the initial design. Firstly, the flux-focusing effect of the spoke-type PM machine provides sufficient flux linkage to the stator, allowing a certain degree of

margin on the excitation, which permits this trade-off. Secondly, based on the initial predicted design performance, the flux saturation on the rotor core suggests that the initial design of the magnet has not fully utilized the potential from the excitation sources.

Given the saturation state of the rotor shown in Fig 4-3, the magnet thickness in radial direction was reduced from 35 mm to 30 mm to decrease flux saturation at the rotor edge. This reduction helps prevent the flux linkage from being diverted into the endplates. The effect on the output power density will be investigated in the following sections.

4.2.3 Revised design to meet the turn-down ratio

After the previous modification on the aspect ratio, the new proposal machine geometry is shown in Fig 4-10. Given the increase in the stator outer diameter of the machine while maintaining the same stator and rotor structures, the non-magnetic hub has consequently been adjusted.

To further increase the turn-down capability by minimising flux-leakage through the inner edge of the magnet, the hub was partially extended into the region occupied by the original rotor core design, as shown in Fig 4-10. This modification increases the surface area facing the Hub, consequently increasing the flux passing into the flux-diverting endplate, further boosting the flux turn-down capability. The remainder of the machine geometry remains the same, and the winding pattens is also the same as the initial D1 design for a direct comparison. Th resulting design, the FE model of which is shown in Fig 4-10 referred to as design D2.
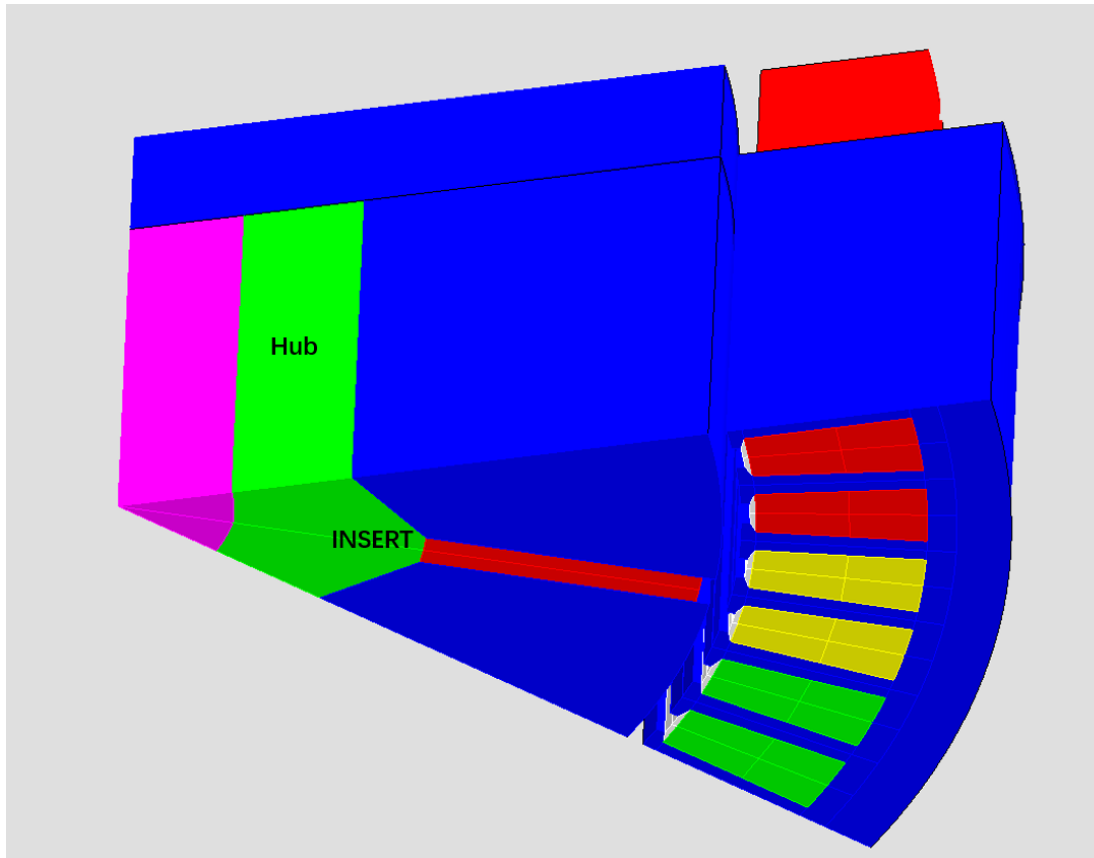
Fig 4-10 Model with updated aspect ratio (D2)

The flux density distribution under open-circuited conditions is shown in Fig 4-11. It can be seen that, under the same condition, the magnitude of flux density on the endplate has increased from 1.7T to 2T compared to Fig 4-7. This is close to the typical saturation knee point of cobalt iron [52]. Moreover, the flux density distribution is not localized but spread across the entire endplate, indicating an improved capability of the endplate to divert flux. The output phase voltages of the D2 machine and the associated harmonic spectra are shown in Fig 4-12 and Fig 4-13 respectively. the magnitude of the fundamental component of the open-circuit voltage for maximum and minimum space-off are 49.0V and 20.3V at 5,400 RPM, respectively, resulting in a turn-down ratio for D2 of 2. 4.

It needs to be point out that the simulation shown above using a 1 turn per coil notional winding, as one of means to improve computation efficiency of 3D simulation in the early optimization process.
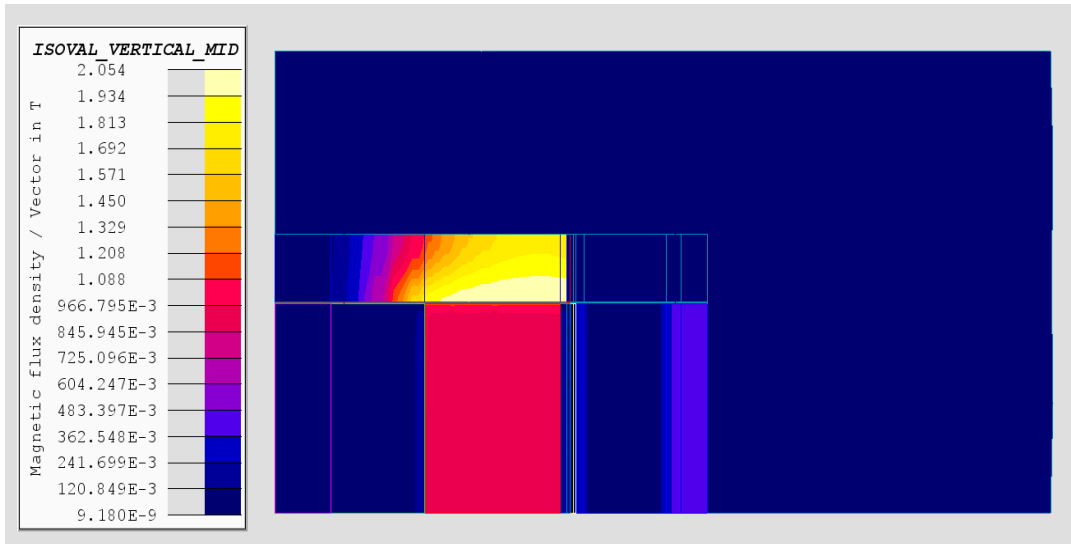
Fig 4-11 Flux distribution side view for D2 model under open-circuit conditions
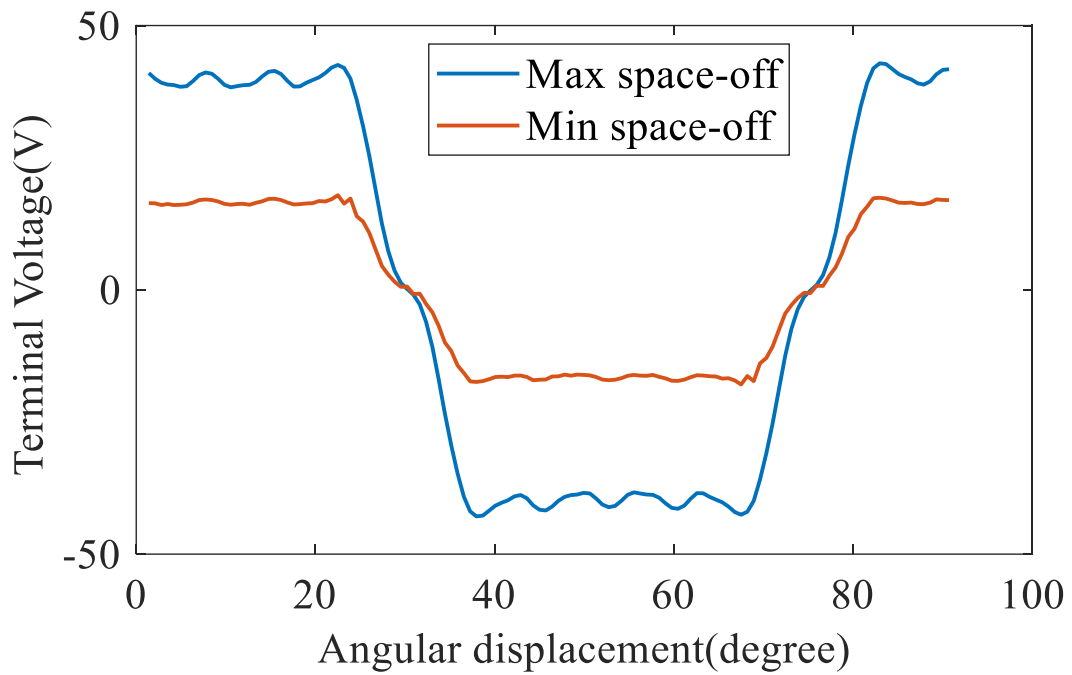
Fig 4-12 Output phase voltage waveform at different space-off (5,400 RPM) of D2 model under open-circuit conditions
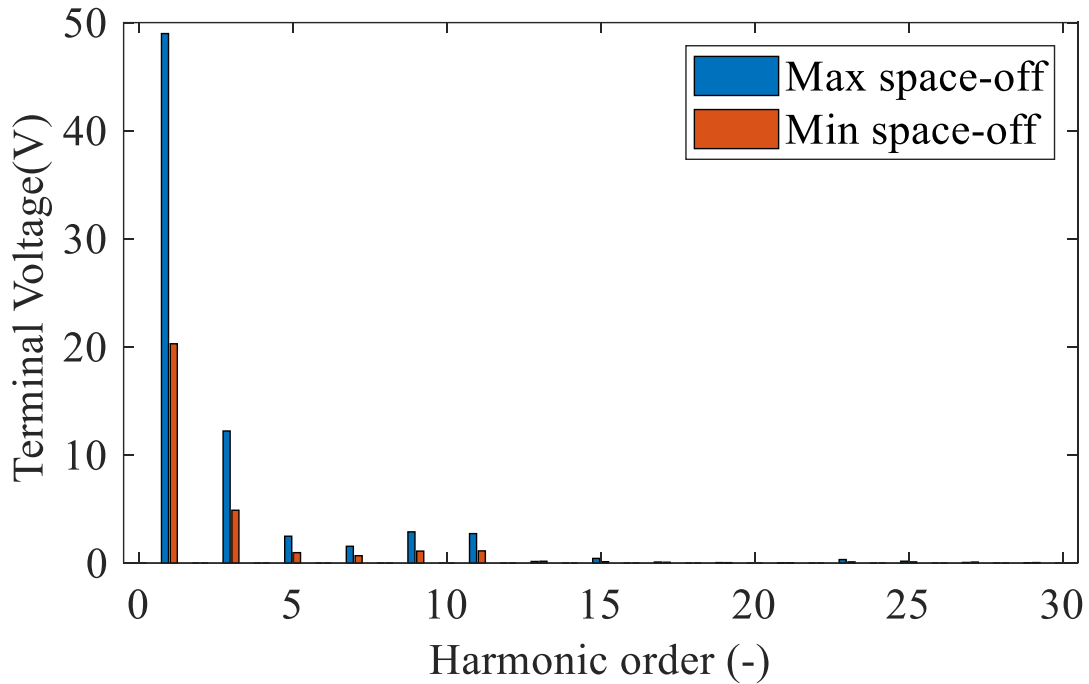
Fig 4-13 Output phase voltage spectra at different space-off (5,400 RPM) of D2 model at Open-circuited condition

However, by increasing the radial air-gap length from 1mm to 2mm and altering the aspect ratio, the fundamental component of the output phase voltage for minimum speed maximum space-off condition drops from 87.4V to 49V, resulting in a 44% reduction. Moreover, in order to isolate the voltage reduction due to the increase of air-gap, a separated simulation has been conducted based on D1 model with 2mm airgap showing the output phase voltage for minimum speed maximum space-off condition is 56.6V.

4.3 Load regulation capability

4.3.1 Full load condition

Fig 4-14 shows the schematic of the electric circuit used in the FEA model to load the generator with a unity power factor load. The component A1-A4, B1-B4 and C1-C4 are lumped parameter coils which couple into the winding regions of the finite element model. RA, RB and RC represent the load resistors.

For open-circuit calculations, RA, RB, and RC are set to 1MΩ while for the full load conditions, the value of those load resistances was set to draw specific power.
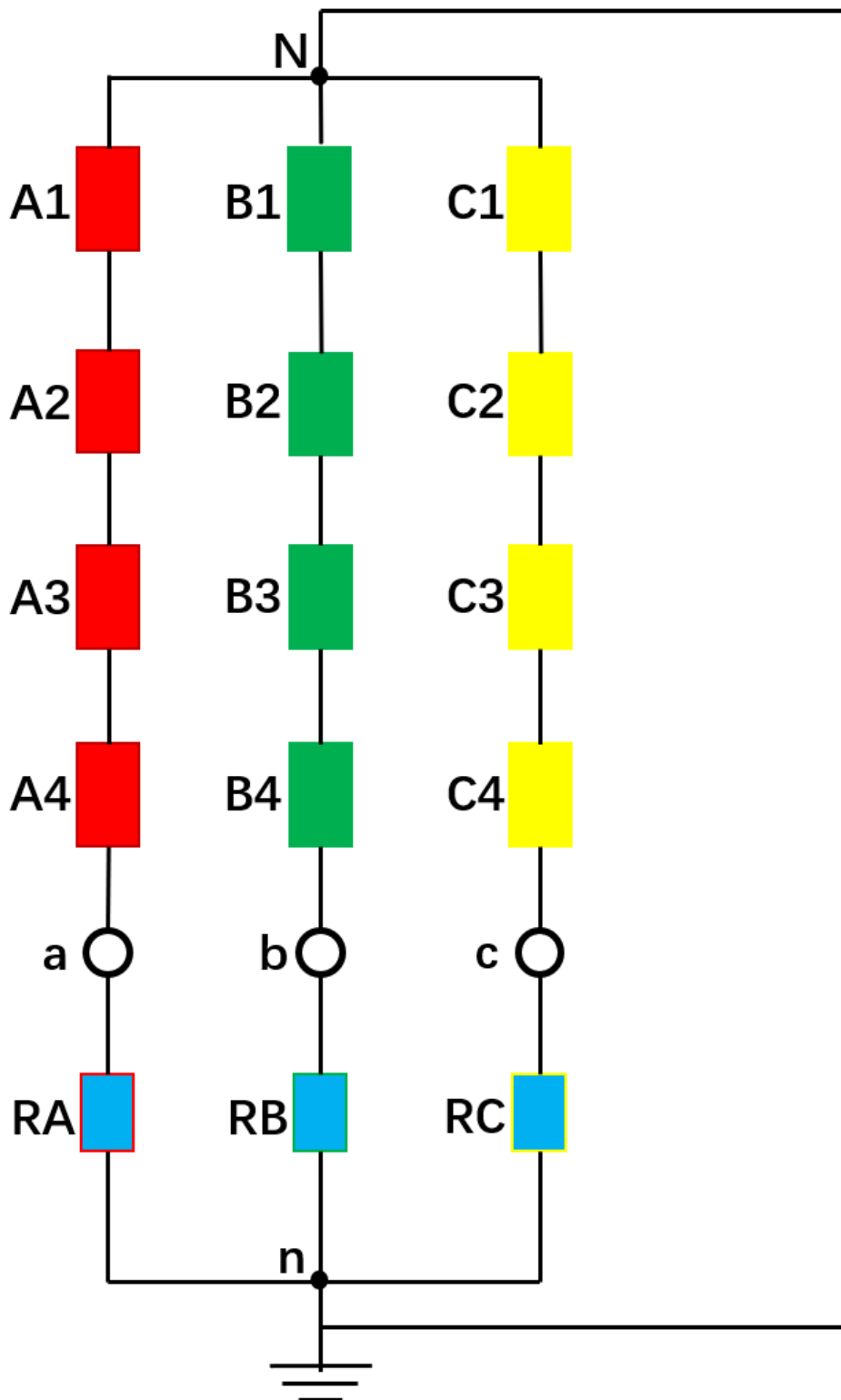
Fig 4-14 Coupled electric circuit layout for Altair flux model D2

A parametric sweep of the load resistances has been performed at 5,400rpm and

maximum space-off, to find out the load resistance that draws the maximum output power. The resulting variations in the voltage and output power as a function of the load resistance are shown in Table 4-1. It can be seen that at the lowest speed of 5,400rpm the machine generates the maximum output power of ~10.4 kW with a 0.1 Ohm load resistance per phase.

Table 4-1 Output power at various load resistances for D2 model at 5,400rpm and maximum space-off

Voltage rms(V)	Resistor(ohm)	Current rms(A)	J(A/mm2)	Output power (kW)
23.6	2,0	11.8	0.5	0.83
23.4	1.0	23.4	1.0	1.64
23.2	0.6	38.7	1.6	2.70
23.1	0.5	46.2	1.9	3.20
22.9	0.4	57.2	2.4	3.93
22.5	0.3	75.1	3.2	5.11
21.6	0.2	107.9	4.6	6.98
21.2	0.18	117.9	5.0	7.51
20.5	0.15	136.8	5.8	8.42
19.4	0.12	161.9	6.9	9.43
18.8	0.1	188.4	8.0	10.65
17.7	0.09	196.3	8.4	10.40
15.8	0.08	198.1	8.5	9.42
14.9	0.07	212.3	9.0	9.46
13.7	0.06	227.7	9.7	9.34
12.2	0.05	244.6	10.4	8.97

4.3.2 D2 performance summary

Table 4-2 summarises the phase voltages (fundamental component, RMS voltage) and distortion factors as defined in Section 1.3.3 at the four corner points of the generator operation envelope, i.e. open-circuit at maximum and minimum speeds, and full load at maximum and minimum speeds. Both maximum space-off and minimum space-off

conditions are analysed for each corner point.

Table 4-2 D2 DESIGN PERFORMANCE SUMMARY WITH PER-TURN DESIGN

	Operating point	Phase Voltage fundamental (rms)		Distortion factor	
		0.25mm space-off	4mm space-off	0.25mm space-off	4mm space-off
Open-circuit	12,000rpm	32.9V	79.7V	26.1%	26.9%
	5,400rpm	14.8V	35.9V	26.1%	26.9%
Full load	12,000rpm	8.1V	21.8V	29.1%	31.4%
	5,400rpm	7.1V	18.8V	28.1%	30.1%

As shown in the Table 4-2, the terminal volage under open-circuit condition at 12,000rpm and 0.25mm space-off is 32.9V, higher than that at full load, 5,400rpm and 4mm space-off, 18.8V. In other words, there is no overlap region between the voltage for open-circuit, 12,000rpm and full load, 5,400rpm operation. Therefore, for D2 design, it is not possible to regulate the terminal voltage within the desired voltage range by adjusting the space-off for a load equivalent to the maximum power.

This mismatch on the voltage regulation indicates that under full load conditions, the machine cannot supply the grid with required voltage (recognising that the number of turns per coil would be scaled to meet the voltage magnitude standards) and hence the D2 design requires further optimization. The main cause of the poor regulation is that the large winding reactance leads to a large voltage drop as shown in Fig 4-15, resulting in insufficient output voltage at full load, maximum space-off and minimum speed condition. Therefore, reduction of the winding reactance via geometry optimization was adopted at the next design change.
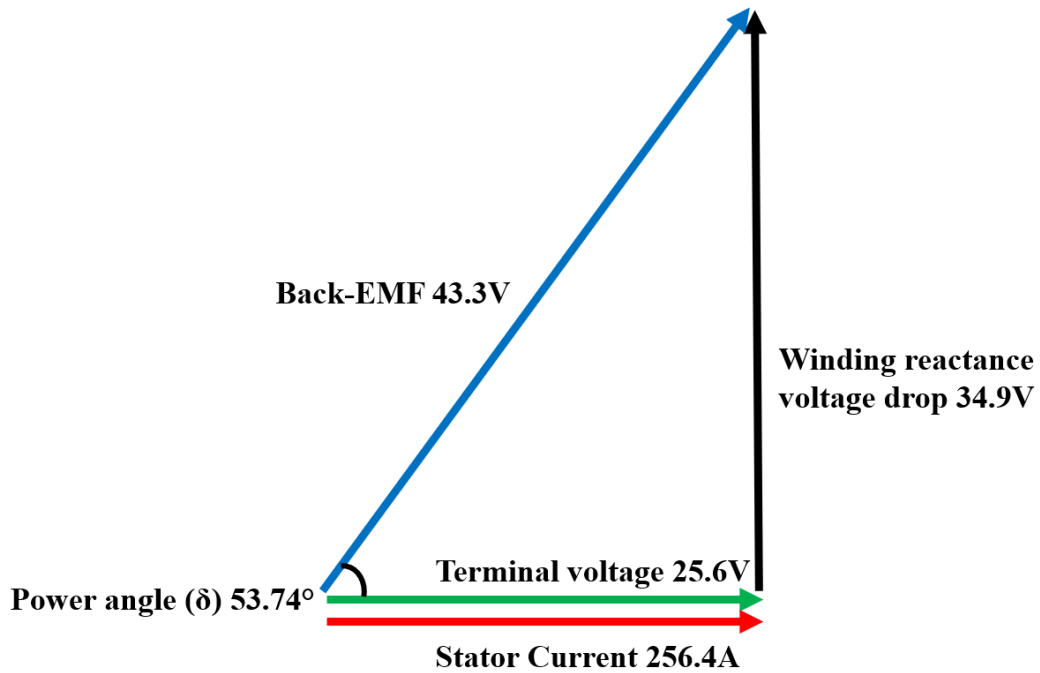
Fig 4-15 Phase diagram of D2 (single turn per coil) loaded with 0.1ohm resistor at
5,400 rpm and maximum space off

4.3.3 Design changes to reduce winding reactance

To reduce the winding reactance, a design with no tooth tip and increased air-gap length
was investigated as D3. Fig 4-16 compares the two tooth schematics of the D2 and D3
designs, while Fig 4-17 shows the cross-sectional view of the one pole FEA model of
the D3 design. Since the change from D2 to D3 involves simply removing the tooth tips
and not extending the tooth body to fill the gap, the air-gap length increases from 2mm
to 3.6mm.

Removing the stator tooth tips and increasing air-gap length inevitably reduce the
induced back-EMF, and hence this approach to improving load regulation capability
only yields dividends when the reactance reduction is larger than the induced back-
EMF reduction. Even if this condition is satisfied, this improved regulation is achieved
at the expense of a reduced power capability due to the compromised back-EMF.

D2 tooth   **D3 tooth**
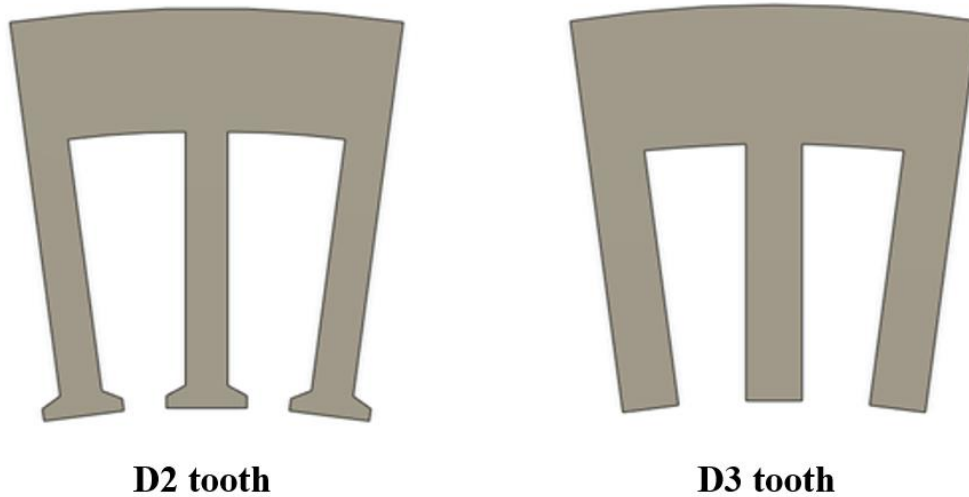
Fig 4-16 Schematics of the stators for the D2 design and D3 design with removal of tooth tip and increased air-gap length.

Table 4-3 shows the voltage regulation performance for D3. As can be seen by comparison with the corresponding data in Table 4-2 for D2, in this case D3 achieves the overlap between the voltage at full-load, minimum speed and maximum endplate off (21.2V) and the voltage at open-circuit, maximum speed and minimum end-plate space-off (23.6V). Hence, the removal of the tooth tips and increased air-gap length allows D3 to meet the voltage regulation requirements.
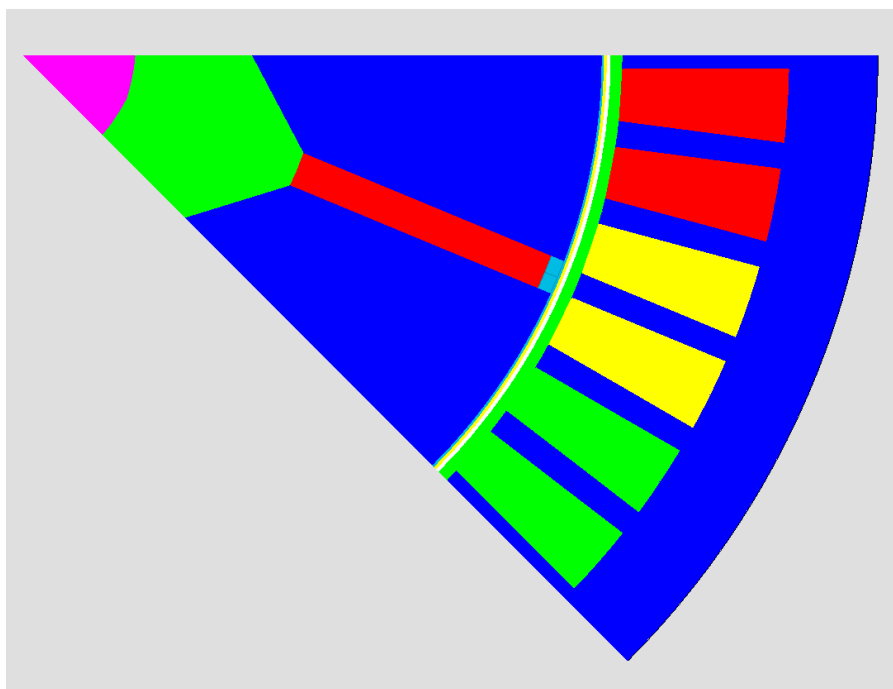
Fig 4-17 Cross-section of D3 design

To investigate whether the output voltage meets the MIL704 standard [15], the distortion factors of the D3 are evaluated from the simulations. The variation in the distortion factor at the four corner operating points are listed in Table 4-3. The distortion factors of all the operation points in Table 4-3 are above 20%, which is well beyond the required distortion factor limit of 5% for aerospace applications [15]. It is interesting to note that the distortion factor is much worse at the full-load and full-speed condition.

Table 4-3 D3 DESIGN PERFORMANCE SUMMARY WITH PER-TURN DESIGN

	Operating point	Phase voltage fundamental (rms)		Distortion factor	
		0.25mm space-off	*4mm space-off*	*0.25mm space-off*	*4mm space-off*
Open-circuit	12,000rpm	21.2V	63.1V	22.7%	22.2%
	5,400rpm	11.4V	28.4V	22.7%	22.2%
Full load	12,000rpm	8.2V	26.9V	51.6%	59.3%
	5,400rpm	6.7V	23.6V	29.8%	33.9%

4.4 Output power quality

From the previous sections, the third iteration of the design (D3) meets the requirements for the flux turn-down capability and load regulation capability. This section will focus on refinements to the design to meet the power quality requirement.

The phase back-EMF waveforms at open-circuit, 4mm space-off and 5,400 rpm for D3 are shown in Fig 4-18, with corresponding harmonic spectra in Fig 4-19. It is important to note that the grounding of the star point allows a significant third harmonic to be present in the phase voltages. The third order harmonic magnitude is ~25% of the fundamental counterpart, while the 5th, 7th, 9th, 11th and 13th order harmonics reach 4.8%, 2.9%, 5.5%, 6.4% and 4.8%, respectively.
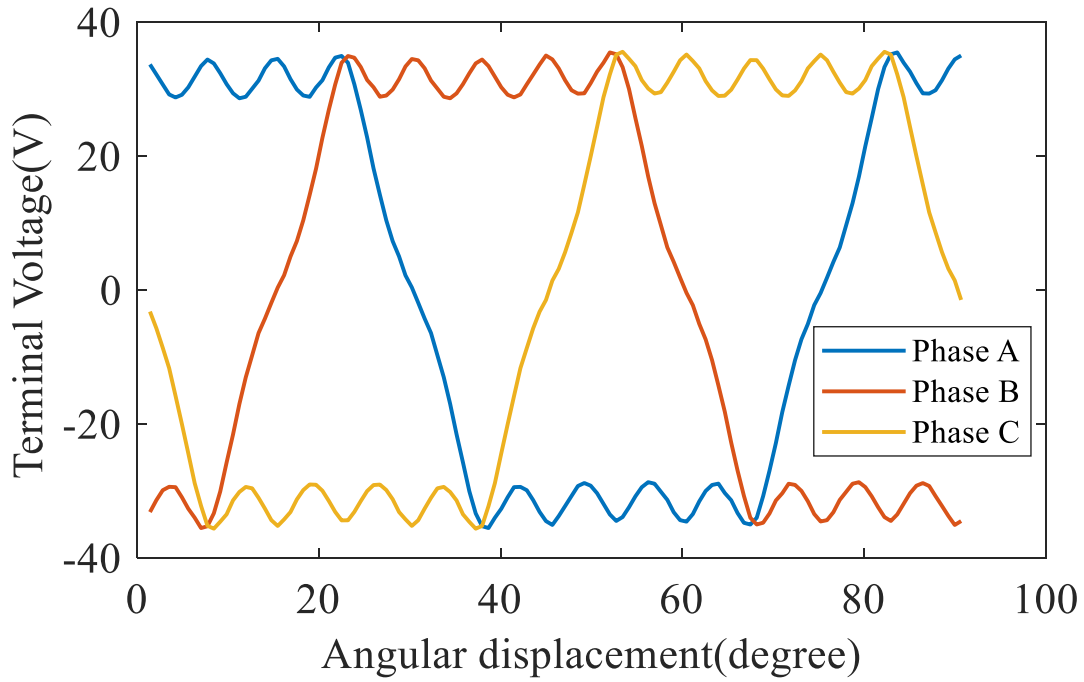
Fig 4-18 D3 open-circuit output phase voltage waveform at 4mm space-off and 5,400 rpm
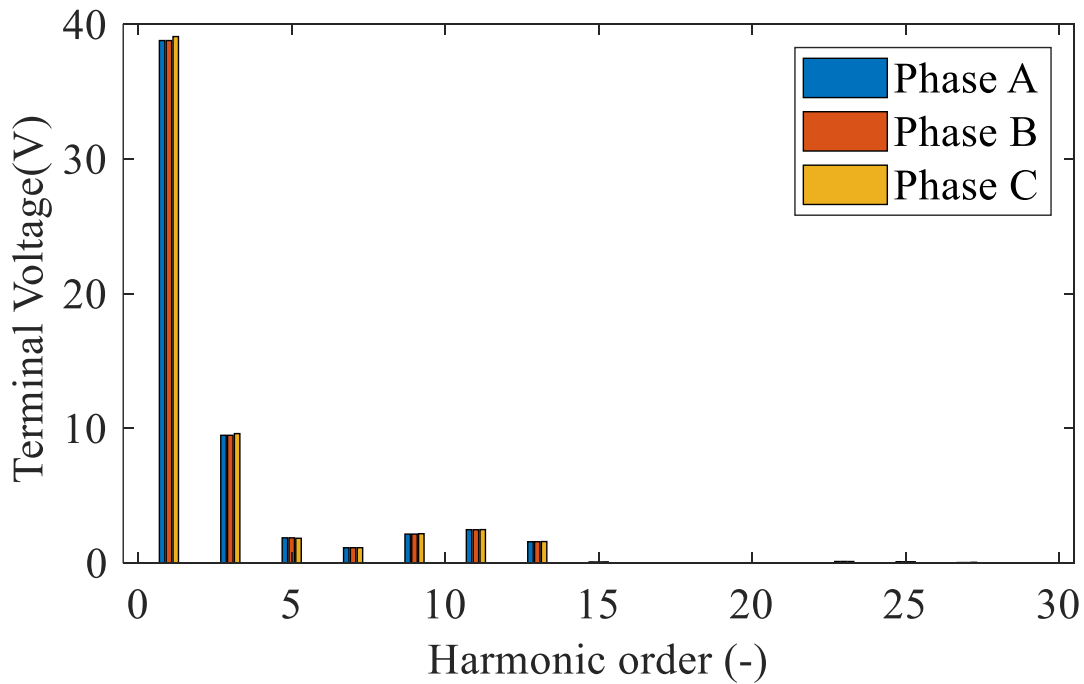
Fig 4-19 D3 open-circuit output phase voltage spectra at 4mm space-off and 5,400 rpm

In order to reduce the dominant 3rd harmonic, shorting pitch of the winding was investigated. Note that short pitching compromises the fundamental winding factor and hence the output power capability. Table 4-4 lists the key winding factors with full pitch,

one slot short pitch and two slots short pitch for 48 slot, 8-pole winding configurations. It can be observed that a one slot short pitch can reduce the 3rd harmonic winding factor from 0.707 to 0.5 while the fundamental winding factor drops from 0.966 to 0.933. Two slots short pitch can reduce the 3rd harmonic winding factor to zero while the fundamental winding factor drops to 0.837.

Table 4-4 Winding factor s for a 48 slot, 8-pole stator winding

Harmonic	Fully pitched	Short-pitched by one slot	Short-pitched by two slots
Fundamental	0.966	0.933	0.837
3rd	0.707	0.500	0.000
5th	0.259	0.067	0.224
7th	0.259	0.067	0.224
9th	0.707	0.500	0.000
11th	0.966	0.933	0.836
13th	0.966	0.933	0.836

4.4.1 One slot short-pitched winding

Given the result shown in Fig 4-19 for D3, the total distortion factor is approximately 30%, most of which is caused by the 3rd order harmonic in the phase back-EMF, while the short pitch winding configurations can reduce the 3rd order harmonic winding factor, as shown in Table 4-4. Hence, this section investigates the design with one slot short-pitched winding while Section 4.4.2 will use two slots short-pitched winding.

The schematic of the machine with one slot short-pitched winding (designated as D4) is shown in Fig 4-20. The distortion factors at open-circuit and full-load conditions are 19.6% and 26.1% respectively, which are still much higher than the required 5% distortion factor limit. Hence, the two slots short-pitched winding configuration was explored despite the lower fundamental winding factor and is discussed in the next section.
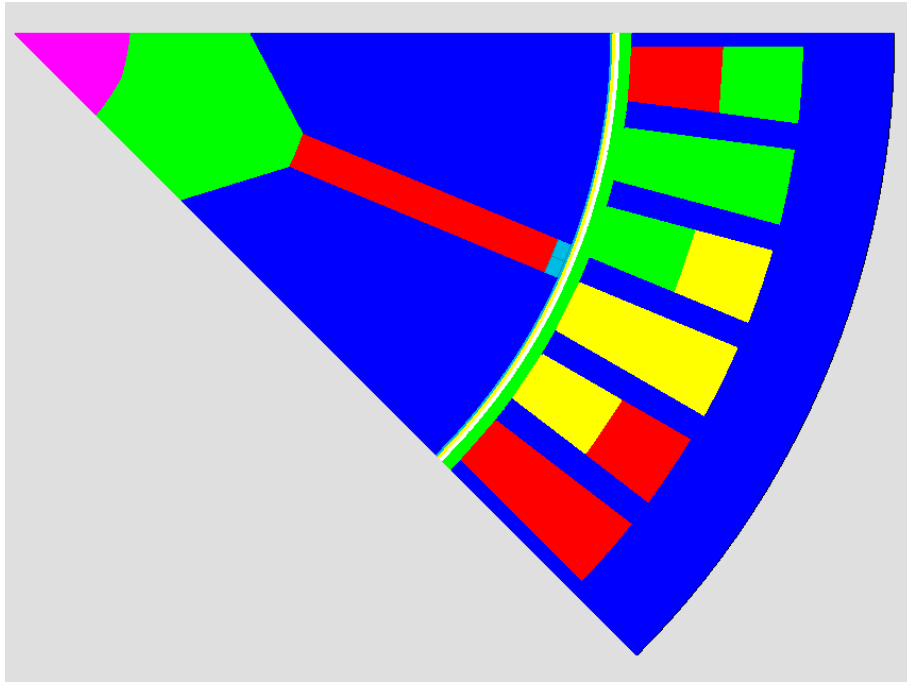
Fig 4-20 Schematics D3 design with one slot short-pitched winding (D4)

4.4.2 Two slot short-pitched winding

In order to further reduce the distortion factor, the two slots short-pitched winding configuration is applied to the D3 model and the schematic of the machine designed in this section (designated as D5) is shown in Fig 4-21.
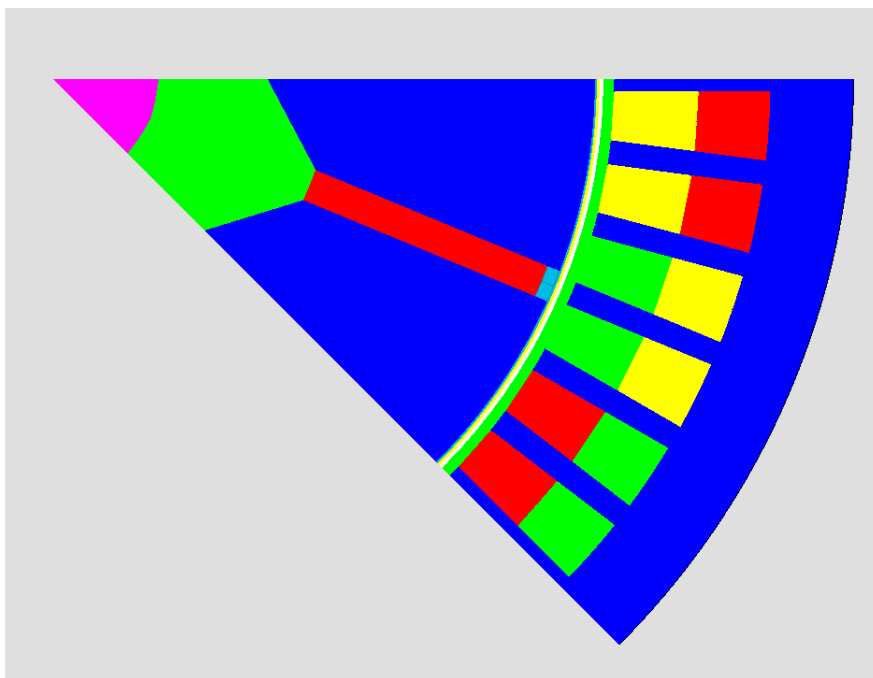
Fig 4-21 Schematic of design D5 (based on D3 design but with two slot short-pitched winding)

The phase volage waveforms and harmonic spectra at 4mm space-off and 5,400 rpm for the design D5 (D3 design but with two slots short-pitched winding) are shown in Fig 4-22 and Fig 4-23. It can be seen that the two slots short-pitched winding configuration fully eliminates the 3rd order harmonic contents of the phase voltages at both open-circuit and full-load conditions. The distortion factors at open-circuit and full-load conditions are 9.5% and 2.3% respectively.
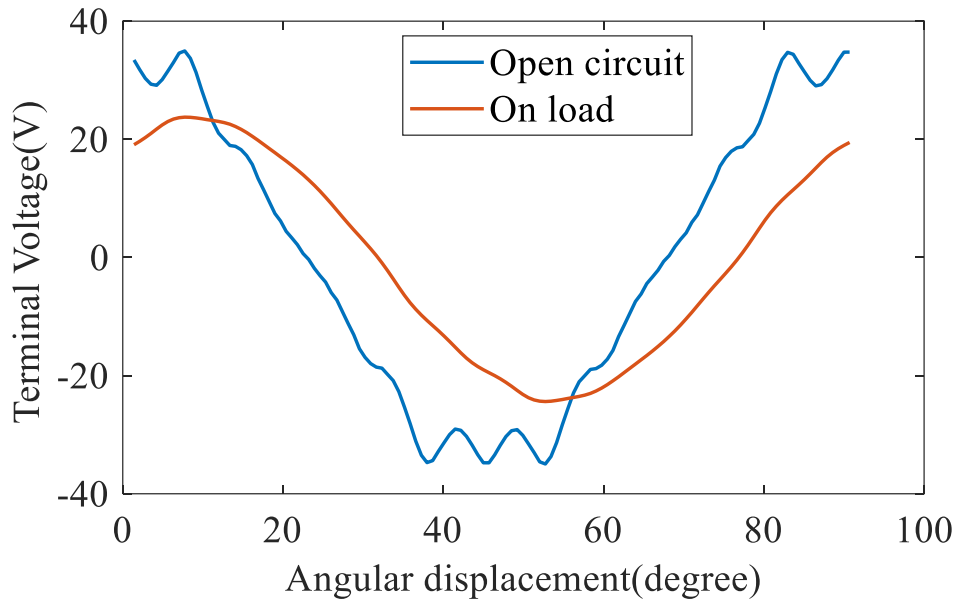
Fig 4-22 D5 output phase voltage waveform at 4mm space-off and 5,400 rpm (Phase A)
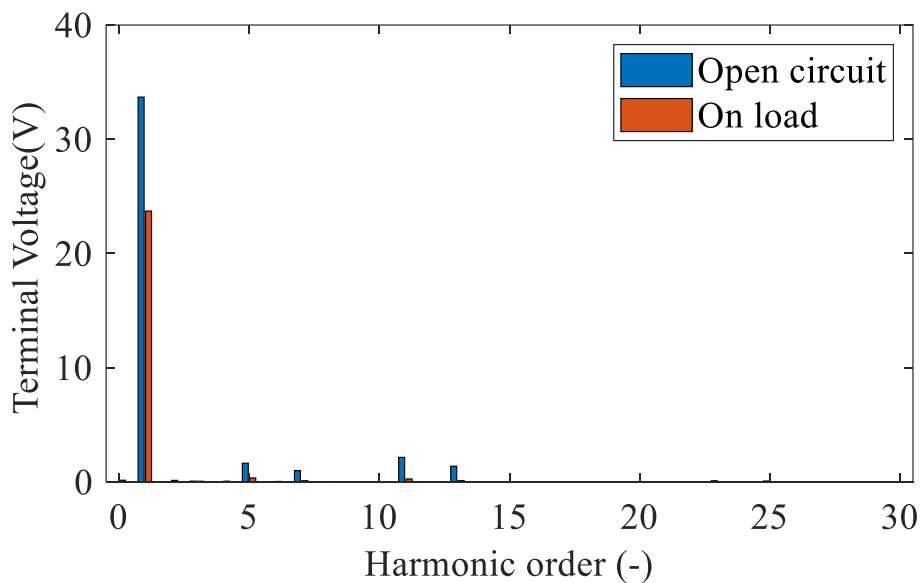
Fig 4-23 D5 output phase voltage harmonic spectrum at 4mm space-off and 5,400 rpm (Phase A)

Table 4-5 compares the distortion factors of the designs with fully-pitched, one slot short-pitched, and two slots short-pitched winding configurations. It can be seen that compared to the design with fully-pitched winding, the short-pitched winding approaches can effectively reduce the distortion factor, but they are still beyond the required distortion factor limit 5% as per MIL704 standard [15].

Table 4-5 Harmonic distortion comparison with various coil spans at 5,400rpm and 4mm space-off for D5 design

	Fully pitched	Short-pitched by one slot	Short-pitched by two slots
Open-circuit voltage (rms)	28.4V	26.8V	23.9V
Full load voltage (rms)	23.6V	17.5V	16.8V
Open-circuit distortion factor	22.2%	19.6%	9.5%
Full load distortion factor	33.9%	26.1%	2.3%

4.4.3 Rotor pole shaping

Given the maximum distortion factors for the design with both one slot (D4) and two slots (D5) short-pitched windings are still beyond the required distortion factor limit, as shown in Section 4.4.2, this section describes an investigation the rotor pole shaping as a method to further reduce the distortion factor.

For this investigation, in which the key quantity is the shape of the voltage waveform, all the optimisations were performed using 2D finite element model running at 5,400 rpm. Whereas this will tend to overestimate the amplitude of phase voltage by around 15% according to previous comparison shown in Table 3-4, it still provides a useful means of rapidly assessing many different rotor profiles.

4.4.3.1 Rotor pole profile for optimisation

The rotor in both D4 and D5 are cylindrical rotors in which the pole-pieces between magnets have a fixed outer radius. In order to vary the rotor pole piece profile, a method was chosen based on specifying a number of points around the rotor periphery whose radius can be varied.

Fig 4-24 shows the schematic of one rotor pole with the definitions of various segments of arcs AB, BC, DE, and EF. Points A and F are fixed, while the radius and angular position of points B and E can be varied. Points C and D are determined by the magnet insert width. Therefore, the polar coordinates of points B and E, along with the depth of the magnet insert, are the five geometric parameters to be optimised.
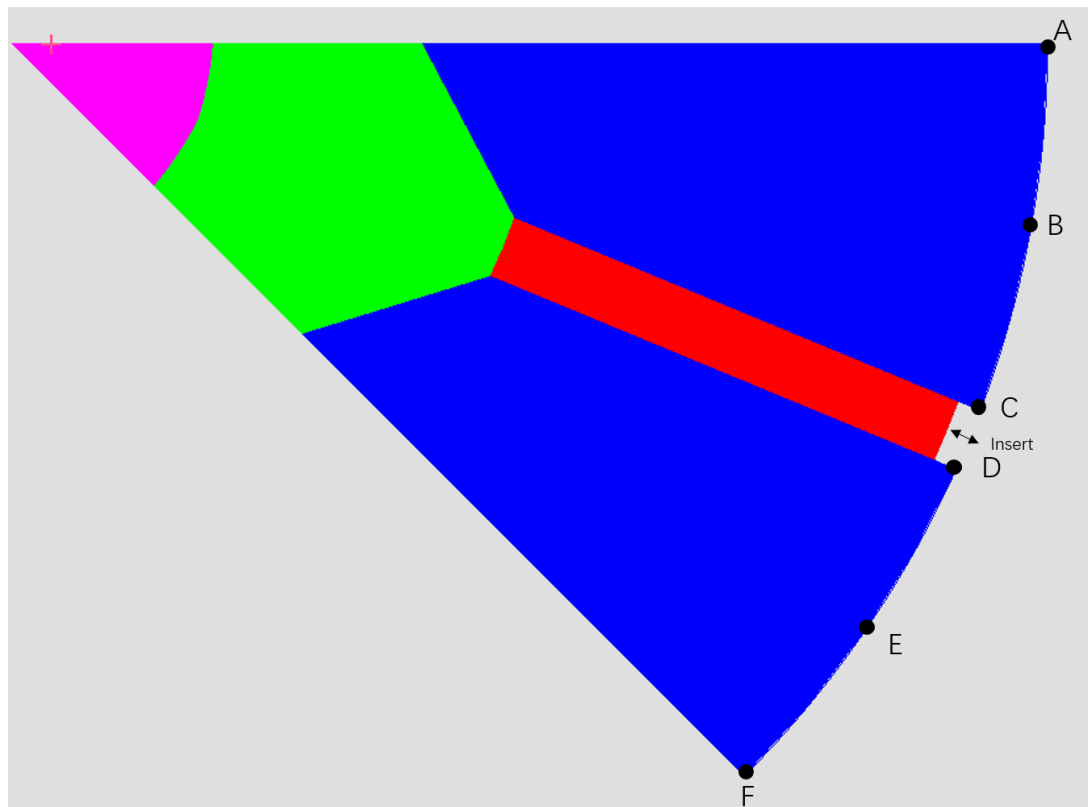
Fig 4-24 Schematics of rotor pole improved segments (D5)

4.4.3.2 Optimisation objective and constrains

Whereas the main goal of this rotor pole shaping is to reduce the distortion factor, the actual optimisation objective is to maximise the fundamental voltage while the meeting the 5% threshold on the distortion factor is set as an optimisation constraint. This is minimising the distortion factor below the required limit can significantly compromise the fundamental voltage (or power capability). As an example, a design with 1% distortion factor does not bring valuable benefits compared to a design with 4% distortion factor, since both meet the required distortion factor limit of 5%, while the design with 1% distortion factor may well compromise electromagnetic performances to achieve such a low distortion factor. Therefore, this optimisation uses maximisation

of the fundamental voltage as the optimisation objective while using ≤5% distortion factor as an optimisation constraint.

The global optimisation tool used was Altair Hyperstudy with algorithms as one of approach that based on global response surface. The details of this algorithm can be found in [53]. Table 4-6 lists geometric parameter variation ranges for the global optimisation and those values are determined by avoiding the geometric violation. The machine

Table 4-6 Boundary value for parameters scan variation in mm unit

	Lower bound	Current	Upper bound
Point B radians (degree)	6	11.45	14
Point E radians (degree)	6	11.45	14
Point B radius (mm)	60	64.75	70
Point E radius (mm)	60	64.75	70
Magnet insert length (mm)	3	6	8

4.4.3.3 Global optimisation for open-circuit condition

This section describes the global optimisation for open-circuit conditions with the objective and constraint described in Section 4.4.3.2, i.e. using the maximisation of fundamental phase voltage at open-circuit condition as the optimisation objective and using ≤5% distortion factor at open-circuit condition as the optimisation constraint.

The iteration process of geometric parameters during the optimisation is illustrated in Fig 4-25 and Fig 4-26. It can be seen that after 6th iterations, the predicted geometric parameters have negligible variations. Similar trends can be observed in the variation trends of the distortion factor and the fundamental phase voltage during the optimisation, as illustrated in Fig 4-27 and Fig 4-28. They indicate that within the given constraints, no further improvements of the fundamental phase voltage can be found after 6th iteration. Considering the distortion factors for all the iterations are within 5%, an increased trend of the fundamental phase voltage before it reaches the saturation means the optimisation is effective in maximising the fundamental phase voltage while satisfying the optimisation constraints.
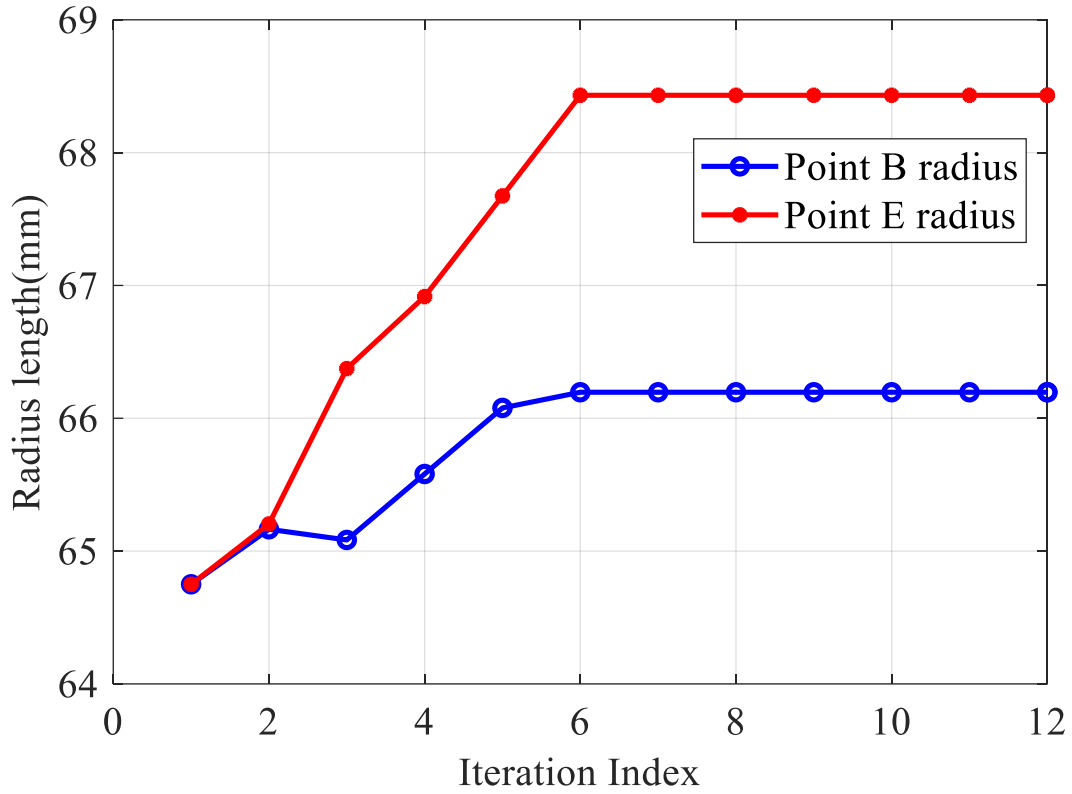
Fig 4-25 Iteration plot for radius of anchor point B and E
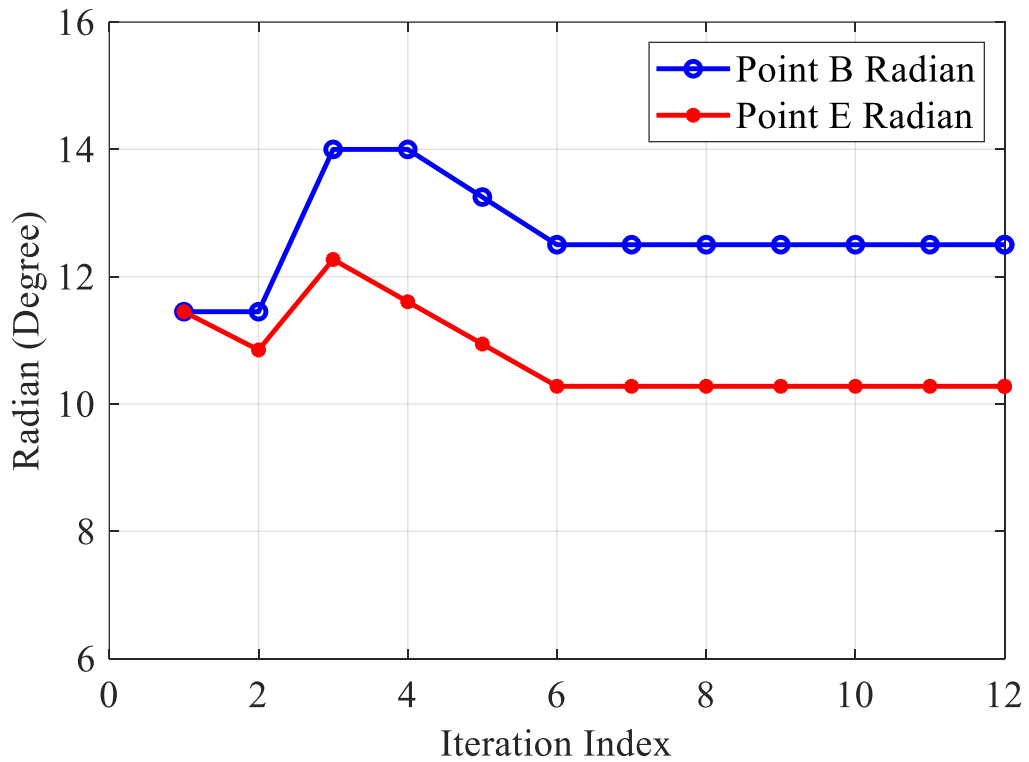
Fig 4-26 Iteration plot for radian of anchor point B and E
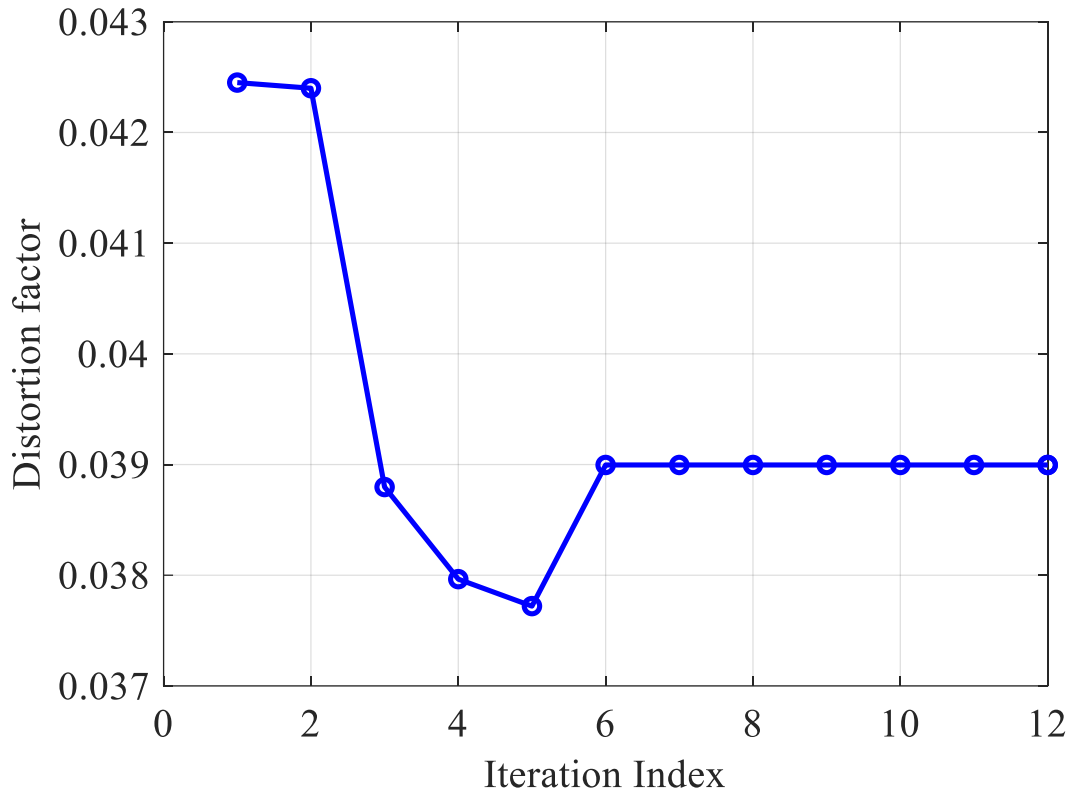
Fig 4-27 Iteration plot for distortion factor
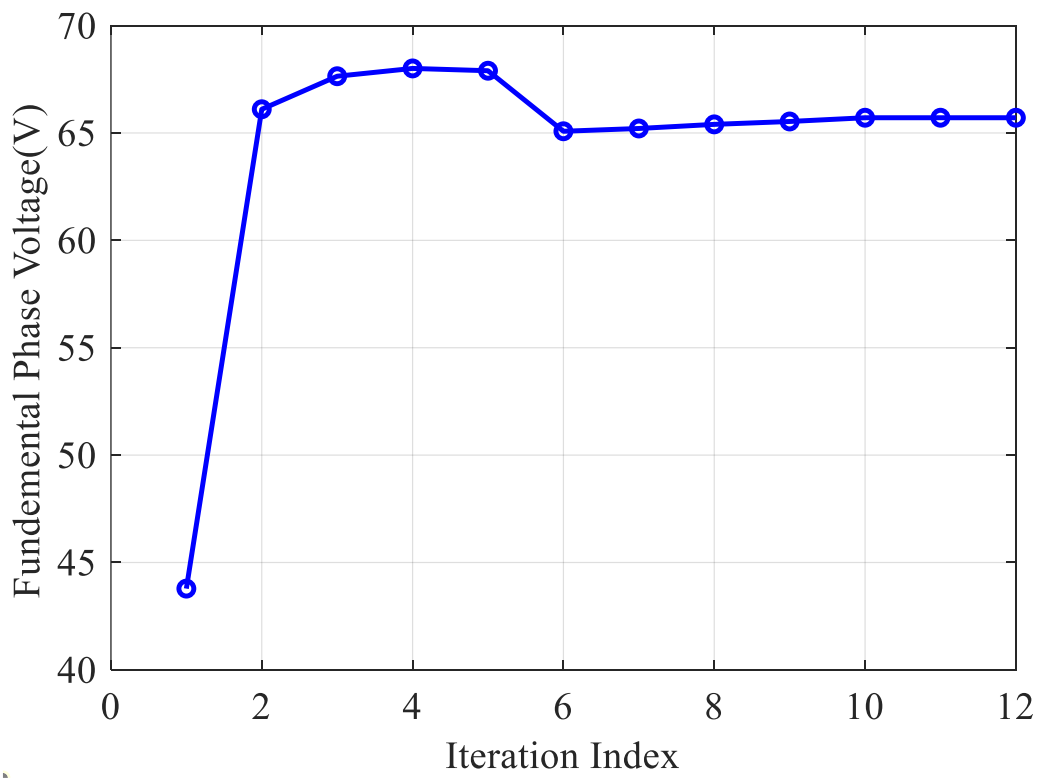
Fig 4-28 Iteration plot for fundamental phase voltage

Table 4-7 lists the optimised geometric parameters, with which the optimised design can achieve 65.2V fundamental phase voltage with 3.9% distortion factor. This compares with a fundamental phase voltage of 47.3V and a distortion factor of 9.5% prior to optimisation of the rotor profile

Table 4-7 Optimized geometric parameters with an optimization at open-circuit condition

	Value
Point B radians (degree)	12.5
Point E radians (degree)	10.0
Point B radius (mm)	66.2
Point E radius (mm)	68.4

4.4.3.4 Global optimisation considering both open-circuit and full load conditions

Based on the optimised design in Section 4.4.3.3, the next stage included the full load condition performances into the global optimisation process to meet the power quality constraints for both open-circuit and full load conditions. In other words, the optimisation objective is the maximise the fundamental phase voltage at both conditions with weight factor as 1:1. while the optimisation constraints are the distortion factors at both open-circuit and full load conditions ≤ 4% (1% margin is considered in this series of optimisations).

The optimised geometric parameters considering both open-circuit and full load conditions are listed in Table 4-8, with which the optimised design can achieve 65.8V the fundamental phase voltage with 3.5% distortion factor at open-circuit condition, and 43.9V fundamental phase voltage with 1.4% distortion factor at full load condition. As previous discussed, the amplitude of phase voltage fundamental components will be an overestimate due to the use of a 2D finite element model.

Table 4-8 Optimized geometric parameters for optimization for both open-circuit and full load conditions

	Value
Point B radians (degree)	7.69
Point E radians (degree)	6.03
Point B radius (mm)	65.22
Point E radius (mm)	67.02

This optimised rotor geometry profile is shown in Fig 4-29. It can be seen that the rotor profile is asymmetric as the optimised coordinates for points B and E are different, as shown in Table 4-8. This asymmetric design is acceptable for generator applications given an aircraft engines rotate in one direction only.
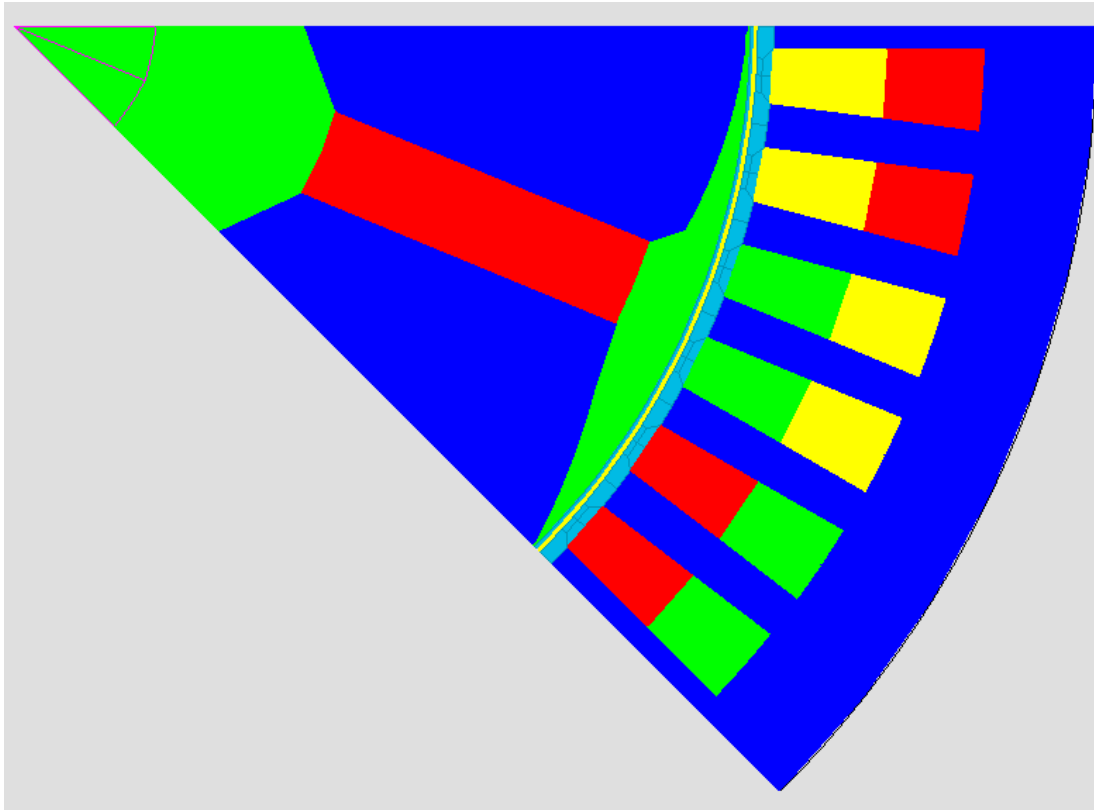
Fig 4-29 Schematic of machine cross-section after global optimization

4.4.3.5 Optimisation of a grounded machine

The global optimisation was based on the D4 geometry and a floating star point, which intrinsically has a greater harmonic content. Another optimisation based on D5 and a grounded neutral configuration was performed and is reported in this section with the same approach described in Section 4.4.3.4.

Fig 4-30 compares the cross section of the rotor pole pieces, while Fig 4-31 shows a superposition of the two geometries to highlight the difference via the overlapped view. Slight differences between the rotors of those two optimised designs can be observed but the asymmetric nature of the rotor is pronounced in both cases. Regarding the fundamental phase voltage, it changes from 65.8V to 61.3V at open-circuit, and changes

from 43.9V to 43.8V at full load. In terms of the distortion factor, it changes from 3.5% to 3.2% at open-circuit, and changes from 1.4% to 3% at full load. Given the distortion factor meets the requirements, the optimisation based on D5, grounded neutral balanced distortion factor on open-circuit and full load condition but give lower terminal voltage output which is less desirable.

Table 4-9 Optimized geometric parameters

	Optimisation based on D4 and ungrounded neutral	Optimisation based on D5 and grounded neutral
Point B radians (degree)	7.69	8.60
Point E radians (degree)	6.03	5.40
Point B radius (mm)	65.22	64.70
Point E radius (mm)	67.02	68.39

Design based on D4 and ungrounded neutral

Design based on D5 and grounded neutral
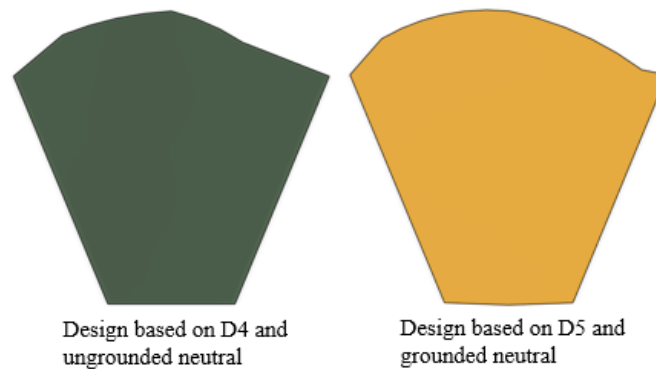
Fig 4-30 Rotor shape comparison for the optimized design based on D4 and ungrounded neutral and that based on D5 and grounded neutral
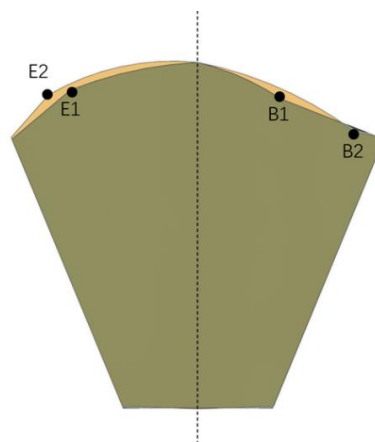
Fig 4-31 Overlapped view of the rotor profile of the optimized design based on D4 and ungrounded neutral and that based on D5 and grounded neutral

4.5 Final design

The optimised design based on D4 and ungrounded neutral configuration is selected as the final design, termed as D6 even though it is to be used with a grounded star-point. Given the previous comparison between the D4 with ungrounded neutral machine and D5 with grounded neutral machine showing the former configuration can produce higher output terminal voltage.

It is important to clarify that different machine structure, which defined by distinct winding configurations and grounding topologies have been globally optimized to obtain the corresponding optimal rotor shape. When the distortion factor performance is similar, the D4 ungrounded neutral configuration exhibits higher output terminal voltage.

Therefore, the rotor shape corresponding to this structure is selected as the final rotor shape. However, as described in section 1.3.3, aerospace generators are practically grounded neutral. The electromagnetic performances with grounded star point are evaluated using 3D FEA in the following sections.

4.5.1 D6 performances with per-turn design

As discussed in Section 3.3.3 , the output voltage predicted by 3D FEA can be ~10% lower than that of the 2D FEA due to end effects. Moreover, the introduction of endplate to the model will also lead to the decrease in the output voltage, even with 4mm space off, as demonstrated previously in Section 0. Hence, 3D FEA is employed in this section to evaluate the electromagnetic performances of the D6 design. The analysis in this section is based on a per-turn design.

The open-circuit phase voltage waveforms and harmonic spectra at the four operating points at the corners of the operation envelope are shown in Fig 4-32 and Fig 4-33, respectively. As would be expected, the 5th and 11th order harmonics are the significant harmonics with their percentage values with respect to the fundamental being 2.4% and 2.6%, respectively. The full-load phase voltage waveforms and spectra at 4 corners of the operation envelope are shown in Fig 4-34 and Fig 4-35 respectively. It can be seen that all the voltage harmonics at full-load condition are negligible.
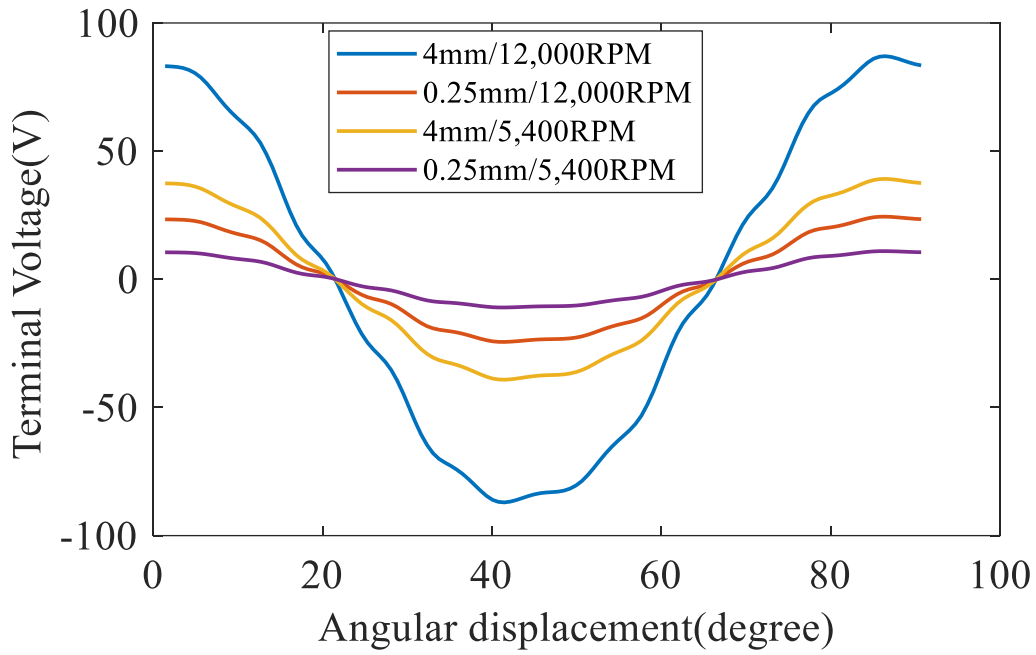
Fig 4-32 Open-circuit output voltage phase A waveform of D6 (per-turn) using 3D
FEA
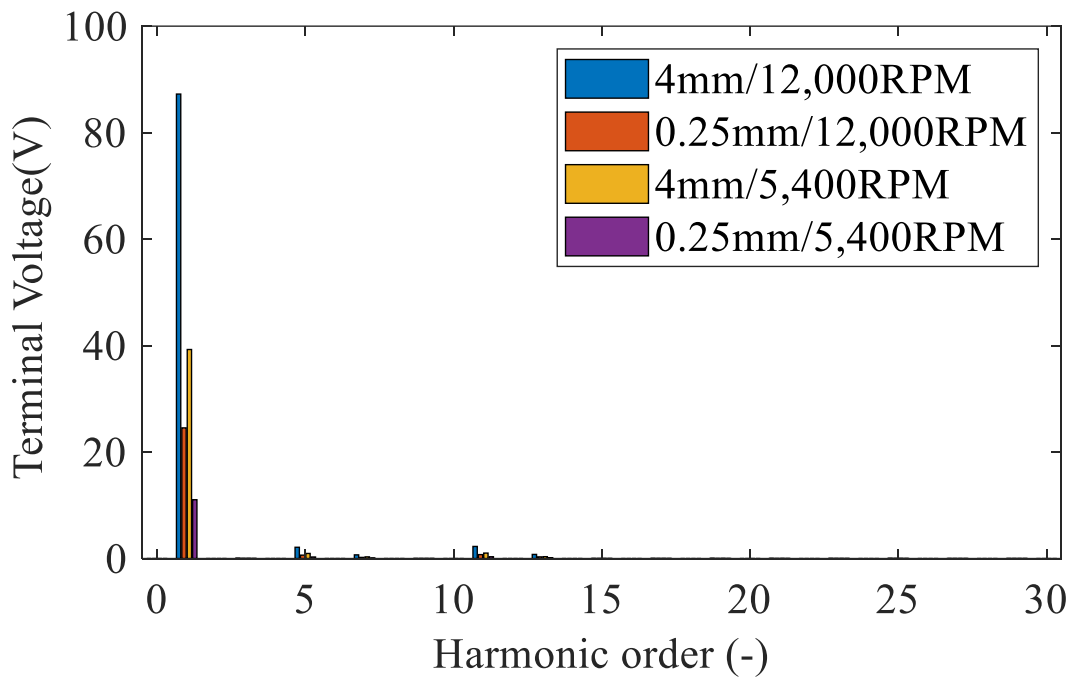
Fig 4-33 Open-circuit output voltage phase A spectrum of D6 (per-turn) using 3D
FEA
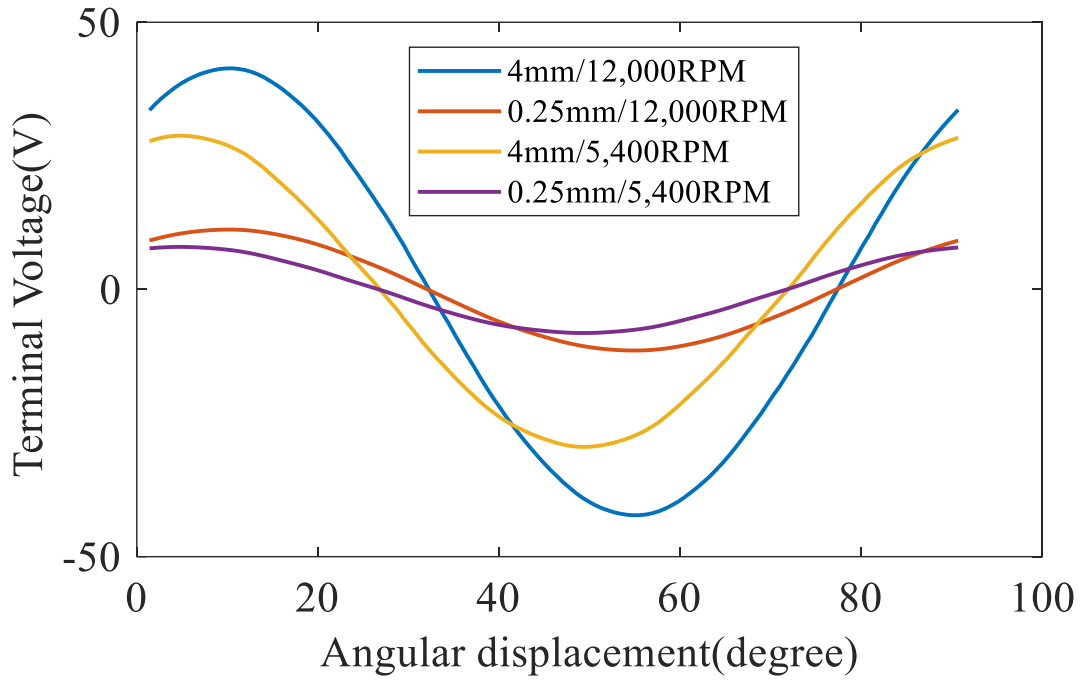
Fig 4-34 Full-load output voltage phase A waveform of D6 (per-turn) using 3D FEA
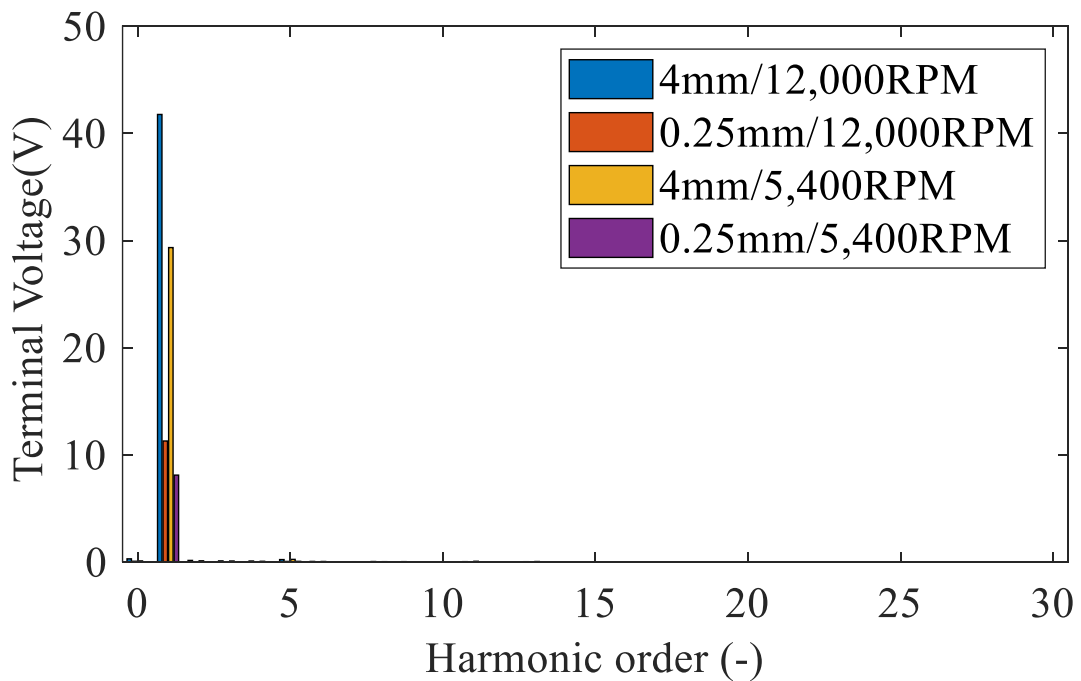
Fig 4-35 Full-load output voltage phase A spectrum of D6 (per-turn) using 3D FEA

Table 4-10 summarises the fundamental phase voltages (in RMS) and the distortion factors of D6 with per-turn design at all those operation points. At open-circuit condition, the distortion factors are 3.7% at 4mm space-off and 4.2% at 0.25mm space-off. At full-load condition, the distortion factors are 1.4% at 4mm space-off and 1.3%

at 0.25mm space-off. All those distortion factors are within 5%. Therefore, D6 design meets the distortion factor requirements specified in MIL704 standard. The fundamental phase volage under open-circuit condition at 12,000rpm and 0.25mm space-off is 17.4V, lower than that at full load, 5,400rpm and 4mm space-off, 20.7V. Therefore, D6 design can meet the voltage regulation requirements after scaling the turn number based on the current per-turn design. This scaling will be performed in the next section.

Table 4-10 D6 DESIGN PERFORMANCE SUMMARY WITH PER-TURN DESIGN

	Operating point	Phase voltage fundamental (rms)		Distortion factor	
		0.25mm space-off	*4mm space-off*	*0.25mm space-off*	*4mm space-off*
Open-circuit	12,000rpm	17.4V	61.7V	4.2%	3.7%
	5,400rpm	7.8V	27.8V	4.2%	3.7%
Full load	12,000rpm	8.0V	29.5V	1.3%	1.4%
	5,400rpm	5.7V	20.7V	1.3%	1.4%

4.5.2 The number of turns calculation

Given that the generator is required to maintain an RMS phase voltage between 108V and 118V, as set out in the standard [15], the number of turns per coil needs to be scaled up to meet this required voltage range.

First, at open-circuit and maximum speed (12,000 rpm) condition, with the endplate positioned at the minimum space-off (0.25mm in this regard), the output phase voltage must not exceed 118V. This is because, in a direct-line connected generator system referred in this thesis, the voltage amplitude is regulated exclusively by the position of the endplate, and a space-off of 0.25mm indicates that the endplate has reached its limit for reducing the voltage. Consequently, if the output voltage surpasses 118V, it would indicate that the voltage has exceeded the range controllable by the endplate.

Similarly, at full-load minimum speed (5,400 rpm), with the endplate set to the maximum space-off (4mm in this regard), the output phase voltage must not drop below 108V. If the voltage falls below this threshold, adjusting the endplate to further space-off would have no effect on increasing the output voltage.

Based on these two conditions, the number of turns per coil is calculated to be 6 turns. This allows the machine to have an output phase voltage of 104.4V at open-circuit and 12,000 rpm with the endplate at the minimum space-off, thereby meeting the criterion of being less than 118V. In order to bring the voltage into the required range, the space off can be increased. Additionally, the machine can output 124.2V phase voltage at full-load and 5,400 rpm with the endplate at the maximum space-off, thus satisfying the criterion of being greater than 108V.

4.5.3 Final machine performances

After scaling up the number of turns per coil to meet the voltage range requirements, the fundamental phase voltages and distortion factors are summarized in Table 4-11. Compared to the results of the per-turn design shown in Table 4-10, the voltage results in Table 4-11 are linearly scaled up by a factor of 6 while the distortion factors do no changes. Hence, the conclusions drawn in this section remain the same as those in Section 4.5.1, i.e. D6 design meets both the voltage regulation requirements and the distortion factor requirements, with cogging torque at 0.2% of rate torque as 25Nm given the torque ripple is about 15.02%

Table 4-11 D6 DESIGN PERFORMANCE SUMMARY WITH 6-TURN DESIGN

	Operating point	Phase voltage fundamental (rms)		Distortion factor	
		0.25mm space-off	*4mm space-off*	*0.25mm space-off*	*4mm space-off*
Open-circuit	12,000rpm	104.4V	435.0V	4.2%	3.7%
	5,400rpm	46.8V	166.8V	4.2%	3.7%
Full load	12,000rpm	48.0V	177.0V	1.3%	1.4%
	5,400rpm	34.2V	124.2V	1.3%	1.4%

4.6 The power capability discussion

The motivation of this research is to investigate whether a direct-line connected generator can achieve the voltage regulations at various speed and load conditions to meet the grid demand in aerospace applications without using power convertors. Despite of the benefits brought by the direct-line connected generators in terms of eliminating the need for a power converter, improved fault management and reduced electromagnetic interference, the mechanical regulation mechanism investigated in this thesis may compromise the overall power density of the generator system. However, these benefits come at the expense of some compromises in power density. This section discussed the power capability of the D6 machine and the aspects that have an impact on its power density.

4.6.1 Power capability baseline

The initial reference model was based on the convertor fed SILOET machine with a 100kW output power at 14,677 RPM rated speed [50]. Designs D1-D6 of the variable flux generator have maintained the same rotor volume and hence a direct comparison of the power ratings.

The first factor which will diminish the power capability is that for a direct-line connected generator, the operation frequency range need to match 360 to 800 Hz [15]. Given the pole pair number selected in this research is 4, the speed range can be derived, i.e. 5,400 rpm to 12,000 rpm. Given that the power density of an electrical machine is to a reasonable approximation directly proportional to its operation speed, the speed difference between the direct-line connected generator operating point of 5,400rpm compared to the 14,677rpm of the SILOET machine means a 63.2% drop in the power density for the direct-line connected generator assuming they achieve the same torque density.

4.6.2 Power capability summary

The power capability of each of the design iterations D1-D6 is summarized in Table 4-12 running at the 5400rpm base speed with maximum space-off.

It is important to note that for the D1 model, the terminal load that achieves maximum power output is 0.25 ohms, whereas for models D2 to D6, the corresponding maximum output load is 0.1 ohms. Considering that the iteration from D1 to D2 involved changes in the aspect ratio and an increase in the main air gap, a D1 model with a 2mm air gap was separately recorded to distinguish the effects of these two factors on the power capability. As can be seen from Table 4-12, there is a very significant drop in output power between the high-speed converter connected SILOET machine in [50] and the direct connected machine.

Table 4-12 Power capability of per turn model iterations at 5,400 rpm with maximum space-off

	Terminal voltage rms (V)	Distortion factor (THD)	Output power(kW)
SILOET baseline at 14,677rpm	Not provide in [50]	Converter feed	100
D1	44.3V	28%	23.5
D1 with 2mm airgap	21.1V	29%	13.3
D2	18.8V	30%	10.7
D3	17.6V	30%	9.3
D4	17.5V	26%	9.1
D5	16.8V	23%	8.4
D6	20.7	1.3%	13

4.6.3 Power capability reduction due to the optimization

A large proportion of the reduction in power density is due to the reduced speed imposed by the combination of pole number and the lower end of the VF range. The baseline SILOET machine would have a power rating of 36.8KW at 5,400rpm for the same torque as its rated 100kW operating point.

The second most significant factor is the increase in the air-gap, which was introduced to achieve sufficient turn-down capability, i.e. make axial leakage of flux. The effects of other features and design changes on power capability are summarized in Fig 4-36. It is interesting to note that the pole shaping not only helps reduce the harmonic content but also increases the power capability by 4.6%.
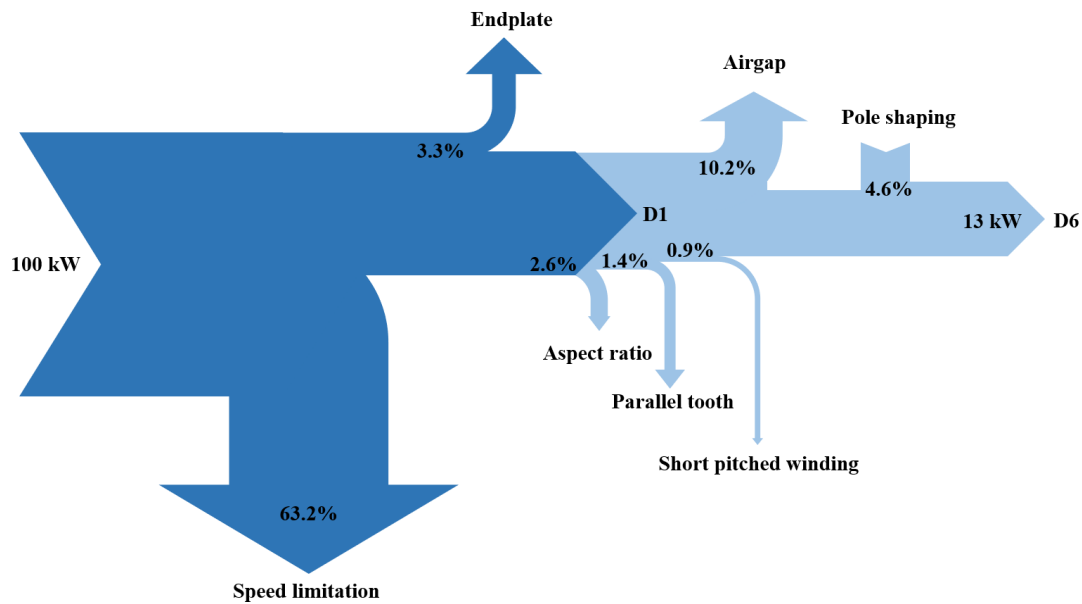
Fig 4-36 Sankey diagram for factors affect power capability

4.7 Impact of star-point grounding

As mentioned in Section 1.3.3, the grounding of electrical systems in aircraft does not fit to the conventional concept of grounding but instead designates a PVR as the reference point. However, for star-connected generators, the connection of the star-point to the PVR is rarely discussed in detail, which directly impacts the output power quality of machines. In this section, the impact of star-point grounding state will be discussed. In Table 4-13 presents the comparison for different design iterations of model with both grounding star-point connection and ungrounding (floating) star-point connection.

As would be expected, for designs which do not eliminate the 3rd harmonics through the winding configuration, i.e. designs D1-D4, there is a significant difference between

the grounded and floated cases. Once, the third harmonic is eliminated in D5 and D6, the two grounding cases come into line, although the rotor pole shaping introduced in the final design D6 is required to bring the distortion factor below the 5% threshold in the standards.

Table 4-13 Comparison of output power quality across different iterations of per turn models at 5400 rpm under maximum space-Off, open-circuit condition with various grounding configurations

	Grounding star-point		Floating star-point	
	Distortion factor	Terminal voltage rms value (V)	Distortion factor	Terminal voltage rms value (V)
D1	27%	64.1	9.9%	62.3
D2	27%	35.9	8.2%	34.8
D3	27%	28.4	9.5%	27.6
D4	20%	26.8	9.5%	26.8
D5	9.5%	23.9	9.5%	23.9
D6	3.7%	27.8	3.7%	27.8

The large distortion factors in the cases with the grounding star-point configuration are caused by the fact that the triplen harmonics in phase back-EMF can generate triplen harmonics in phase terminal voltage considering the phase terminal voltage directly mirrors the voltage from the terminal to the machine neutral point (i.e. $\overrightarrow{V_{an}} = \overrightarrow{V_{aN}}$, as shown in Fig 4-37a). However, for the floating (ungrounded) star-point configuration, as shown in Fig 4-37b, the triplen harmonics in a Kirchhoff's Voltage Law (KVL) loop across any two phases cancel out each other because the three-phase triplen harmonics at any order are in-phase and have the same magnitudes. Hence, the triplen harmonics do not present in the phase terminal voltages (terminal to ground voltages) for a floating star-point configuration.
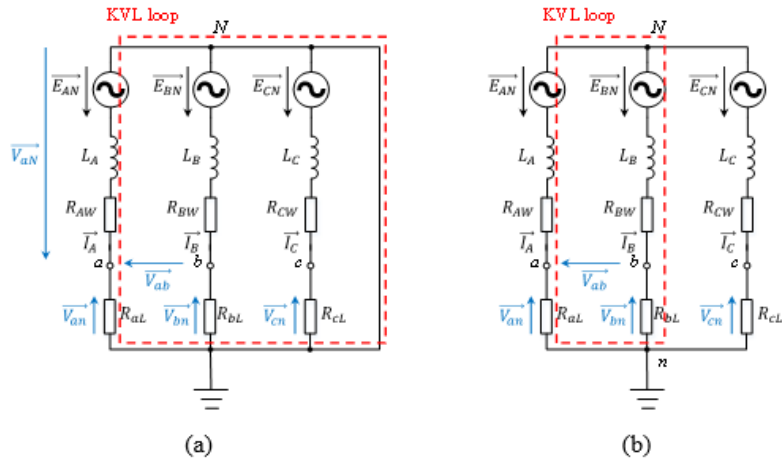
Fig 4-37 Circuit diagrams of the generator with load connection. (a) Grounding star-point. (b) Floating (ungrounding) star-point.

4.8 Machine optimization summary

In this chapter, the operating performance specification deducted from the relevant aerospace standards were used to guide the model optimization, which include improve flux manipulation ability, enhancing the load regulation capability, and the most importantly optimizing output power quality through improvements in winding configuration and rotor geometry. The final model is predicted to meet the target performance requirements.

Chapter 5 - The endplate actuation system

5.1 Introduction

The previous chapters have developed the concept of a variable-flux machine with movable endplates and optimized the electromagnetic performance resulting in an optimized design D6. However, a critical factor in the concept is the mechanism to control the position of the endplates. This requires an additional actuated mechanical structure that integrates with the other parts of the generator. In this chapter, the design of a mechanical structure for manual setting of the endplate position and some preliminary concepts for actuation systems will be presented.

The electromagnetic modelling performed in chapters 3 and 4 has been based on a minimum axial separation of 0.25mm. This very small airgap provides the necessary turn-down ratio for full exploitation of the frequency range but may be difficult to achieve in practice, although it is worth noting that this is a controlled gap and so if a suitable gap sensor was used this could accommodate most geometric and assembly tolerances and thermal expansion. Hence, if operation over the full VFAC range is not required or the power envelope can be met at rated voltage without full turn-down in the voltage, there may not be a need to meet this 0.25mm specification.

5.2 Design requirements and objectives

As discussed previously, the mechanical structure supporting and moving the endplates must ensure its stability during operation of the machine while simultaneously allowing the endplate to controllably move within a stroke of ~4 mm. Any actuation system or manual system for prototype testing must meet several requirements:

Precision and resolution of control - Since the output voltage is highly sensitive to changes in the endplate space-off, the mechanical actuation structure must provide extremely precise control over the displacement of the endplate. In an actuated system, this control of space-off would be done in closed-loop to manage changes in speed, load

and temperature (which affects magnet remanence and so magnet flux).

Rigidity – In order to bring the endplates up very close to the end of the rotor, it is essential that end-plates and the end of the rotor remain parallel. This means that the end-plate displacement mechanism must be rigid and not result in any bending.

High force capability – The arrangement of end-plates and the rotor magnets means that there will be a large attractive reluctance force between the rotor and the endplates at each end. The magnitude of the attractive force was predicted over a range of space-off conditions in the down-selected design D6. Fig 5-1 shows that the predicted force increases dramatically as the gap closes, with a 1650N force at 0.25mm. In order to have control over the end-plate position, there will need to be a method for counteracting this very significant force. It is worth noting that in an implementation with controlled actuation of the endplate position, this force would not need to be matched by the actuator on its own, and for example, stiff springs could be used to down-size the actuator requirements.

For the prototype build, which is described in detail in chapter 6, it was decided to simply use an entirely manual mechanical adjustment of the end-plate position. This would allow the performance of the generator to be measured at a range of fixed set-points. The design of this manual adjustment mechanism is described in Section 5.3 of this chapter. The preliminary design consideration for an actuated system is discussed in Section 5.4 of this chapter.
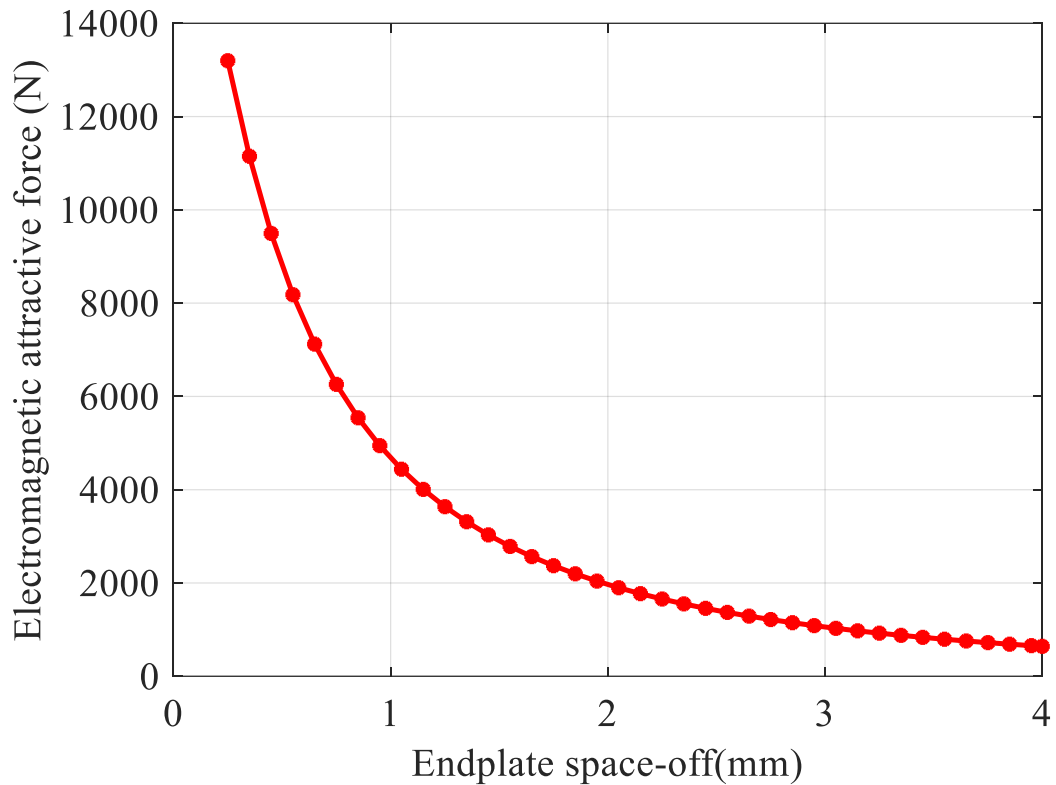
Fig 5-1 Finite element predicted variation of electromagnetic attractive force between each individual endplate and rotor body as a function of space-off

5.3 Design of the manual adjustment system

In order to test the electromagnetic performance of generator D6 it was necessary to design a mechanical mechanism to vary the space of the flux-diverting end-plates from the end face of the rotor. The adjustment of the gap would be performed manually with the rotor stationery and between operating test points. The different components and structures designed to provide a manual adjustment system are described in the following sub-sections.

5.3.1 Endplate retaining structure

The need to bring the magnetic diverting endplate close to the end of the rotor, possibly as close as 0.2 mm which means that the end-plate must be held from the rear as there is no room in the space-off gap to incorporate any mechanical structures. In order to minimize the core losses in the flux-diverting endplate, these would need to be

manufactured from laminated cores, most likely from spiral tape wound circular cores. This means that the cores themselves would not be reliable mechanical structure for incorporating bolts or other fasteners.

The geometry of the optimized generator rotor in design D6 is shown in the cross-section of Fig 5-2. There is a substantial non-magnetic hub between the rotor core and the shaft. The region of the flux-diverting endplate nearer the axis of rotation which faces this hub does not perform a significant electromagnetic function although it could have a small effect on magnetic saturation. There is therefore the possibility to increase the central bore of the flux-diverting endplate up to diameter which is similar to the non-magnetic rotor hub.
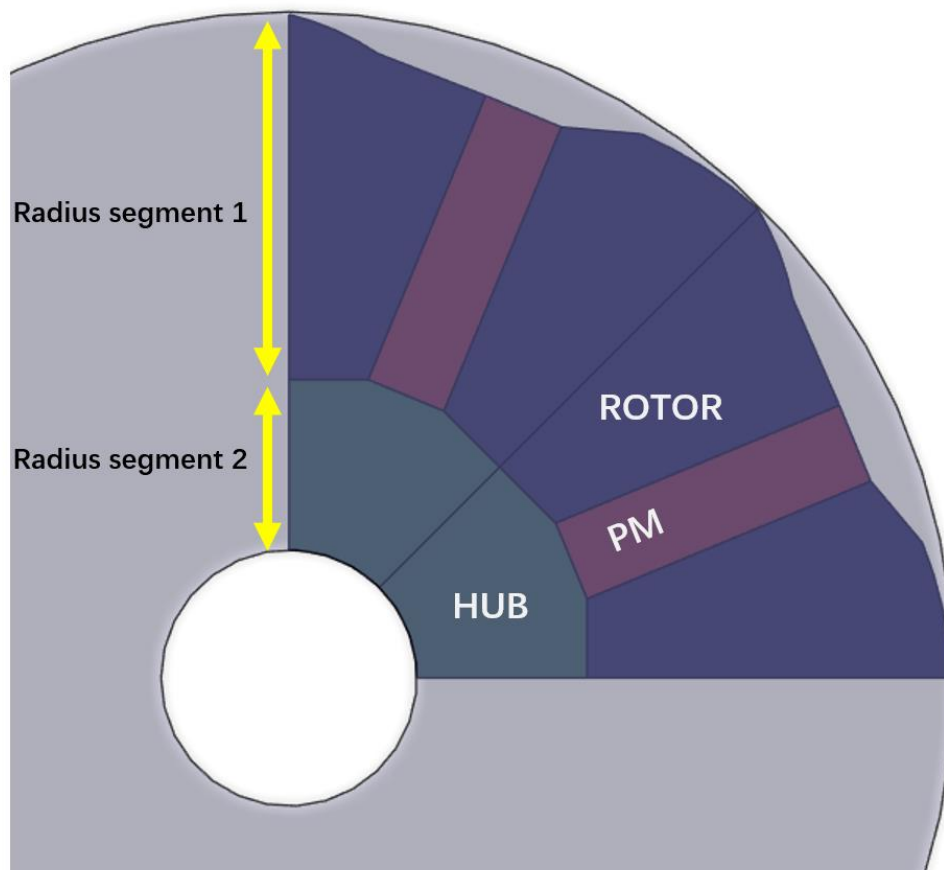
Fig 5-2 End-face geometry of D6 rotor

If a circular hole is introduced into the flux-diverting endplate in the region that faces the non-magnetic rotor hub then the core can be joined to a structural back-plate by tapering the bore of the hole outwards in the direction of the face that faces into the

space-off gap as shown in Fig 5-2. The top face in Fig 5-3 faces into the space-off airgap. This would then be fixed to a non-magnetic back-plate using a matched tapered insert as shown in Fig 5-4. This tapered insert is then bolted into the structural back-plate
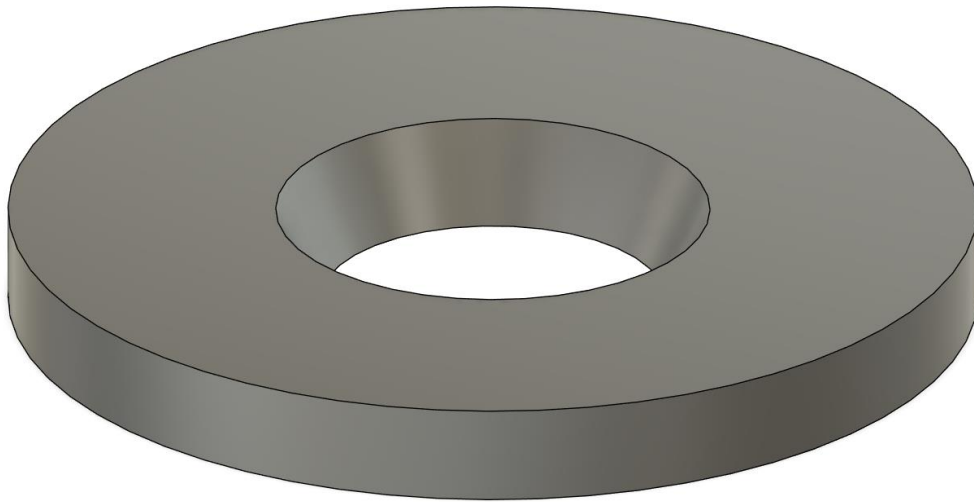
Fig 5-3 Endplate with centre taper angle cutout
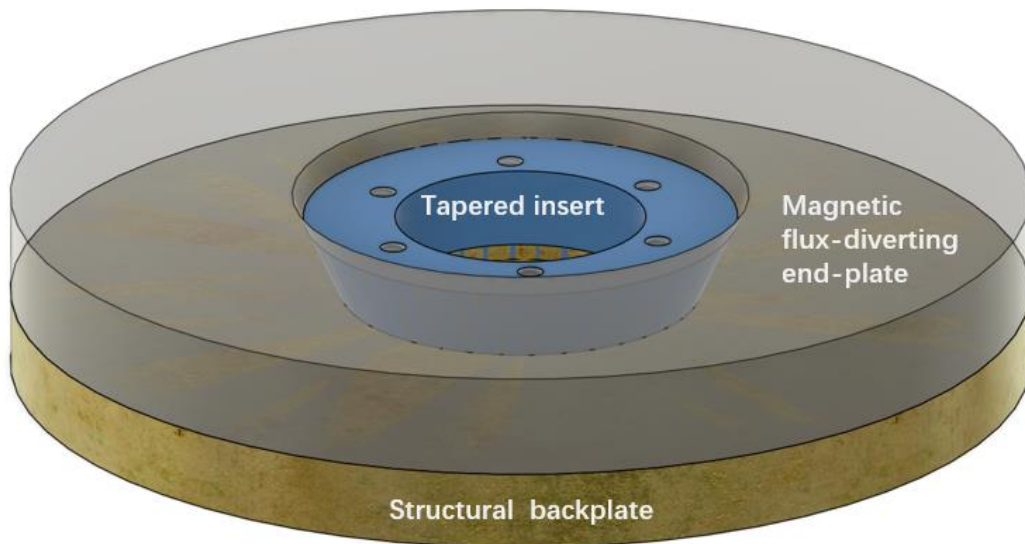
Fig 5-4 Endplate tapered groove fixation Structure

5.3.2 Sliding mechanism for the end-plate

After establishing a method to attach the core to a structural back plate the next stage is to consider design an arrangement which allows the structural backplate to slide in

an axial direction. As noted previously, avoiding bending in the structure is important to maintain a parallel space-off gap and so the approach used in the design is to use multiple ground steel shafts distributed around the structural back plate and not one central sliding shaft. The features in the structural back-plate to attach the series of the ground shafts is in Fig 5-5. The structure of the individual sliding shafts is shown in Fig 5-6, with threaded sections to fix the shafts into the structural back-plate at one end and a profile and threaded section at the other end to attach to the adjustment mechanism. This series of 6 shafts slide in a corresponding series of linear bearings which are mounted in the machine end-cap as shown in Fig 5-7.
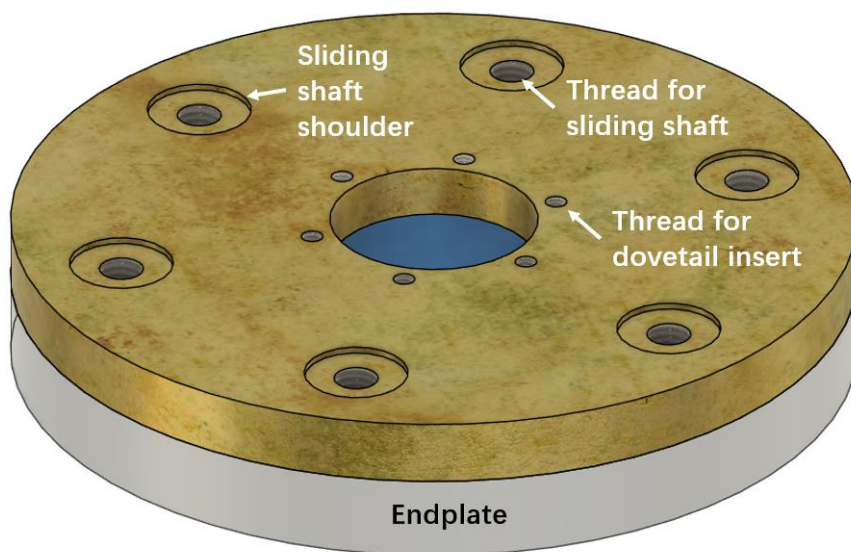
Fig 5-5 Endplate structure backplate thread and shoulder schematic
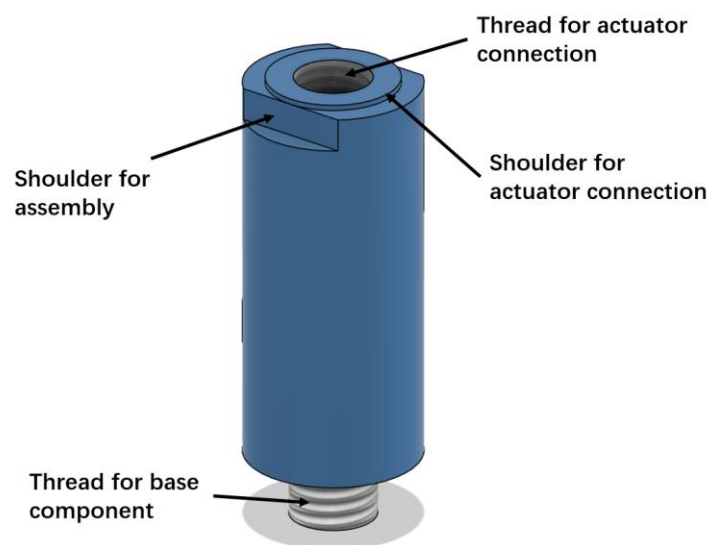
Fig 5-6 Sliding shaft details
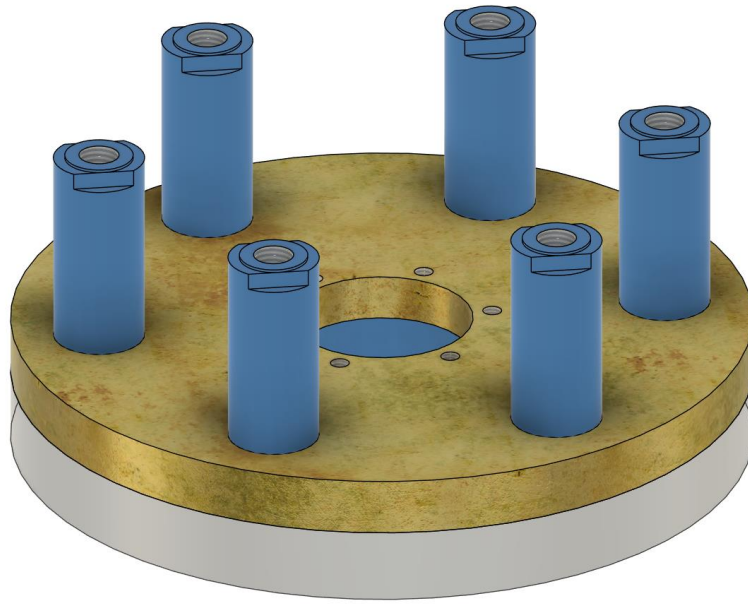
Fig 5-7 Sliding shaft locations on the structural backplate

5.3.3 Machine endcap

The machine endcap needs to incorporate a series of linear bearings which align with the sliding shafts of Fig 5-7. The machine endcap needs to be a precision component to ensure that all the shafts run smoothly and must also be rigid to ensure that there is no deflection in the structure. The endcap design is shown in Fig 5-8. The surface that points towards the rotor include a recess for the main rotating bearing of the machine and six thicker regions to support the linear bearings on the other side of the endcap. The other face contains recesses for six commercial linear bearings (Model 6676K31).
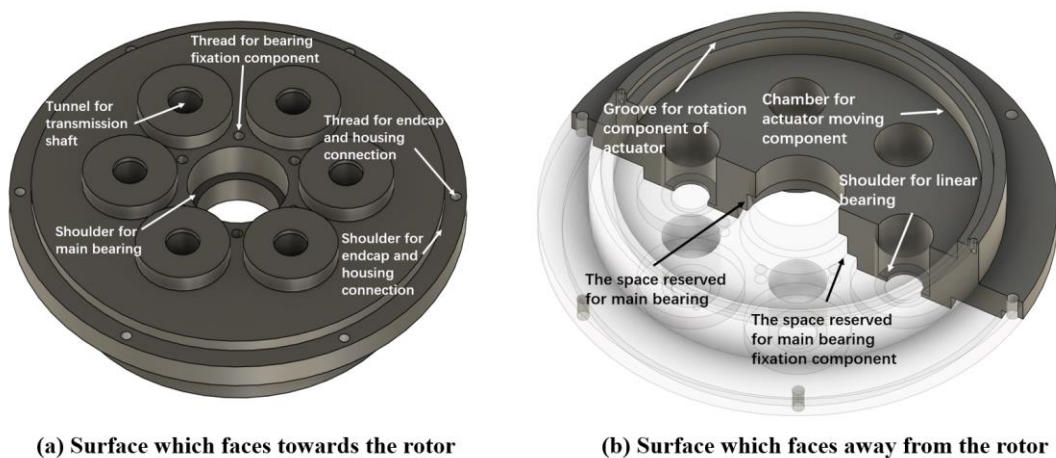
(a) Surface which faces towards the rotor   (b) Surface which faces away from the rotor

Fig 5-8 Machine endcap schematic

5.3.4 Position adjustment mechanism

This section discusses the design of a manual adjustment mechanism to move the endplate accurately and ensure that the displacement can be set in a precise and controlled way. The magnetic force of attraction between the flux diverting magnetic end-plate and the end of the rotor can be partly offset by a spring. However, as shown later in Section 5.4.1, the design of a suitable spring is complicated and hence no spring was included in the manual adjustment mechanism for the demonstrator machine. This means that the full magnetic force of attraction must be resisted by the adjustment mechanism. Given this requirement, it was decided that a heavy duty screw-thread would provide a simple and robust adjustment mechanism that would allow fine and repeatable adjustment. The two main components of this mechanism are shown in Fig 5-9. The first rotation component consists of a large circular plate with a hexagonal raised section that contains a tapped hole (M42 thread). The hexagonal profile of the raised section enables a custom spanner to be used to rotate the plate. The other transmission component is in a circular plate with a raised central section with a matching thread to the plate on the left. This contains a series of circular 8mm diameter clearance holes through which a series of machine screws are used to connect to the top of the 6 sliding shafts. As shown in Fig 5-10, the underneath of the plate with the hexagonal raised section includes a groove to accommodate the machine screw heads and other plate includes recesses to locate the profile on the top of the sliding shafts.
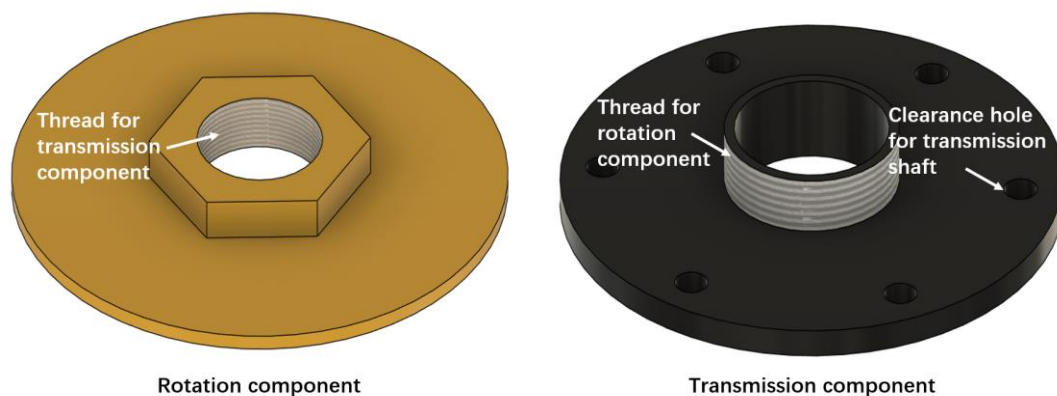
Fig 5-9 Position adjustment mechanism component schematic (top view)
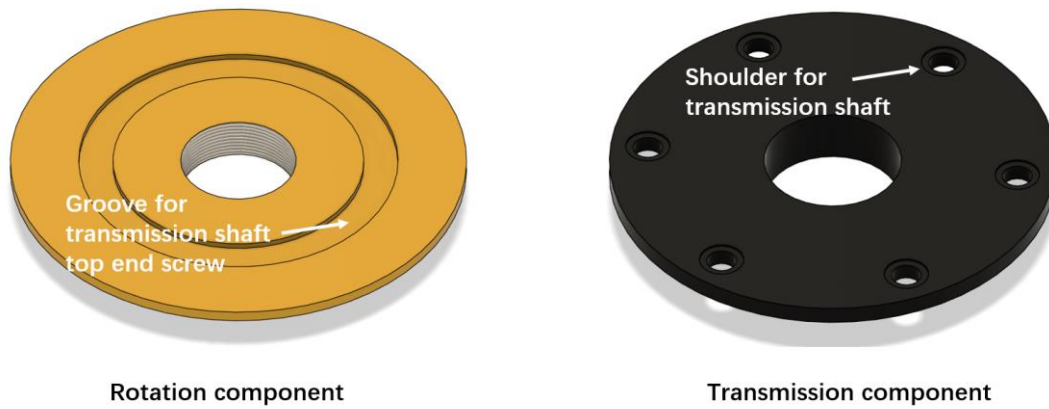
Fig 5-10 Position adjustment mechanism component schematic (bottom view)

Fig 5-11 shows the complete assembly for the adjustment mechanism in which the rotating plate with the hexagonal profile rotates in a groove formed by a recess in the machine end-plate and a retaining ring. By rotating the ring with the hexagonal raised section, the other threaded plate moves axially hence causing the six shaft to slide.
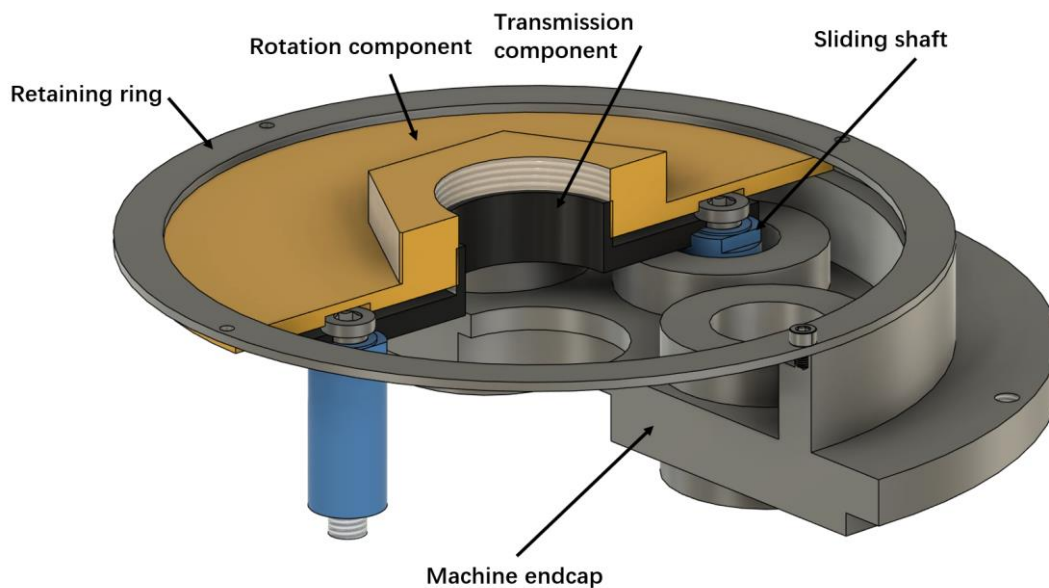
Fig 5-11 Adjustment mechanism component and sliding shaft assembly schematic view

5.3.5 Main generator shaft and bearings

The design of a shaft and bearing assembly has many of the same considerations as conventional machines but it is also necessary to consider the axial force of attraction with the magnetic flux-diverting endplates. The attractive forces produced by the

endplates at either end are in opposite directions and hence the net force is only due to any imbalances between the space-off gap and any magnetic asymmetry. Since the gaps would be controlled at each end, the net force on the rotor is likely to be small and not a major factor in designing the bearing system. Fig 5-12 shows the shaft design which is very similar to a shaft for a conventional machine although the shaft is longer due to the space taken up at each end by the flux-diverting plate and its adjustment mechanism.
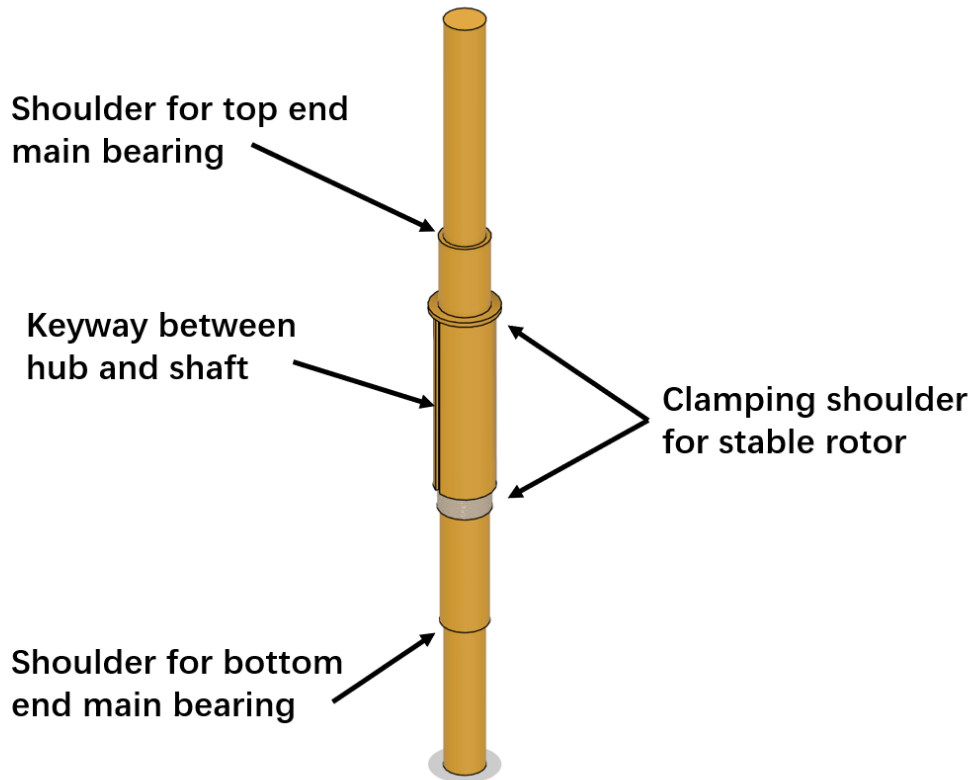
Fig 5-12 Machine shaft schematic

The mechanical design of the bearing system for any machine needs to allow a small amount of relative axial motion between the rotor and the stator case to accommodate any differences in overall thermal expansion between the rotor and stator casing. If the bearings were firmly fixed to both the rotor shaft and the stator casing at both ends, then any difference in thermal expansion will result is significant stress in the rotor shaft and/or stator casing and could result in shaft bending and seizing of the rotor. This is usually avoided by firmly fixing one of the bearings into the bearing housing with a press-fit and using a sliding fit with a wavy or Bellville washer at the other end. The bearing arrangement at the sliding end which was designed for the prototype is shown in Fig 5-13. It is important to note that such a spring and sliding bearing should not be

added to both ends. If both ends had sliding bearings, the shaft would have axial compliance and would be able to oscillate radially within the machine. Fixing the one bearing firmly in its housing gives the rotor a high axial stiffness.
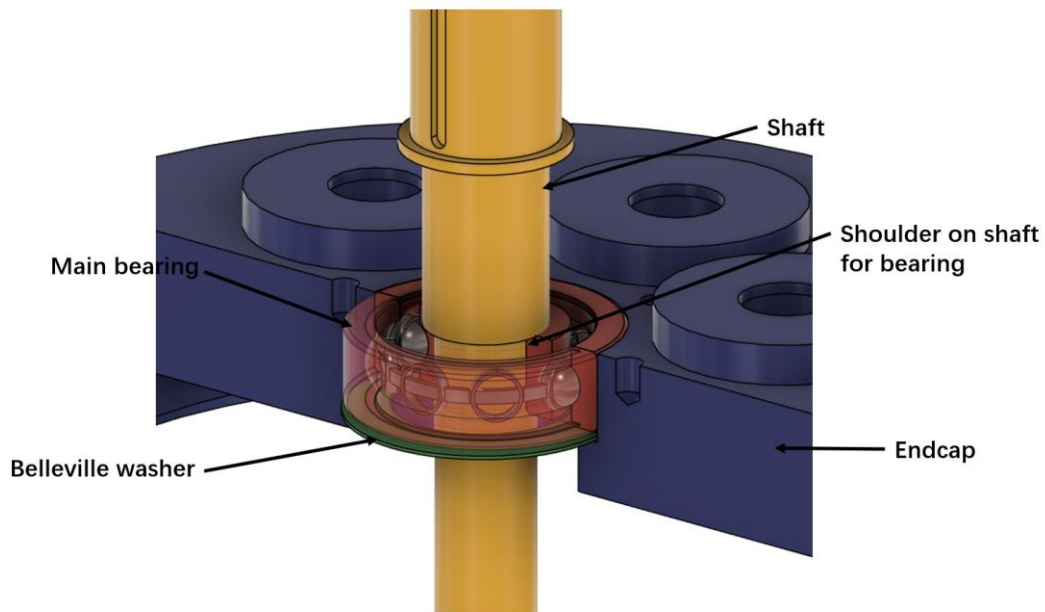
Fig 5-13 Illustration of main bearing and Belleville washer location

5.3.6 Hub and rotor

In order to enhance magnetic flux levels in the machine, the rotor was designed with a non-magnetic hub to minimize flux leakage around the ends of the magnets nearest the machine shaft. It is common in IPM type machines to have such non-magnetic hubs even though this complicates the mechanical connection between the hub and the rotor core and magnets. Attachment and location of the individual rotor pole pieces was done with a dovetail groove structure as shown in Fig 5-14. This provides a stable and precise connection. However, it is important to recall that this rotor is designed to have a high-strength carbon fiber sleeve around the entire active region of the rotor and hence the dovetail is not expected to resist much of the centrifugal load on the pole-pieces.
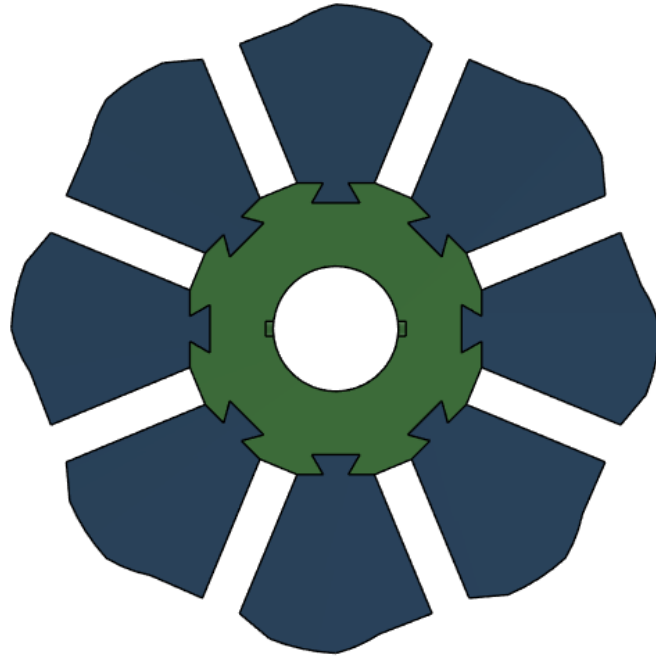
Fig 5-14 Hub and rotor core with dovetail attachment (permanent magnets not shown)

5.3.7 Overall mechanical design and integration

An exploded view of one end of the generator is shown in Fig 5-15 (stator winding not shown for clarity). As will be clear from this exploded view and the detail provided in this chapter, incorporating movable flux-diverting plate involves significant additional complexity to the mechanical design of the casing even with a manual adjustment.
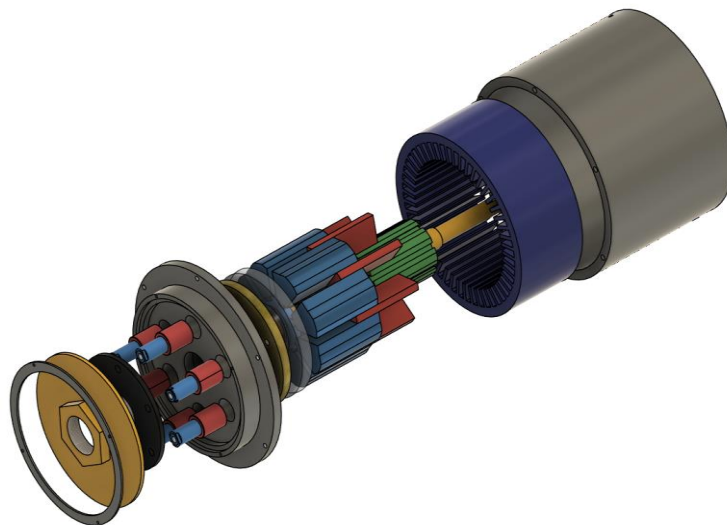
Fig 5-15 General assembly of machine one end exploded view

5.4 Investigation of actuation options

Although a manual mechanical adjustment of flux diverting plate position was chosen for this first demonstrator machine, it is important to consider the feasibility and options for controlled actuation as this will have a significant influence on whether the proposed concept will be feasible and competitive with converter connected permanent magnet generators. This section considers some options for the actuator.

5.4.1 Spring mechanisms to reduce actuator force requirement

As noted in Section 5.2, each individual flux-diverting end-plate is subjected to large attractive magnetic forces of up to 1650N for the case of a 0.25mm space-off gap. In order to have control over the position of the flux-diverting endplates it is necessary to have a counteracting and controllable force which exceeds the maximum attractive magnetic force acting on each end-plate value. As noted previously in this chapter, this force can be produced by a combination of a spring and the actuator which is useful in reducing the force which needs to be produced by the actuator and hence, its size, weight and power consumption

.

If the force-gap characteristic of the magnetic force could be exactly matched by a non-linear spring force-displacement characteristic then only a small electromagnetic force would need to be produced. As an example, Fig 5-16 shows the attractive magnetic force between the rotor and the endplate, an idealised non-linear spring characteristic which produces a restoring force which tracks the electromagnetic force characteristic but only with 90% of the magnitude and the net attractive force which must be counteracted by the actuator. In these characteristics a positive force corresponds to a force in the direction of a closing the space-off. In the case of this idealised non-linear spring, the net force would still attract to the endplate to the end of the rotor in the absence of any actuation force, but the actuator would only need to produce ~165N to exert full control over the space-off. It is also worth noting that the force required by the actuator (which would be negative according to the convention in Fig 5-16) is in

the same direction across the full stroke range and could therefore be produced by a uni-directional force actuator such as a pure reluctance actuator. It is also useful that the variation in spring force is monotonic, i.e. it continuously increases as the space-off decreases which makes stable operation easier to implement.
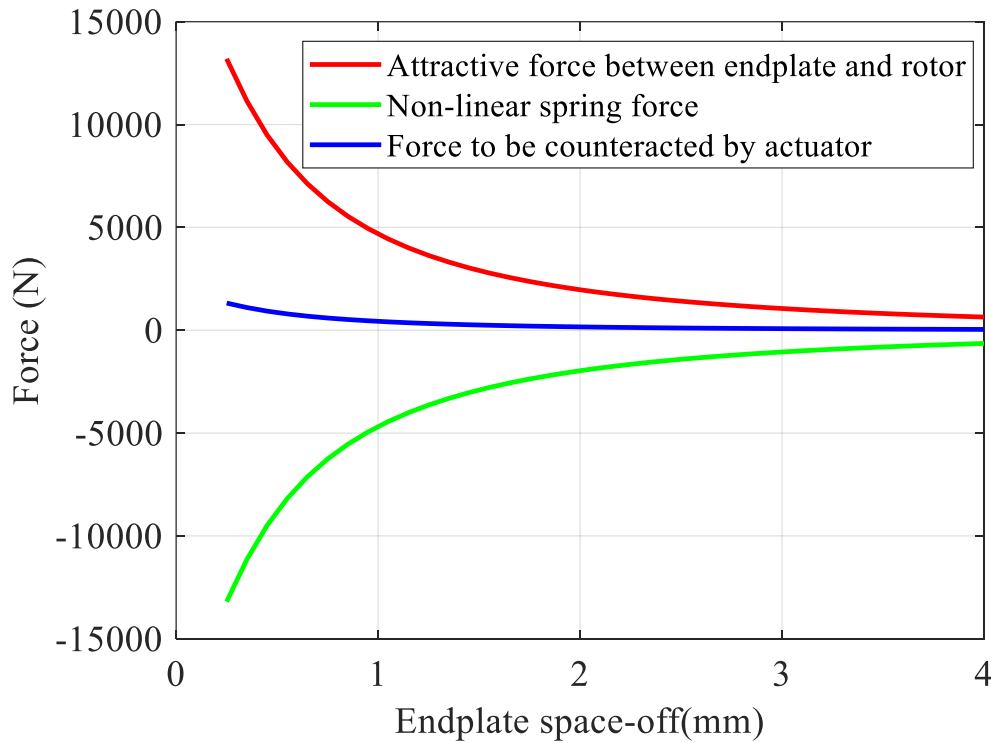
Fig 5-16 Non-linear Spring force profiles

If a linear spring is used then to ensure that the force required by the actuator is uni-directional then the spring must produce a force which is greater than the electromagnetic force of attraction, such as the example in Fig 5-17, This produces a force of 110% of the magnetic force of attraction at the minimum gap of 0.25mm. This then results in a net force which is always trying to cover up the space-off gap and hence although a unidirectional force actuator could still be used, it would need to be turned around compared to the non-linear spring case in Fig 5-16.

The force characteristics in Fig 5-17 show that a linear spring characteristic requires an actuator with a much greater force capability and also has a non-monotonic force versus gap requirement which could lead to some control challenges due to unstable equilibrium at a space-off of ~1.25mm.
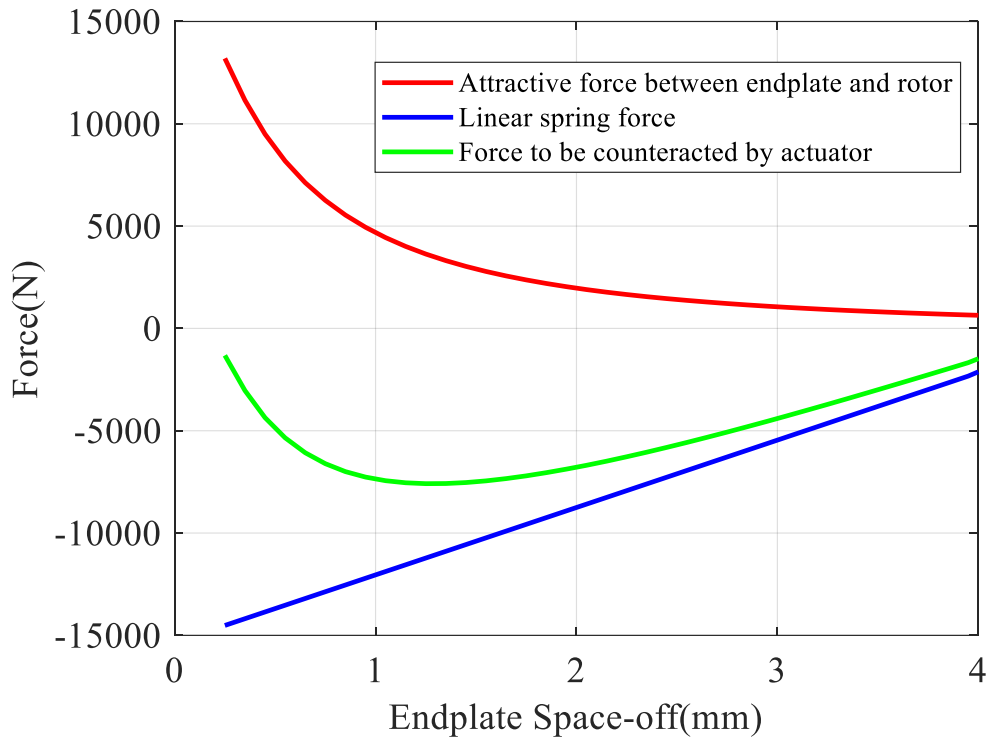
Fig 5-17 Linear Spring force profiles
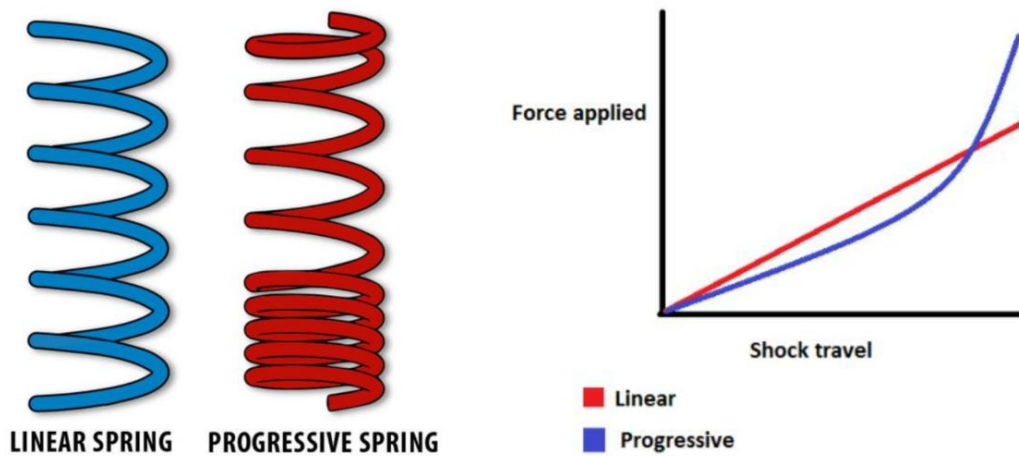
Fig 5-18 Schematic of different coil spring design options[55]

The force-displacement of spring can be tailored by careful design of the spring shape, geometry and materials. Non-linear stiffening coil springs, which are sometimes called progressive springs or variable-rate springs [54] can be designed with uneven separation between coils as shown in Fig 5-18. With characteristics such as that in Fig 5-16. Progressive coil springs are commonly used in vehicle suspensions and hence tend to be available in very high force ratings although they tend to be large.

Chapter 6 - Prototype construction

6.1 Introduction

Having established the electromagnetic features of the prototype design in chapter 4 and the mechanical components in chapter 5, this chapter is concerned with the manufacture and assembly of the numerous components that make up the prototype. Some of the components were manufactured in-house, while other such as the cores and magnets were sourced from external suppliers

6.2 Generator rotor components

6.2.1 Shaft

Fig 6-1shows the shaft for the prototype machine which was machined from a circular bar of Stainless Steel. The total shaft length is 340mm and as shown there are various steps in the diameter to accommodate the hub and provide shoulders for the bearing.
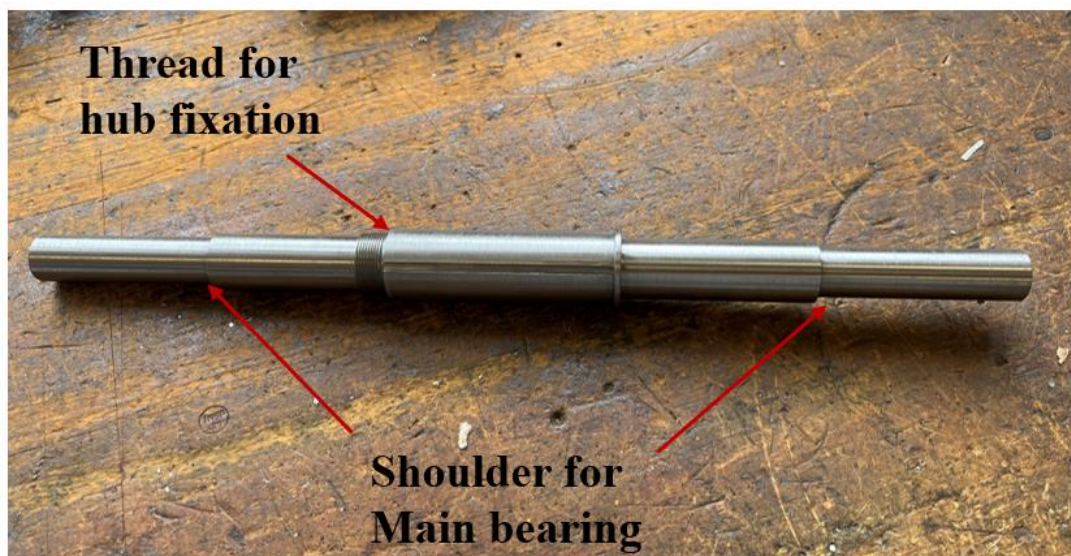
Fig 6-1 Prototype Shaft

6.2.2 Rotor hub

The non-magnetic hub which was manufactured from Aluminium using wire electro-discharge machine (Wire EDM) is shown in Fig 6-2. The central bore for the shaft includes two keyways to ensure reliable torque transmission. This is preferable to shrink fit because of the very significant difference in thermal expansion between the Aluminium hub and the stainless-steel shaft. The outer surface has 8 dovetail slots and precision flat regions to precisely locate the individual magnets and rotor pole pieces. Since the hub was cut with wire EDM, all internal corners with have a radius of ~0.16mm (wire radius + an allowance for cutting) as shown in the close up of Fig 6-3. Since the rotor pole pieces are a precision fit it was necessary to specify a matching radius on the corners of the pole pieces.
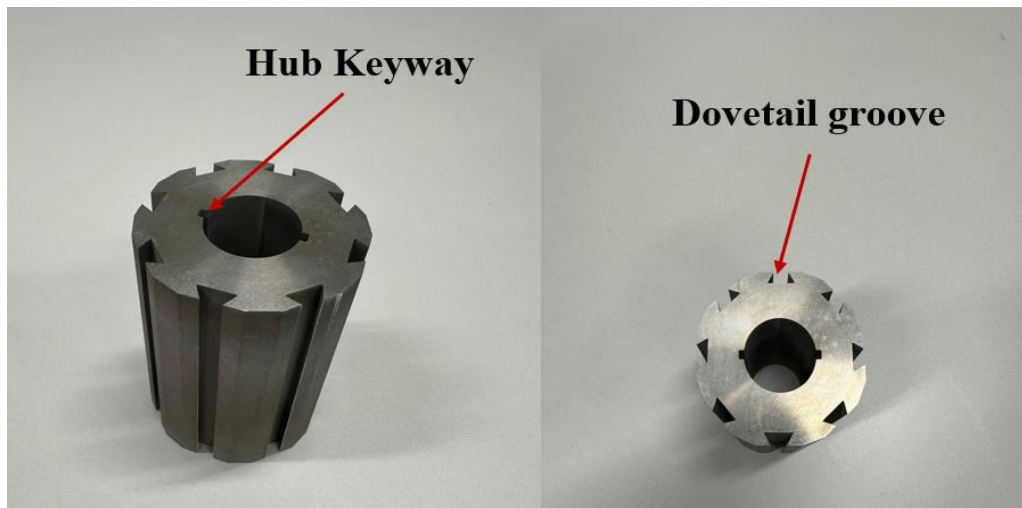
Fig 6-2 Aluminium Prototype Hub
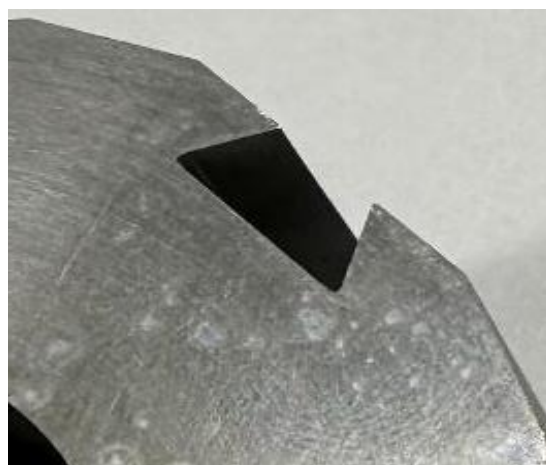
Fig 6-3 Close up of dovetail slot in rotor hub showing the fillet radius on the internal corner

6.2.3 Rotor core pole pieces

The rotor pole pieces were manufactured by an external supplier, using 0.35 mm thick laminations of Cobalt iron. The specific grade supplied was 1J22 which has characteristics equivalent to Hiperco-50 which is a commonly used alloy in the aerospace sector and was used in the modelling studies of chapters 3 and 4. The 80mm long pole pieces were manufactured by welding together a stack of lamination on the four faces as shown in Fig 6-4.
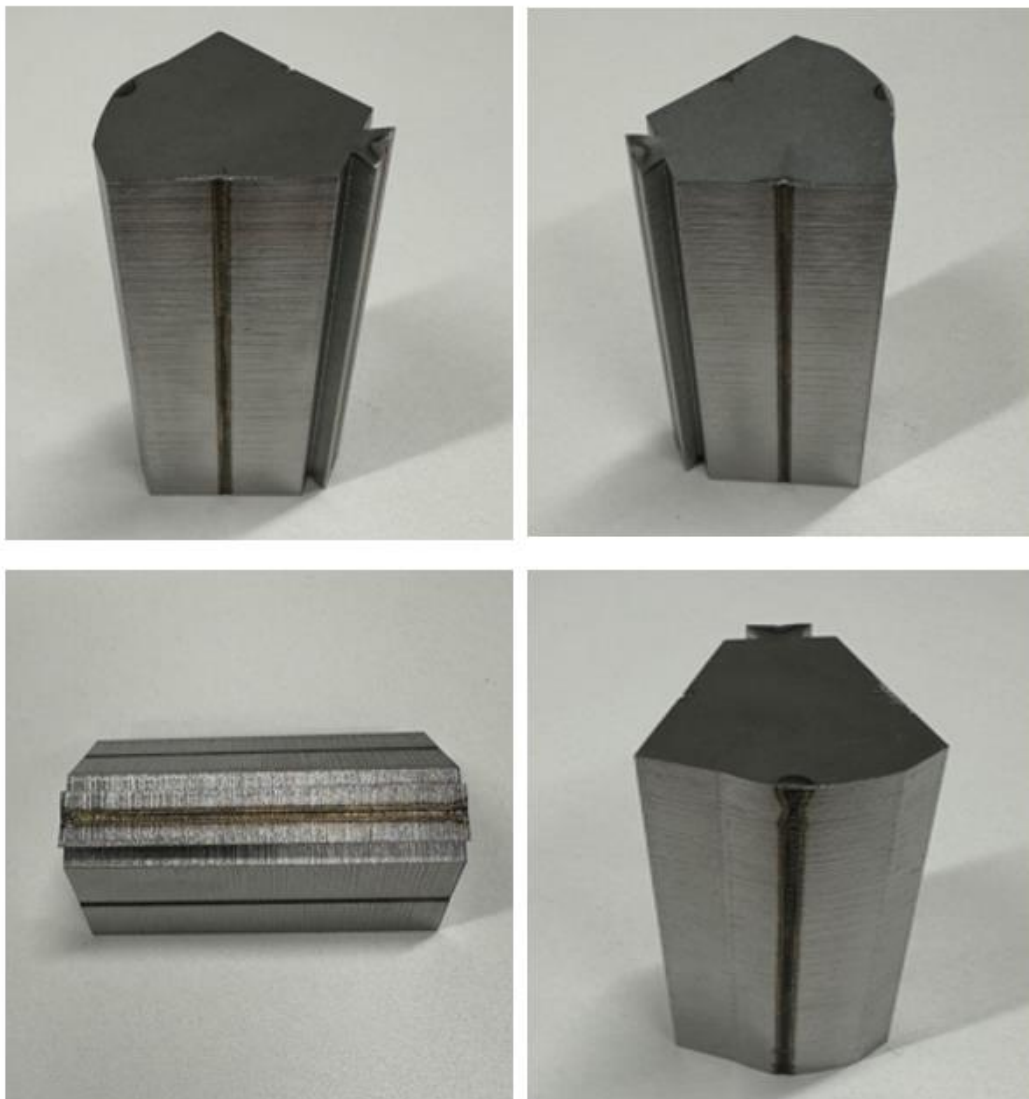
Fig 6-4 Rotor pole piece showing welds on 4 faces

6.3 Stator components

6.3.1 Stator core

The stator core was also manufactured from a welded stack of the same 0.35mm thick IJ22 Cobalt iron laminations. The finished stator core is shown in Fig 6-5. The stack was formed with 12 welds located on the outer surface of the stator. Fig 6-6 shows a close-up of the weld lines on the back of the stator core.

Stator NE view **Stator Top view** **Stator front view**
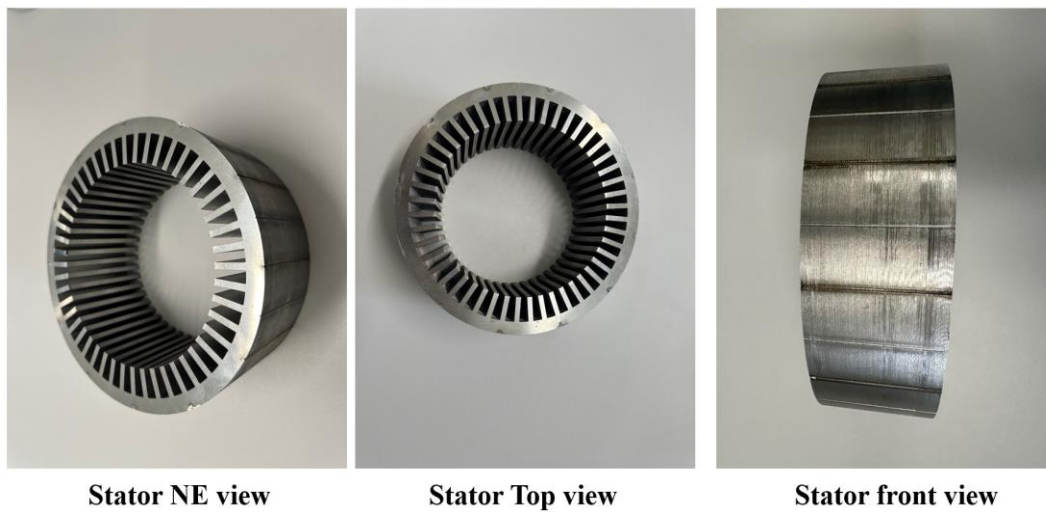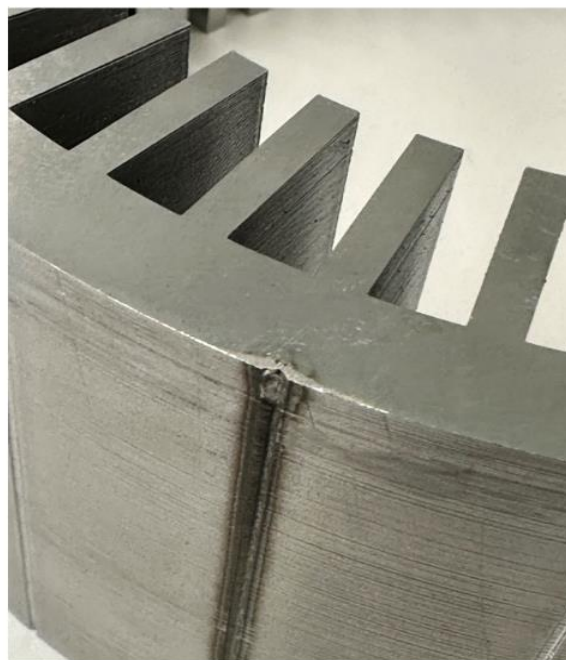
Fig 6-5 Stator core

Fig 6-6 Stator core close-up showing welds

6.3.2 Stator structural endcap

As discussed in detail in chapter 5, the main structural endcap of the stator needs to resist significant axial force. Fig 6-7 and Fig 6-8 show the machined end cap for the prototype machine. As detailed in chapter 5, in order to reduce weight, the design of the endcap included significant detailing to hollow-out the end cap to reduce weight. Whereas this would be important in a final product, this is not a critical feature for a prototype and hence this detailing was not incorporated in the prototype.

Endcap top view   **Endcap NE view**

Fig 6-7 Endcap top and NE view

Endcap bottom view   **Endcap SW view**

Fig 6-8 Endcap bottom and SW view

6.3.3 Flux varying system components

The flux-adjustment mechanism whose design was described in chapter 5 contains numerous structural components and the magnetic flux-diverting endplate. The magnetic endplates, one of which is shown in Fig 6-9 was a custom tape wound Cobalt-iron core manufactured from 0.1mm thick strip of cobalt-iron alloy (Supermendur) by LH component. A key feature of this core is the incorporation of a taper which locates and retains the core. This could not be included by the core manufacturer and an attempt was made to wire EDM the taper but this proved unsuccessful due to the epoxy between each layer.

Fig 6-9 Untaped wound Cobalt Iron core

Accordingly, a rotary cutting technique was employed to process the laminated core. To preserve the integrity of the interlaminar epoxy, tapering was applied exclusively to an 8-mm thick segment, while the remaining 5 mm was left untampered and the final toroidal core are shown in Fig 6-10.

Fig 6-10 Tapered wound Iron core

As discussed in chapter 5, the rotating plate in the adjustment mechanism included a hexagonal raised section to allow precise rotation using spanner. However, during construction it was decided to change to a simple cylindrical raised section with a series of holes that would match up to a series of dowels in an adjustment tool. These modified Aluminium rotating endplates are shown in Fig 6-11.

Adjustment plate Top view   **Adjustment plate Bottom view**

Fig 6-11 Adjustment plate

The Aluminium retaining ring which forms the closed groove in which the adjustment plate rotates is shown in Fig 6-12.

Retaining ring Top view   **Retaining ring Bottom view**

Fig 6-12 Retaining ring

The adjustment mechanism plate which locates the sliding shafts and includes the threaded section that interfaces with the rotating plate in the adjustment mechanism is shown in Fig 6-13.

Non-rotating adjustment plate top view   **Non-rotating adjustment plate NE view**

Fig 6-13 Non-rotating adjustment plate

Fig 6-14 shows the assembled adjustment mechanism before and after fitting to the main stator casing. Also shown the custom adjustment tool that was manufactured to allow the adjustment plate to be rotated.
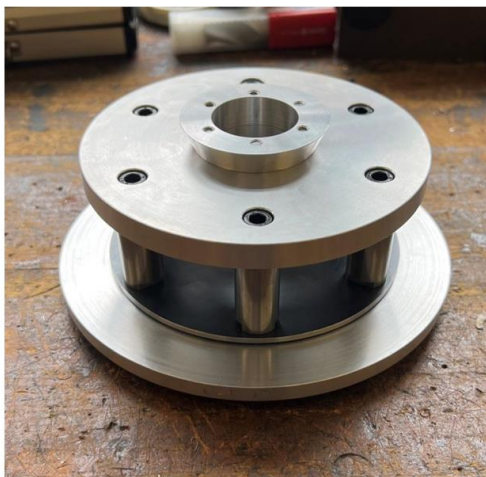
Internal configuration (bottom view)   **Outer view**
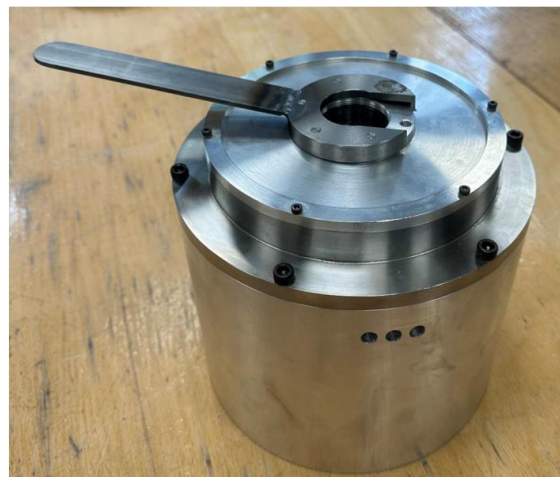
Fig 6-14 Assembled adjustment mechanism

6.3.4 Assembly of the rotor

As is common in prototypes, the rotor was constructed using pre-magnetised permanent magnets. The total axial length of 80mm of each pole was made up of 4 long individual magnet pieces. This poses significant challenges in terms of the forces acting on the magnet and other magnetic rotor components. The magnets were attached to the rotor pole pieces using Loctite 648 adhesive. In order to ensure that the magnets remain in place when other magnets are brought into close proximity with other magnets it is usual to allow the glue used on each magnet to cure. In the case of the Loctite SF7471 used, the majority of strength is achieved within an hour of application s and hence for this manual one-off prototype each magnet piece was attached to the pole piece with a thin layer of adhesive and then clamped into position as shown in Fig 6-15.

Fig 6-15 Magnet clamping arrangement during bonding of magnets to rotor pole pieces

This clamping and alignment of the magnet pieces required to two tooling components shown in Fig 6-16. These plastic tooling elements were manufactured using 3D printing.
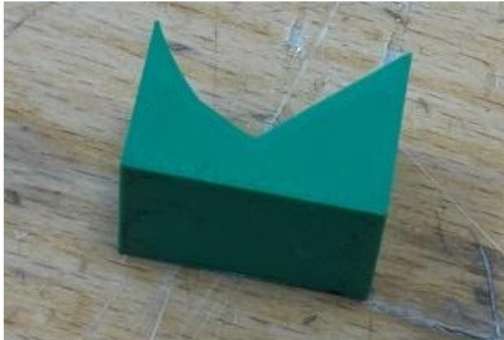
Tools for clamp support   Tools for stable magnet location

Fig 6-16 Tooling for magnet clamping

The magnet poles were gradually built up using the clamping with the tooling of Fig 6-16. Fig 6-17 shows the clamp arrangement during attachment of the second magnet piece in the pole. After all the magnet pieces had been bonded to the pole pieces, the 8 rotor pole pieces were mounted in the hub. The assembled 8-pole rotor part-way through assembly and after the assembly process are shown in Fig 6-18.
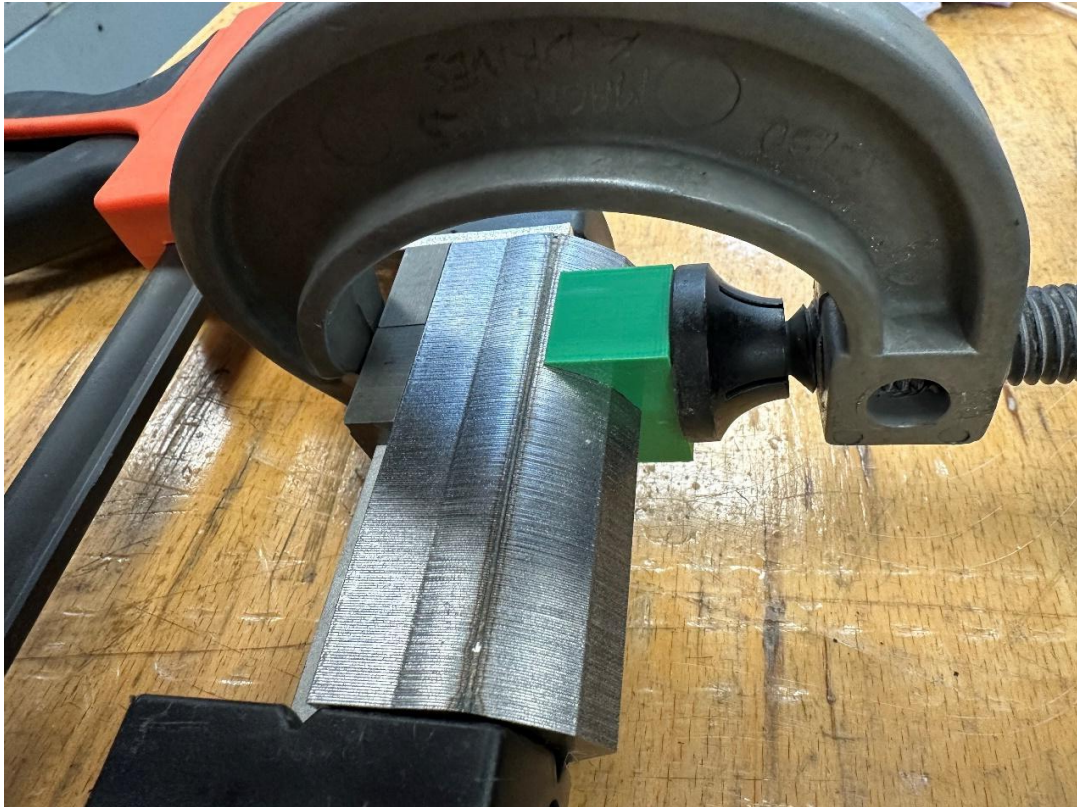
Fig 6-17 Magnet piece clamping arrangement during the build-up of one pole

Fig 6-18 Assembled active elements of the rotor

Having attached the rotor poles and magnets, the next step in the rotor manufacture was to fill in the voids around the periphery of the rotor with a high fibre-reinforced putty. The material used was epoxy resin (CV-1108 A) and hardener (CV-1108B) manufactured by Dolph Von-Roll. This is a two-part putty with glass fibre reinforcement which is applied as a thick putty and cures at room temperature. Fig 6-19

121

shows the rotor after the putty was applied and cured in-situ.
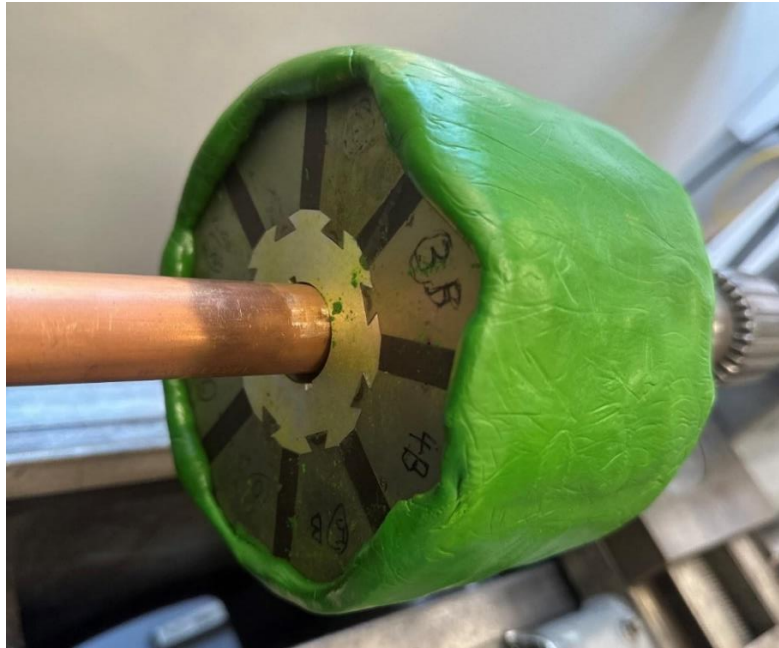
Fig 6-19 Rotor after hand application of Dolph glass fibre reinforced putty

After curing, the putty was machined to the final dimensions as shown in Fig 6-20.

Fig 6-20 Rotor after machining of fibre reinforced putty

Unfortunately, during machining of the putty, due the fracture in the putty, the last lamination on the end of two pole pieces were damaged as shown in Fig 6-21. In order to remedy this, it was necessary to peel away the last lamination on each pole piece, although this does leave the magnet slightly proud.

Fig 6-21 Damaged pole piece ends due to fracture of putty during machining

After removing the damaged laminations, additional reinforcement of the rotor periphery is necessary, considering the machine's maximum operating speed of 12,000 RPM. Conventional fiberglass sleeves lack sufficient strength and the ability to conform to the rotor body without additional fixation measures. Therefore, using the carbon fibre wrapping for the rotor lamination is the optimal choice, as it provides superior mechanical strength and has self-adherence ability, as shown in Fig 6-22 where the rotor was first encapsulated with pre-impregnated dry fibre and subsequently enclosed within a vacuum bag, then to an eight-hour curing process under controlled conditions of 90°C and 3 atmospheres.

Fig 6-22 Rotor inside carbon fibre curing chamber

The final appearance of the rotor is shown in Fig 6-23.
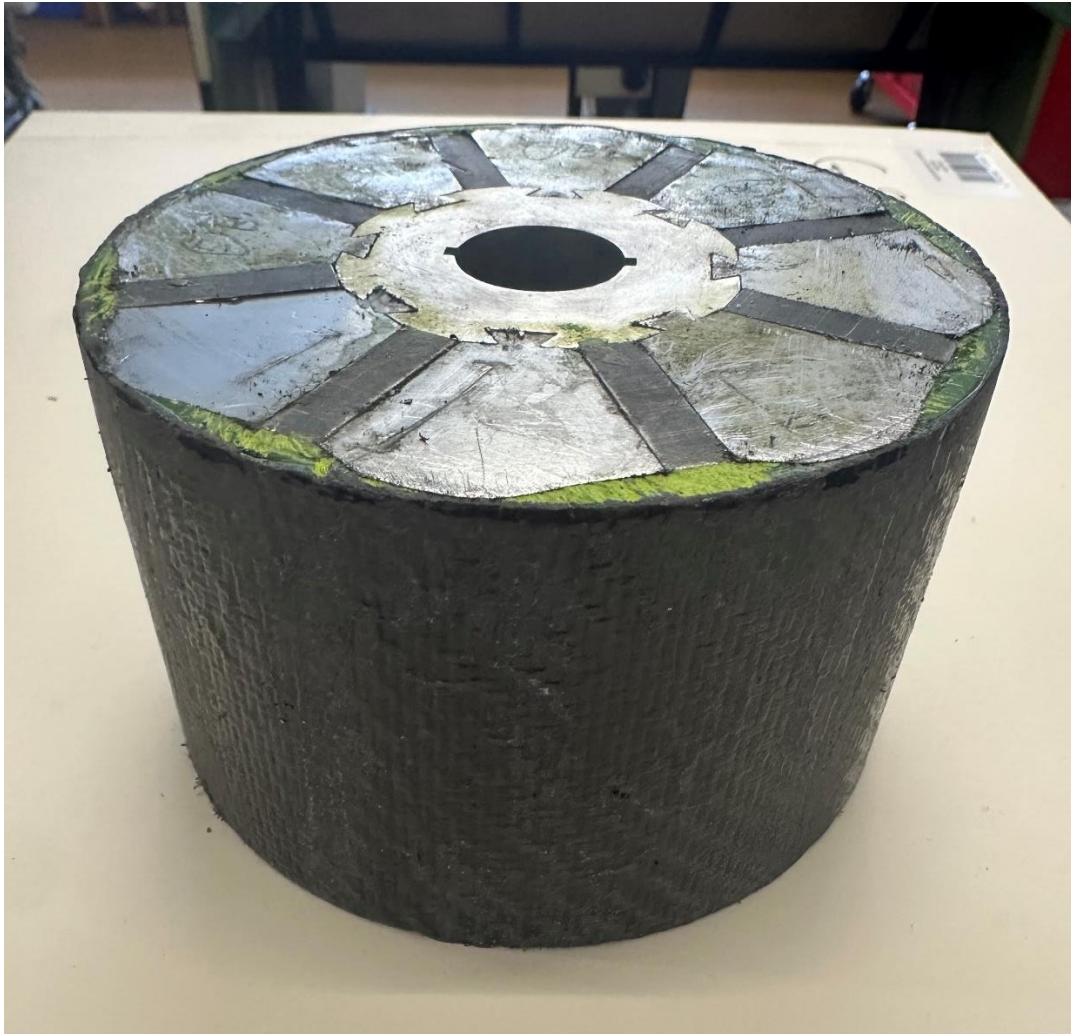
Fig 6-23: Finished rotor

6.6. Stator winding

The stator was wound with a 48 slot, 8 pole, double-layer winding with a two-slot short pitched winding. The finished winding is shown in Fig 6-24. Each coil consists of 7 series turns made up of 8 parallel strands of 0.71mm circular wire.

A key requirement of the stator winding was compact end-windings since this has an impact on the space available to fit in the flux-diverting place and any actuation mechanism. The coils were manually inserted in the slots and with good attention to detail, the end-windings around the entire machine were limited to a ~25mm space as shown in Fig 6-25.

Fig 6-24 Stator winding

Fig 6-25 Close up of end-winding detail

In addition, the slot wedge was processed separately and subsequently installed. Given the substantial thickness of the slot wedge, a laser cutting method was employed, which resulted in visible scorch marks on the cut surface, as illustrated in Fig 6-26.

Fig 6-26 Slot wedges separated with laser cutter

The stator with installed slot wedges is shown in Fig 6-27.
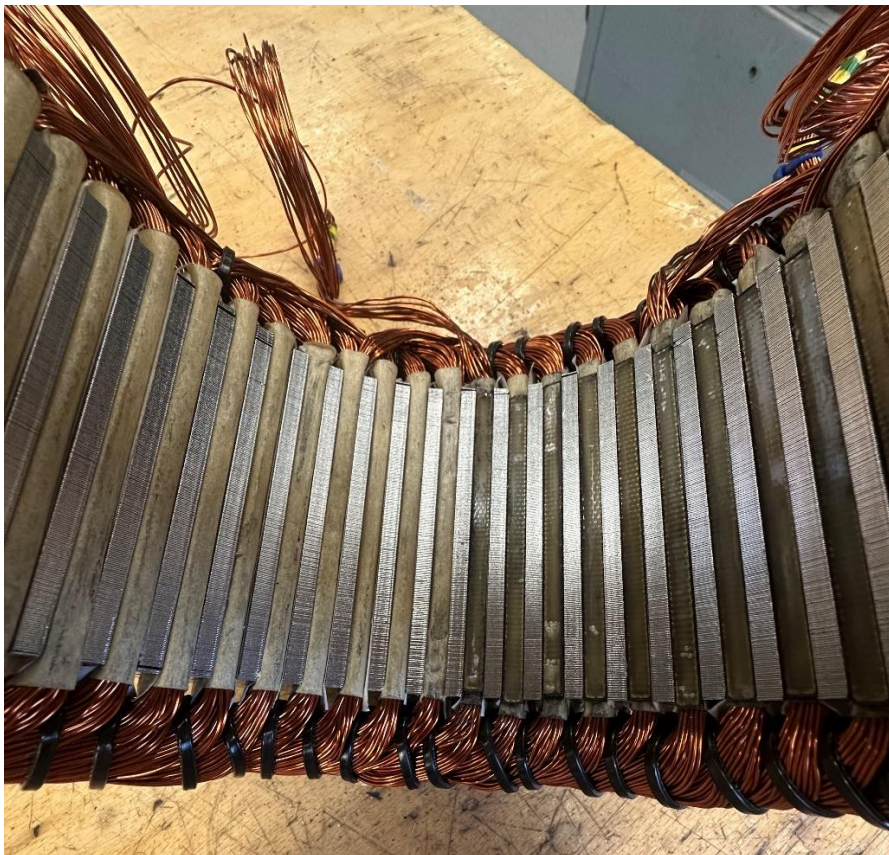
Fig 6-27 Slot wedge installed within stator

6.7   Prototype power capability comparison

After finalizing the structural design of the prototype components, an important validation analysis involves comparing the weight of the prototype developed shown in Table 6-1 this study with that of the prototype from [50]. It is worth noting that due to time constraints, the prototype in this study was not tested before the dissertation submission deadline. As a result, a comparison of power density could not be conducted. Additionally, it is important to highlight that the prototype in [50] features a specifically designed enclosure to enhance thermal capabilities, whereas the prototype in this study does not include such a design.

Table 6-1 Measured components mass comparison between prototype machine and proposal machine from [50]

	Components	Prototype from this research	Prototype from [50]
		Mass, Kg	Mass, Kg
Active	Stator lamination stack	5.10	4.67
	Rotor lamination stack	3.23	1.29
	Stator winding	3.86	4.63
	Magnet and carbon fibre (Putty for this research)	2.63	1.56
	Total mass	14.82	12.15
Non-active	Rotor shaft	1.40	1.80
	Rotor Hub	0.98	1.03
	Casing	2.69	3.69
	DE endcap	6.18	1.22
	NDE endcap	6.11	1.18
	Ancillary components	1.93	1.69
	Flux diverting plate	2.38	N/A
	Plate variation system	2.48	N/A
	Total mass	24.15	10.60
	Overall mass	38.97	22.75

6.8 Summary and current prototype status

This chapter provides a comprehensive summary of the essential processes involved in the fabrication of the prototype machine. It covers the design of the shaft, the installation and stabilization of the permanent magnets, the design of the hub, the post-treatment of the flux diverting plate, the measures implemented to ensure the mechanical stability of the rotor including the glass fibre putty shaping and carbon fibre wrapping, and the installation of the stator slot wedge.

Moreover, the flux varying system was evaluated, as illustrated in Fig 6-28. Consider the feasibility of test, two red components made by 3D-printed part are used as the substitute for the flux diverting plate. When the endcaps at both ends were secured with the main bearings, a space offset of 4 mm was measured.
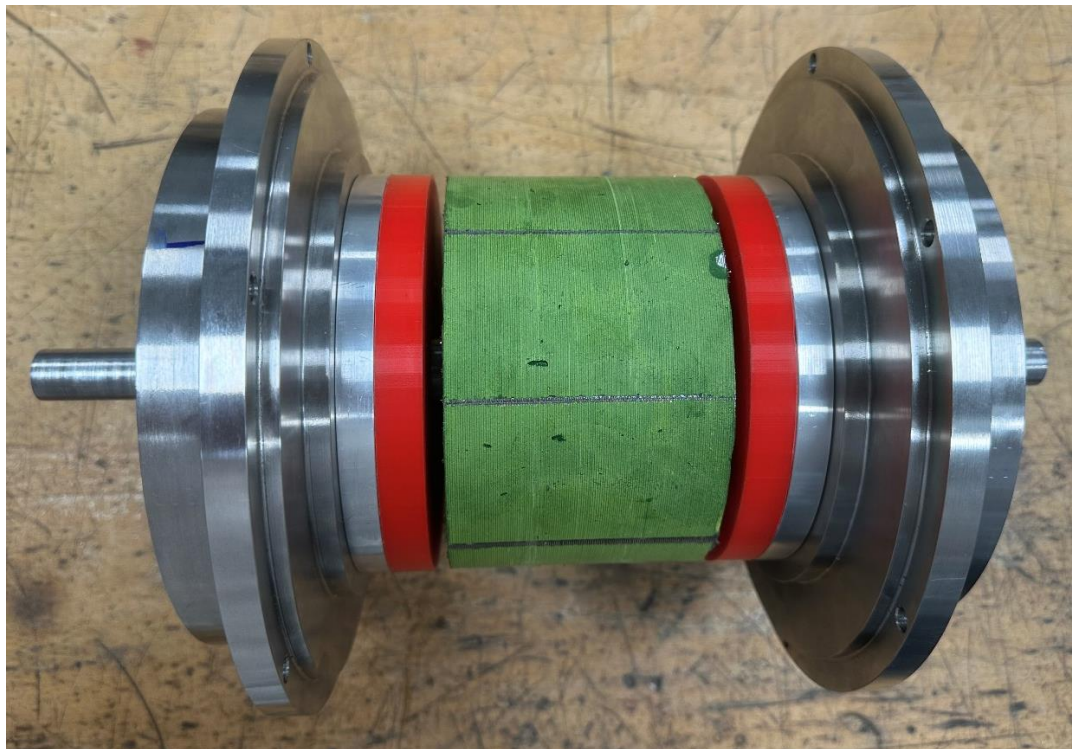
Fig 6-28 Flux varying system test

Furthermore, the installation of the flux diverting plate has been completed shown in Fig 6-29.

Fig 6-29 Flux diverting plate assembled with endcap

Although significant progress in the build was achieved as shown in this chapter, unfortunately the full assembly could not be completed within the project time-frame due to extended difficulties in manufacturing the rotor. However, the prototype is well developed and will be picked in a future study to take it through to test.

Chapter 7 - Conclusions

7.1 Main conclusions

The main research question which has been investigated in this thesis is whether variable-flux permanent magnet machines can be a competitive technology for direct line-connected and variable frequency aerospace generators. Following a review of different solutions for achieving variable-flux in permanent magnet excited machines, a concept based on using axial leakage flux to reduce the flux crossing the main working airgap flux by using moving magnetic flux-diverting endplates was selected.

Using extensive two- and three-dimensional finite element modelling, the basic operating principle of the machine concept was demonstrated. Starting from a published baseline permanent magnet aerospace generator design and by careful optimisation of the rotor aspect ratio, sufficient flux-linkage variation was achieved to regulate the generator output voltage over the full operating speed and load range of the machine. However, meeting power quality standards (specifically output voltage distortion factor) in a direct connected permanent magnet machine under both open-circuit and full-load is challenging, particularly in an IPM rotor which introduces significant harmonic content in the airgap field.

A combination of stator tooth geometry changes, short-pitching of windings and rotor profiling resulted in a machine design was established (designated D6) which was able to meet the 5% distortion factor. Although features such as selection of winding configuration is commonly used to improve waveform quality. To meet the very tight distortion specification with an IPM type rotor, it was necessary to include some novel asymmetric shaping of the iron pole. Achieving low distortion levels across the full speed and load range was made more challenging by the industry practice of connecting the star point to the local aircraft point of voltage reference (PVR). This grounding results in 3rd harmonics in the voltage waveform which can then only be removed by using a winding with a slot-pole combination that eliminates the triplen harmonic. For the 48 slot-8 pole rotor, short-pitching the winding by 2 slots eliminates the 3rd harmonic.

Although the basic functionality of the proposed concept was demonstrated by simulation and a design established which was capable of both covering the maximum operating envelope and meeting demanding power quality requirements, there remain two main obstacles to this concept being competitive with existing wound-field or converter fed permanent magnet generators. These are power density and the very large forces produced on the magnetic endplates.

The final optimised design of the generator had a maximum power capability of only 13kW compared to the 100kW baseline machine design of the same size. This was despite significant effort to maintain power capability while also meeting the power quality requirements for direct line connection. As discussed in detail in Section 4.6 of chapter 4, there are many factors that cause this dramatic reduction in power capability, with the restrictions on speed set by the VAFC frequency range being the most significant, accounting for ~62% of the reduction in power capability from the baseline. This is an inevitable consequence of the direct line connection and although the mechanical speed could be increased by reducing the pole number, the IPM type rotor structure which is essential to the variable-flux concept is not well suited to low pole numbers because of de-focussing effects. It is important to note that this limitation on mechanical speed is common to all directly connected generators with 4 pole and 6 pole being common in wound-field machines. It was shown in chapter 4 that scaling the power capability of the 100kW baseline generator back to the same 5,400rpm operating speed would reduce its power rating to 36.8kW, which is still a factor of 3 times higher than design D6 of variable flux-machines. This is a false comparison however and does not account for one of the main benefits of converter connected machines which is the de-coupling of the mechanical speed from grid frequency.

The force of attraction between the flux-diverting end-plates and the end face of the rotor has been recognised in this study and typical magnitudes calculated. The large forces which arise, particularly if small space-off gaps are required, will impose significant structural loads on the components and require high force capability mechanisms to control the endplate position. It is also worth noting that the manual adjustment mechanism which was designed and part-built used engineering judgement to size the components and ultimately the suitability of the mechanism was not tested in a demonstrator machine. As well as resisting the large magnetic forces from a

structural point of view without bending, the actuation forces required could result in large and heavy actuators which could offset any weight savings from eliminating the converter.

It is important to note that the specification set was extremely challenging in that it covered operation over the full 360 to 800 Hz speed range. In practice, most engine shafts which drive generators via gearboxes do not operate over such a wide frequency range, e.g. 400 to 800Hz [56] or 360 to 650Hz[16]. Any reduction in speed range below 2.2:1 has benefits such as a narrowing of the turn down requirements. This would allow the flux-diverting plates to operate with larger space-off and hence reduced force of attraction. There would also be less compromised in the electromagnetic design and the ability to operate with a smaller radial airgap.

Overall, this programme of research has proposed some features and operating concepts for a novel machine topology which from an electromagnetic point of view is capable of being used as a variable-flux generator with sufficient flux-varying capability to meet VFAC requirements including power quality. However, there remain unresolved questions around mechanical integrity, actuation and power density which mean that without further work this machine cannot be regarded as a competitive technology to wound-field machines or converter connected permanent magnet machines.

7.2 Future work

Due to time limitations and the numerous challenges encountered in manufacturing a prototype, the final build and testing of the demonstrator machine could not be completed. The testing of this demonstrator is clearly an important part of future work as this would validate the modelling and prove the viability of the electromagnetic aspects of this variable-flux machine. It was recognised towards the end of this research programme that it might have proved more productive to have set out to build a much smaller generator (100s of W) which could have provided the necessary experimental proof and a more straightforward mechanical adjustment in terms of force levels.

Additionally, due to time constraints, the thermal performance of the machine could not be elaborated on. This includes both the overall thermal behaviours and the thermal performance of the flux diverting plate. Although a toroidal core structure was used,

the plate remains stationary relative to the rotor, making its heating risk and cooling requirements aspects that need additional consideration. In this regard, provisions for thermal coupling have already been made in the stator slots and stator end-winding during prototype fabrication, and the plate's temperature can be monitored using an infrared probe. Therefore, more in-depth analysis can be conducted in future studies.

Another key aspect which has not been addressed in any detail is the actuation of the end-plates. A particular challenge is the very large magnetic force of attraction on each plate. As discussed at the end of Chapter 5 there is potential to use a complex spring arrangement to balance out most of the electromagnetic force. The design of the springs and the actuator is a very complex task which was beyond the scope of this thesis but is a key element in determining the viability of this concept.

As noted in Section 7.1, the design specification was based on the VFAC power range from 360 to 800Hz. Having established a proof of concept based on this wide frequency range, it would be interesting to work with an aero-engine specialist to understand the improvements in power density that could be achieved with narrower specific engine shaft speed variations.

One final aspect that would be interesting to explore, particularly if this concept was being considered for commercial use, is whether the claimed reliability improvements by removal of the power converter would be achieved in practice. This would require a very detailed failure-mode and effects analysis to determine the reliability of the actuation systems and its sensors and control system.

Reference

[1] Kuropatwa, M., Wegrzyn, N., & Kozuba, J. (2022). Turbofan Engines Efficiency, Historical Trends, and Future Prediction. Safety & Defense, 8(2), 82-90. https://doi.org/10.37105/sd.186.

[2] Adu-Gyamfi B.A., Good C., 'Electric aviation: A review of concepts and enabling technologies', Transportation Engineering, Vol 9, 2022. Ref: 100134.

[3] M. J. Provost, "The More Electric Aero-engine: a general overview from an engine manufacturer," in International Conference on Power Electronics, Machines and Drives, 2002, pp. 246-251.

[4] J. Li, Z. Yu, Y. Huang and Z. Li, "A review of electromechanical actuation system for more electric aircraft," 2016 IEEE International Conference on Aircraft Utility Systems (AUS), Beijing, China, 2016, pp. 490-497, doi: 10.1109/AUS.2016.7748100.

[5] S. E. de Lucena and E. Y. Suzuki, "Electro-Hydraulic Actuator Tester for Fly-By-Wire Aircrafts," 2007 IEEE Instrumentation & Measurement Technology Conference IMTC 2007, Warsaw, Poland, 2007, pp. 1-3, doi: 10.1109/IMTC.2007.379213.

[6] Hoffman, A. C. et al. (1985) 'ADVANCED SECONDARY POWER SYSTEM FOR TRANSPORT AIRCRAFT', NASA Technical Paper.

[7] C. R. Avery, S. G. Burrow and P. H. Mellor, "Electrical generation and distribution for the more electric aircraft," 2007 42nd International Universities Power Engineering Conference, Brighton, UK, 2007, pp. 1007-1012, doi: 10.1109/UPEC.2007.4469088.

[8] X. Roboam, "New trends and challenges of electrical networks embedded in "more electrical aircraft"," 2011 IEEE International Symposium on Industrial Electronics, Gdansk, Poland, 2011, pp. 26-31, doi: 10.1109/ISIE.2011.5984130.

[9] X. Roboam, B. Sareni and A. D. Andrade, "More Electricity in the Air: Toward

Optimized Electrical Networks Embedded in More-Electrical Aircraft," in IEEE Industrial Electronics Magazine, vol. 6, no. 4, pp. 6-17, Dec. 2012, doi: 10.1109/MIE.2012.2221355.

[10] O. Hockmeyer and Hockmeyer, IO (1946) 'The generation and regulation of electric power in aircraft: a survey of design features of generators and their control', The journal of the Institution of Electrical Engineers., 93(31), pp. 2–14. doi: 10.1049/ji-2.1946.0002.

[11] Xu, Kelu & Xie, Ning & Wang, Chengmin & Shi, Xudong. (2017), 'Modeling and Simulation of Variable Speed Variable Frequency Electrical Power System in More Electric Aircraft, The Open Electrical & Electronic Engineering Journal, 11, pp. 87-98. doi: 10.2174/1874129001711010087.

[12] V. Madonna, P. Giangrande and M. Galea, "Electrical Power Generation in Aircraft: Review, Challenges, and Opportunities," in IEEE Transactions on Transportation Electrification, vol. 4, no. 3, pp. 646-659, Sept. 2018, doi: 10.1109/TTE.2018.2834142.

[13] Kennett, R.J., 'Integrated drive generators for aircraft', Electronics& Power, 1971, 17, (2), p. 73-76, DOI: 10.1049/ep.1971.0047.

[14] R. J. Kennett, "Integrated drive generators for aircraft", Electron. Power, vol. 17, no. 2, pp. 73-76, 1971.

[15] Aircraft, US Military, MIL-STD-704F, "Characteristics and Utilisation of Electric Power", 1991.

[16] RTCA, Inc., "Environmental conditions and test procedures for airborne equipment," DO-160G, Dec. 2010.

[17] European Committee for Standardization (CEN), "Aerospace series - Characteristics of aircraft electrical supplies," EN 2282, 1992.

[18] Qwik-Connect, Special Edition on Grounding and Bonding, Glenair, Vol. 27(3), July 2023.

[19] International Organization for Standardization (ISO), "Aerospace - Airframe bearings - Characteristics, loads, and classification," ISO 1540, 2006.

[20] S. L. Arevalo, P. Zanchetta, P. W. Wheeler, A. Trentin and L. Empringham, "Control and Implementation of a Matrix-Converter-Based AC Ground Power-Supply Unit for Aircraft Servicing," in IEEE Transactions on Industrial Electronics, vol. 57, no. 6, pp. 2076-2084, June 2010, doi: 10.1109/TIE.2009.2034180.

[21] Bento, A. et al. (2021) 'On the potential contributions of matrix converters for the future grid operation, sustainable transportation and electrical drives innovation', Applied sciences, 11(10), p. 4597. doi: 10.3390/app11104597.

[22] Balachandran, A., Boden, M., Sun, Z., Forrest, S.J., Ede, J.D. and Jewell, G.W. (2019), Design, construction, and testing of an aero-engine starter-generator for the more-electric aircraft. The Journal of Engineering, 2019: 3474-3478. doi: 10.1049/joe.2018.8235.

[23] [Diagram of APU APS5000], Pratt and Whitney. [Online]. Available: https://www.prattwhitney.com/en/products/auxiliary-power-units

[24] [Diagram of RAT], SAFRAN. [Online]. Available: https://www.safran-group.com/products-services/ram-air-turbine

[25] B. Adkins, W. Philipp and A. Hossle, "Electrical machines for aircraft", Proceedings IEE-A Power Eng., vol. 103, no. 1S, pp. 116-127, 1956, [online] Available: http://digital-library.theiet.org/content/journals/10.1049/pi-a.1956.0017.

[26] Jayarajan, R., Fernando, N. and Nutkani, I. U. (2019) 'A Review on Variable Flux Machine Technology: Topologies, Control Strategies and Magnetic Materials', *IEEE access*, 7, pp. 70141–70156. doi: 10.1109/ACCESS.2019.2918953.

[27] Wan, Yihong (2019) Fault behaviour and management of a permanent magnet aerospace starter-generator. PhD thesis, University of Sheffield.

[28] R. Owen, Z. Q. Zhu, J. B. Wang, D. A. Stone and I. Urquhart, "Review of variable-flux permanent magnet machines," 2011 International Conference on Electrical Machines and Systems, Beijing, 2011, pp. 1-6

[29] Ostovic, V., 2003. Memory motors. *IEEE Industry Applications Magazine*, 9(1), pp.52-61.

[30] I.R. Harris, G.W. Jewell, 'Rare-earth magnets: properties, processing and applications', chapter 19 in Functional Materials for Sustainable Energy Applications, Woodhead Publishing, 2012, pp. 600-639, ISBN 9780857090591.

[31] M. Wang et al., "Analysis of a Novel Hybrid-PM Variable-Flux Machine Using New Magnet Material CeFeB," in IEEE Transactions on Magnetics, vol. 55, no. 7, pp. 1-7, July 2019, Art no. 8106207

[32] T. Kosaka, Y. Kano, N. Matsui and C. Pollock, "A novel multi-pole permanent magnet synchronous machine with SMC bypass core for magnet flux and SMC field-pole core with toroidal coil for independent field strengthening/weakening", 2005 European Conference on Power Electronics and Applications, 2005.

[33] R. Owen, Z. Zhu, J. Wang, D. Stone and I. Urquhart, "Mechanically adjusted variable-flux concept for switched-flux permanent-magnet machines", 2011 International Conference on Electrical Machines and Systems, 2011.

[34] Lei Ma, M. Sanada, S. Morimoto and Y. Takeda, "Advantages of IPMSM with adjustable PM armature flux linkage in efficiency improvement and operating range extension", Proceedings of the Power Conversion Conference-Osaka 2002 (Cat. No.02TH8579).

[35] Ozawa, T. Kosaka and N. Matsui, "Less rare-earth magnet-high power density hybrid excitation motor designed for Hybrid Electric Vehicle drives," 2009 13th

European Conference on Power Electronics and Applications, Barcelona, 2009, pp. 1-10.

[36] S. Thomas, Z. Q. Zhu, R. L. Owen, G. W. Jewell and D. Howe, "Multiphase Flux-Switching Permanent-Magnet Brushless Machine for Aerospace Application," in IEEE Transactions on Industry Applications, vol. 45, no. 6, pp. 1971-1981, Nov.-dec. 2009, doi: 10.1109/TIA.2009.2031901.

[37] W. Hua, M. Cheng, Z. Q. Zhu, and D. Howe, "Design of flux-switching permanent magnet machine considering the limitation of inverter and flux-weakening capability," in Conf. Rec. IEEE IAS Annu. Meeting, 2006, pp. 2403–2410.

[38] M. C. Kulan, N. J. Baker and S. Turvey, "Split Rotor Concept for Permanent Magnet Electrical Machines," 2019 IEEE International Electric Machines & Drives Conference (IEMDC), San Diego, CA, USA, 2019, pp. 700-707

[39] Simon Turvey, Keir Wilkie "Split Rotor for Permanent Magnet MAachines- A patent application report," Control Data Services, Rolls-Royce plc, UK, Report 2018.

[40] Kou Baoquan, Li Chunyan and Cheng Shukang, "A new flux weakening method of permanent magnet synchronous machine," 2005 International Conference on Electrical Machines and Systems, Nanjing, 2005, pp. 500-503 Vol. 1

[41] Lei Ma, M. Sanada, S. Morimoto, Y. Takeda and N. Matsui, "High efficiency adjustable speed control of IPMSM with variable permanent magnet flux linkage," Conference Record of the 1999 IEEE Industry Applications Conference. Thirty-Forth IAS Annual Meeting (Cat. No.99CH36370), Phoenix, AZ, USA, 1999, pp. 881-887 vol.2

[42] W. Huijun, A. Zhongliang, T. Renyuan and N. Yingli, "Design of a hybrid excitation permanent magnet synchronous with low voltage regulation", Proceedings of the Eighth International Conference on Electrical Machines and Systems 2005. ICEMS 2005, vol. 1, pp. 480-483, 27–29 Sept. 2005.

[43] Xiaogang Luo and T. A. Lipo, "A synchronous/permanent magnet hybrid AC

machine," in IEEE Transactions on Energy Conversion, vol. 15, no. 2, pp. 203-210, June 2000,

[44] S. Roggia, G. Roggia, C. Francesco and M. Galea, "Rotor configuration comparison for the design of a PM conical machine," 2019 IEEE Energy Conversion Congress and Exposition (ECCE), Baltimore, MD, USA, 2019, pp. 3976-3982

[45] F. Chai, K. Zhao, Z. Li and L. Gan, "Flux Weakening Performance of Permanent Magnet Synchronous Motor With a Conical Rotor," in IEEE Transactions on Magnetics, vol. 53, no. 11, pp. 1-6, Nov. 2017, Art no. 8208506, doi: 10.1109/TMAG.2017.2708139.

[46] Kazuyuki, PATENT: P2007-244040a

[47] T. A. Lipo and M. Aydin, "Field weakening of permanent magnet machines-design approaches," in Proc. EPE-PEMC, Riga, Latvia, Sep. 2004, pp. 1–7.

[48] Lawrence, P.Z.; Jerry, W.M. Brushless Permanent Magnet Motor with Variable Axial Rotor/Stator Alignment to Increase Speed Capability. U.S. Patent 6,492,753 B2, 10 December 2002

[49] Y. Zhao, D. Li, T. Pei and R. Qu, "Variable Turn Rectangular Wire Winding Permanent Magnet Machine," 2020 International Conference on Electrical Machines (ICEM), Gothenburg, Sweden, 2020, pp. 366-372, doi: 10.1109/ICEM49940.2020.9270797.

[50] Balachandran, M. Boden, Z. Sun, S. J. Forrest, J. D. Ede, and G. W. Jewell, "Design, construction, and testing of an aero-engine starter generator for the more-electric aircraft," J. Eng., vol. 2019, no. 17, pp. 3474–3478, Jun. 2019.

[51] D. Wu and Z. Q. Zhu, "Influence of Slot and Pole Number Combinations on Voltage Distortion in Surface-Mounted Permanent Magnet Machines With Local Magnetic Saturation," in IEEE Transactions on Energy Conversion, vol. 30, no. 4, pp. 1460-1471, Dec. 2015, doi: 10.1109/TEC.2015.2436065.

[52] Vacuumschmelze GmbH & Co. KG, *"Cobalt-Iron Alloys,"* Brochure. [Online]. Available: https://vacuumschmelze.com/03_Documents/Brochures/Cobalt-Iron%20Alloys.pdf

[53] Global Response Surface Method," Altair Hyperstudy 2021.2 Help, https://2021.help.altair.com/2021.2/hwdesktop/hst/topics/design_exploration/method_global_response_surface_method_r.htm

[54] Danun, A. N., Poole, O., Tarter, E., Beutler, P., & Meboldt, M. (2023). (Non-)linear stiffness customisation of metallic additive manufactured springs. Virtual and Physical Prototyping, 18(1).

[55] RTS Auto, "Progressive Vs Linear Springs," RTS - Your Total BMW Enthusiast, July 13, 2017. [Online]. Available: https://www.rtsauto.com/progressive-vs-linear-springs/.

[56] A. Eid, H. El-Kishky, M. Abdel-Salam and M. T. El-Mohandes, "On Power Quality of Variable-Speed Constant-Frequency Aircraft Electric Power Systems," in IEEE Transactions on Power Delivery, vol. 25, no. 1, pp. 55-65, Jan. 2010, doi: 10.1109/TPWRD.2009.2031672.